A Molecular Trigger for Sea Anemone Stinging

HARVARD UNIVERSITY
Graduate School of Arts and Sciences

DISSERTATION ACCEPTANCE CERTIFICATE

The undersigned, appointed by the

Division of Medical Sciences

Program in Neuroscience

have examined a dissertation entitled

A Molecular Trigger for Sea Anemone Stinging

presented by Keiko Weir

candidate for the degree of Doctor of Philosophy and hereby certify that it is worthy of acceptance.

Signature: Bruce Bean
Bruce Bean (Feb 23, 2021 10:25 EST)

Typed Name: Dr. Bruce Bean

Signature: David Corey
David Corey (Feb 24, 2021 05:43 EST)

Typed Name: Dr. David Corey

Signature: David Ginty

Typed Name: Dr. David Ginty

Signature: Harold Zakon
Harold Zakon (Feb 2[illegible]021 08:50 CST)

Typed Name: Dr. Harold Zakon

Date: February 11, 2021

A Molecular Trigger for Sea Anemone Stinging

A dissertation presented

by

Keiko Weir

to

The Division of Medical Sciences

in partial fulfillment of the requirements

for the degree of

Doctor of Philosophy

in the subject of

Neuroscience

Harvard University

Cambridge, Massachusetts

February 2021

Dissertation Advisor: Nicholas Bellono Keiko Weir

A Molecular Trigger for Sea Anemone Stinging

Abstract

Understanding the mechanisms by which cells detect, integrate, and respond to distinct sensory cues is of fundamental importance to biological systems. Cnidarians, such as jellyfish, hydroids, and sea anemones, use specialized stinging cells called nematocytes that facilitate both sensation and secretion during prey capture and defense. Prey-derived mechanical and chemical cues synergistically trigger nematocytes to rapidly fire a venom-covered barb (nematocyst) through a previously unknown mechanism. Here, I show that nematocytes from *Nematostella vectensis* use a specialized voltage-gated calcium channel (nCa_V) to distinguish salient sensory cues and control the explosive discharge response. Unique properties in nCa_V confer unusually sensitive, voltage-dependent inactivation to inhibit responses to non-prey signals, such as mechanical water turbulence. Prey-derived chemosensory signals are synaptically transmitted to acutely relieve nCa_V inactivation, thereby allowing for mechanically-triggered attack. Thus, the distinct voltage-dependent properties of nCa_V allow nematocytes to selectively discriminate prey-derived cues from environmental noise. These findings reveal a molecular basis for the cnidarian stinging response and highlight how single proteins can integrate diverse cellular signals to mediate discrete behaviors.

Table of Contents

Acknowledgments

I started my scientific career determined to push forward our understanding of the human body to help prevent illness or cure disease. After dipping my toe into translational research and feeling unsatisfied, I discovered a passion for unusual organisms and cells. This newfound interest, coupled with my love for electrophysiology, led me to study an organism with tentacles, no brain, and exploding cells. I am very thankful to have had the opportunity to study something unique, challenging, and memorable.

I would like to thank the members of my dissertation advisory committee: Bruce Bean, Sean Eddy, and Rachelle Gaudet, for providing both scientific and career mentorship. I would like to specifically thank Bruce for teaching me how to patch my first cell and instilling rigorous habits that are critical to electrophysiology. I thank Nicholas Bellono for his scientific meticulousness and for opening my eyes to a world of physiology outside of neuroscience. I thank my lab members for their advice and experimental assistance. I thank my many instructors and mentors in the Program in Neuroscience, especially David Ginty, Rachel Wilson, and Lisa Goodrich, for their wise counsel. I thank William Moody for his training and mentorship during my undergraduate years. I would also like to thank the program staff at Harvard, especially Karen Harmin, Jackie Yun, and Janet Daniels, for their guidance and kindheartedness.

I would like to thank my fiancé and best friend, Josef, for his love and support. I am so grateful to have shared this journey with you. I thank my parents, Richard and Hiromi Weir, for supporting my academic ambitions and continuing to provide wisdom and a sympathetic ear. I thank my brother, Tomo, who helped me with my first scientific experiments in our backyard when we were children. I thank, Megan, for her humor and friendship. And lastly, my cat, Felix, who provided constant companionship during the writing of this dissertation.

Introduction

The detection of environmental cues is critical for survival. Animals have evolved an extensive repertoire of sensory systems that have enabled the detection of stimuli across modalities. Such systems contain single cells that can transduce physical stimuli from the external environment into signals that can be processed by the animal to make decisions. Bilaterians, such as mice, humans, flies, and monkeys, have developed extensive nervous systems containing sensory organs with specialized sensory cells. Because native cell function is frequently dependent upon signals from surrounding cells within the tissue or inputs from the nervous system, understanding the mechanism by which these sensory cells process complex environment cues can rarely be studied in an isolated cell. To add further difficulty, the cellular responses to these cues are often unclear, ranging from graded release of molecules to minute differences in electrical activity. Thus, the use of a cellular system in which environmental stimuli and cellular responses can be measured and controlled can help uncover the molecular underpinnings of signal detection, amplification, and processing.

Cnidarians

The phylum Cnidaria, which includes corals, sea anemones, and jellyfish, is thought to be the sister taxon to bilaterians (Simion et al., 2017). Given the phylogenetic position of cnidarians relative to bilaterians, these organisms have been widely studied to understand early body planning, nervous system development, and regeneration (DuBuc, Traylor-Knowles, & Martindale, 2014; Marlow, Srivastava, Matus, Rokhsar, & Martindale, 2009; Watanabe, Fujisawa, & Holstein, 2009). Although cnidarian model organisms do not have the same level of genetic tools available as in bilaterian model organisms, the adaptation of new gene editing technologies, such as CRISPR-

Cas9 and the increasingly streamlined systems available for genetic sequencing have opened new opportunities for molecular characterization in these organisms (Ikmi et al., 2020; Karabulut, He, Chen, McKinney, & Gibson, 2019).

Unlike bilaterians, which are triploblastic, cnidarians are diplobastic, containing only an ectoderm and an endoderm separated by a jelly-like layer called the mesoglea (Layden, Rentzsch, & Röttinger, 2016). Cnidarians contain a simple nervous system organized as a net of neurons, likely connected by bidirectional synapses (Anderson, 1985; Katsuki & Greenspan, 2013).

Nematostella vectensis, also known as the starlet sea anemone, is a species of sea anemone commonly found in brackish water along the east coast of the United States. *Nematostella* is slender and small, typically 1-2 inches in length in laboratory settings. The organism can be divided into three main body sections: a foot, a transparent body column lined with mesenteries, and a crown of tentacles. At the base of the tentacles is a mouth, which opens to the body column for ingesting prey and expelling waste products. In the wild, *Nematostella* typically bury their foot and body column in loose sediment, leaving the tentacles exposed to the water where it can capture unsuspecting prey. *Nematostella* can undergo both sexual and asexual reproduction and are able to tolerate a range of salinities (Stefanik, Wolenski, Friedman, Gilmore, & Finnerty, 2013), making them a very easy organism to maintain in laboratory settings.

Nematocytes

Cnidarians are named for a cell type found exclusively in this phylum called cnidocytes. Cnidocytes are specialized “stinging” cells that are primarily found in the ectodermal layer of tentacles of these organisms, where their apical surface has direct access to the surrounding aquatic environment and the basal surface interacts with other cells in the dermis (**Fig. 1**). If the cell detects

the appropriate environmental cues, the cell explosively releases a specialized organelle called the cnidocyst. Cnidocytes are further classified by the type of cyst that is discharged. One of the two most common types of cnidocytes are spirocytes, which evert an organelle containing a sticky thread used for entangling prey. The other most common are nematocytes, which everts a barbed, venom coated thread from the nematocyst. The discharge of the nematocyst is one of the fastest biological processes in nature – when stimulated, the cyst fuses with the apical surface of the cell and the thread is everted with such speed to achieve an acceleration of over 5,000,000 *g* and has enough force to penetrate the thick cuticle of crustacean prey (Nüchter, Benoit, Engel, Özbek, & Holstein, 2006) (**Fig. 2**).

The nematocyte is an ideal cell to study the relationship between signal transduction and cellular response because of its clear, binary output and simple sensory processing. In most animals, sensory processing involves distinct sensory cells that signal to neural networks to mediate an appropriate behavioral response. Nematocytes are unique because they are hypothesized to use a specific set of cues from the environment to trigger the explosive release of the nematocyst without extensive involvement of the nervous system (Kass-Simon & Scappaticci, Jr., 2002; Pantin, 1942a). Considering that discharge can only occur once, after which the cell dies and is replaced, this clear-cut behavioral response is expected to be tightly regulated to prevent unnecessary cell turnover.

Early work has established that nematocyte discharge is facilitated by both mechanical and chemical sensory cues (Pantin, 1942a; Watson & Hessinger, 1989). N-acetylated sugars and amino acids are commonly found on the surfaces of various prey for cnidarians (Watson & Mire, 2004). Two agonists within these categories have been identified to increase the probability of discharge of nematocytes in various organisms: N-acetylneuraminic acid (NANA) and proline (Thorington

& Hessinger, 1988), potentially by modulating the structure or function of the nematocyte's distinct environmentally-exposed cilium (cnidocil) (Watson & Hessinger, 1992). Importantly, chemical stimulation alone does not appear to induce discharge in isolated nematocytes but modulates discharge when applied simultaneously with a mechanical stimulus (Ewer. & Fox, 1947; McKay & Anderson, 1988a; Pantin, 1942a; Thurm et al., 2004). These studies indicate that chemosensory cues modulate discharge by acting directly on nematocytes or through functionally-connected sensory cells. Thus, the nematocyte is a unique system to study the mechanisms by which cells detect and integrate signals to produce a discrete response.

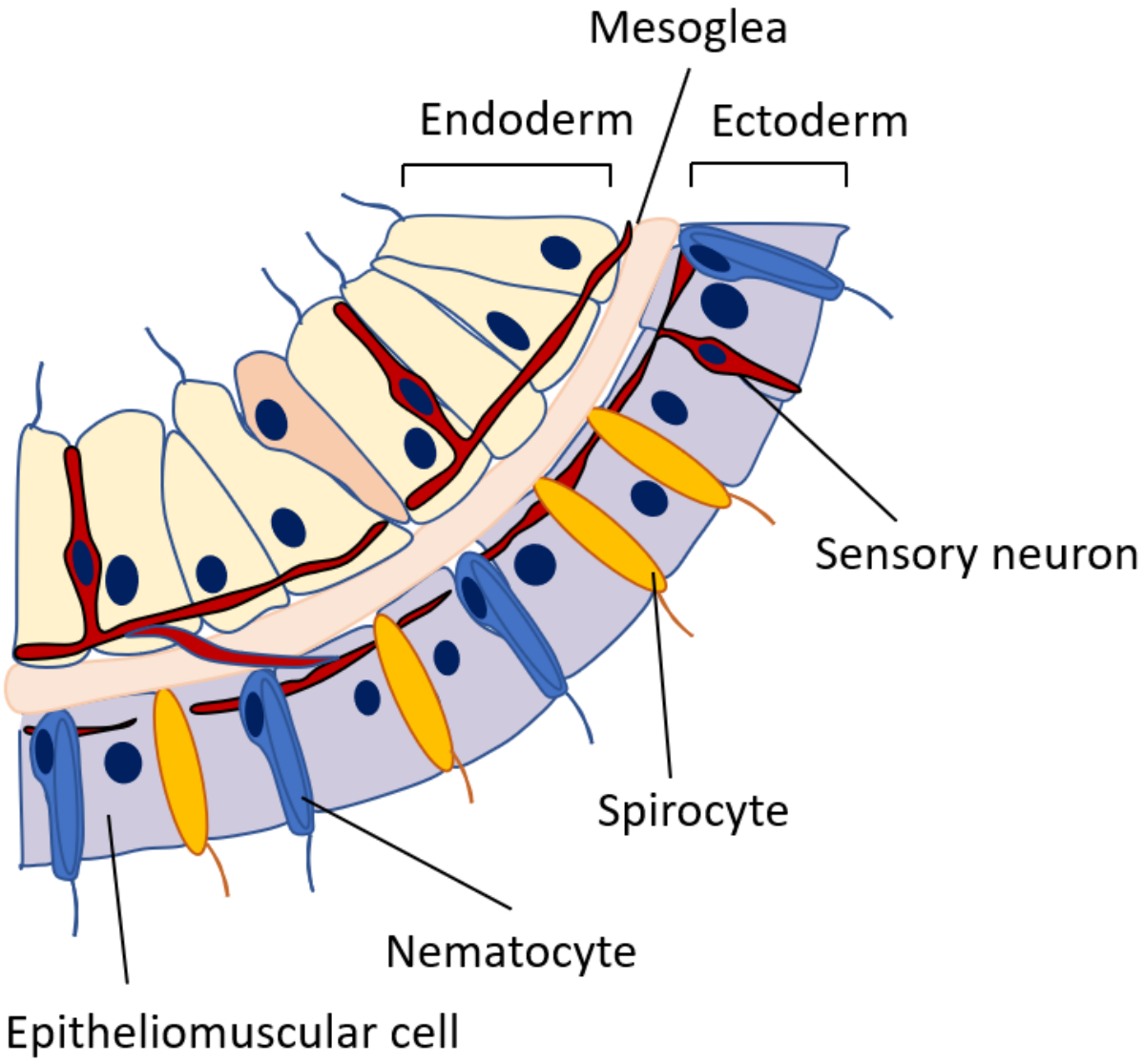

Figure 1: Cross-section of *Nematostella* tentacle. Tentacle tissue is composed of two dermal layers separated by a mesogleal layer. Spirocytes and nematocytes are primarily located in the ectoderm where the apical surface of these cells directly interacts with the surround marine environment and basal surface contacts neural processes and other support cells.

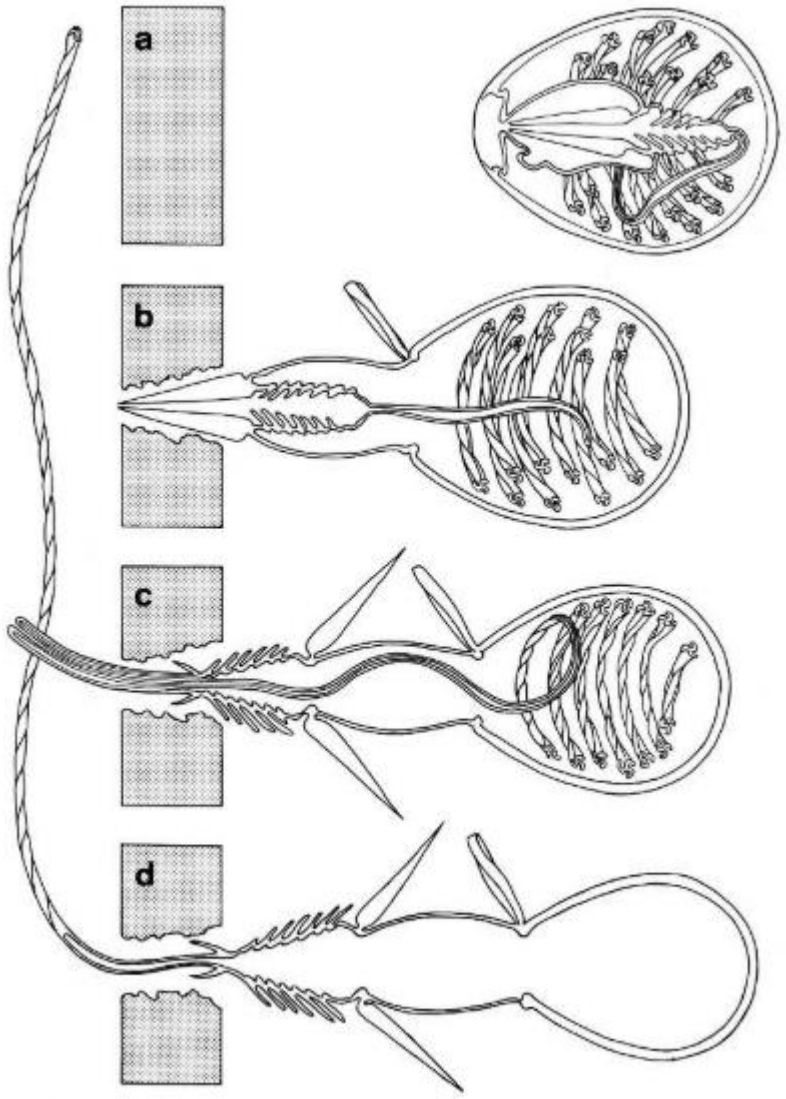

Figure 2: Four stages of discharge of a stenotele nematocyte from *Hydra.* After a nematocyte contacts another organism, the barbed, venom coated thread is discharged from the cell, perforating the epidermis of the target. Adapted from Tardent & Holstein, 1982.

While multiple studies have indicated that nematocytes integrate both mechanical and chemical cues to determine if they should sting, the molecular mechanism underlying this signal processing remains unknown. How does this specialized cell quickly and efficiently detect, amplify and respond to mediate prey capture and predator defense?

One mechanism by which cells quickly transduce and amplify signals is through electrically excitable membranes. Electrically excitable membranes are particularly advantageous for sensory signal transduction because changes are rapid, on the order of milliseconds. Such rapid signaling allows for the initiation of downstream responses within the cell and the fast relay of information to other cells via release of signaling molecules, or through direct electrical coupling. Additionally, electrically excitable membranes can serve to amplify sensory signals using voltage-gated ion channels, which are sensitive to membrane potential changes. The mechanisms underlying electrical signaling are highly conserved and common to many cell types and span multiple phyla.

Despite over 150 years of study (Greene, 1861), the underlying physiology of nematocytes remains largely unknown. Important observations in multiple species have indicated that nematocyte discharge requires calcium influx into the cell (Gitter, Oliver, & Thurm, 1994; McKay & Anderson, 1988a; Santoro & Salleo, 1991), suggesting that calcium-mediated second messenger signaling is critical to the discharge of the cell. However, the calcium-influx in the intracellular space alone cannot explain the rapid extrusion of the nematocyst. Very limited recordings indicate that nematocytes have electrically excitable membranes and can produce action potentials, represented by large acute increases in voltage (spikes) (Anderson & McKay, 1987; Brinkmann, Oliver, & Thurm, 1996; McKay & Anderson, 1988b; Price & Anderson, 2006). Depolarization of nematocytes can be induced by increasing extracellular potassium or by injecting large currents near cells, both of which increase the probability of discharge in a calcium-dependent manner

(Anderson & McKay, 1987; Gitter et al., 1994; Santoro & Salleo, 1991; Watson & Hessinger, 1994). Immediately prior to discharge, the cyst volume also increases rapidly (Holstein & Tardent, 1984). Such change in volume is hypothesized to be mediated by a rapid increase in the osmolarity of the cyst, resulting in a water-induced swelling and providing the necessary potential energy for such a forceful, explosive event (Nüchter et al., 2006). Then, the nematocyst fuses with the apical surface of the cell membrane, akin to vesicular fusion in neuroendocrine or neurotransmitter release (Gitter et al., 1994; Skaer, 1973).

While previous work has established a role for calcium influx in facilitating discharge, the mechanisms of sensory signal transduction, integration, and their relationship to calcium influx remain unclear. Previous work has suggested that nematocytes have electrically excitable membranes, but the electrical properties of nematocytes are poorly understood. Thus, a careful examination of ion channels in nematocytes reveal new insights into the relationship between environmental signals and cellular responses.

Ion channels

The regulation of ions across the cell membrane is critical for life. All cells have a lipid membrane that functions to create a specialized ionic environment inside the cell. The lipid bilayer is impermeable to most hydrophilic molecules, including ions. Thus, specialized transport systems are required to mediate the selective movement of molecules into and out of the cell. One such system that has evolved is the use of ion channels that form a pore, or channel, across the bilayer, allowing selective ions to flow down their electrochemical gradient. Given the biological importance of maintaining ion gradients, it is not surprising that ion channels are highly conserved and found in all phyla of the animal kingdom.

The effectiveness of voltage-gated ion channels in maintaining electrical gradients is based upon the ability to control the passage of ions through the pore. Ion channels typically exist in one of three states and movement between these states requires a conformational change within the pore (**Fig. 3**). Most channels reside in a closed, non-conducting state at physiological resting membrane potentials. Upon membrane depolarization, voltage-gated channels will undergo a conformational change and enter an open, conductive state. With sustained depolarization, these channels will then enter an inactive, non-conductive state. This conformation differs from the closed state because channels in this configuration will not open to the same depolarizing stimulus used in the closed state. Channels will then return to a closed configuration with hyperpolarization, effectively resetting the channel's ability to respond to future depolarizing stimuli.

All electrical signaling requires the movement of ions through ion channels. The stimuli that regulate the opening of this pore vary and includes, but is not limited to, temperature, mechanical stress, the binding of a chemical or another protein to the ion channel, and a change in membrane potential (Hille, 2001). Ion channels that are regulated, or gated, by changes in membrane potential are called voltage-gated ion channels. These proteins are particularly useful for signal amplification because of their regenerative nature. A small depolarization of the membrane triggers the opening of these channels, which can then cause ions to flow across the cell membrane, resulting in further depolarization and additional recruitment of other voltage-gated channels.

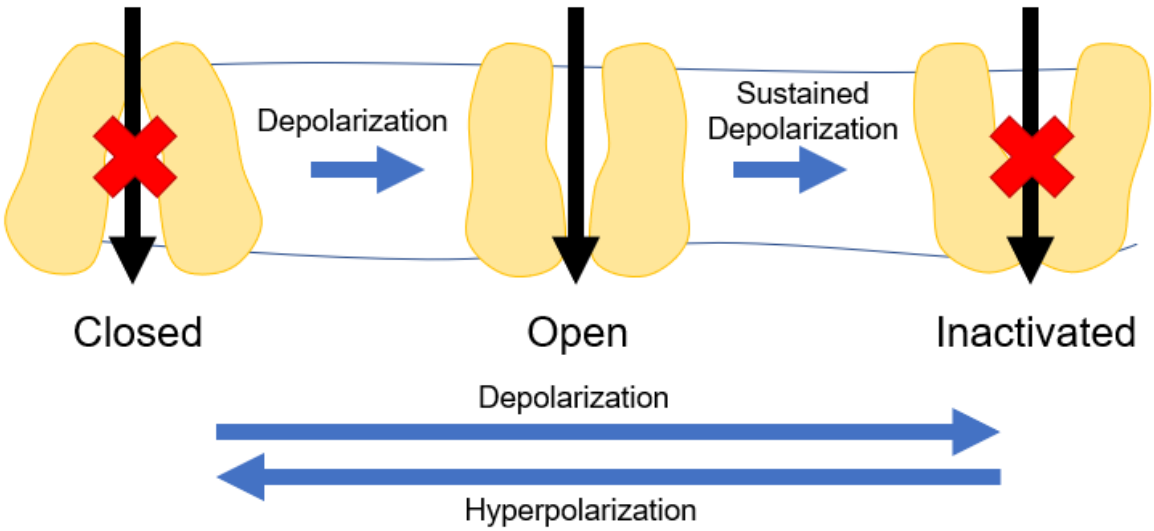

Figure 3: Voltage-gated ion channel states. Most voltage-gated ion channel states can be categorized as either closed, open or inactivated. At rest, a channel typically resides in a closed, non-conducting state. With membrane depolarization, the channel will enter an open state in which the pore of the channel will undergo a conformational change, allowing ions to pass. With sustained depolarization, the channel will then enter an inactive, non-conductive state. In general, a channel can return to a closed state with membrane hyperpolarization.

The superfamily of voltage-gated ion channels includes voltage-gated sodium (Na_V), calcium (Ca_V) and potassium (K_V) channels. Although there are key differences between these subtypes that mediate ion selectivity, generally, these proteins share a similar structure. The pore-forming α subunit is composed of four homologous domains, termed domains I-IV, with each domain containing six transmembrane segments (S1-S6) (Hille, 2001; Jiang et al., 2003; Noda et al., 1986; Tanabe et al., 1988). Voltage-sensing is mediated by the S4 segment, which contains positively charged residues at every third or fourth position and enables the outward movement of the sensor upon change in membrane potential (Catterall, 1986; Hille, 2001). This movement results in a conformational change of the pore and the channel enters an open state configuration, allowing ions to pass through. Selectivity is achieved by specific residues in segments S5 and S6, which are positioned in the lining of the pore and form the aptly named selectivity filter (Gur Barzilai et al., 2012; Wu et al., 2016). While the α subunit is a critical player in voltage-gated ion channels, most channels are a macromolecular complex of proteins. Additional proteins, called accessory subunits, further regulate trafficking, opening of the pore, and other functional properties of the channel (Dolphin, 2016).

The opening of all voltage-gated channels results in a change to the cell membrane potential, however the opening of Ca_V also results in the activation of numerous downstream signaling pathways through the transient increase in intracellular calcium levels (Catterall, 2011). Calcium ions are one of the most ubiquitous signaling molecules employed by cells across all domains of life as calcium can be both spatially and temporally altered and is widely available in the environment (Catterall, 2000). The effectiveness of calcium ions for signaling is attributed to the approximately 20,000-fold concentration difference across the cell membrane, which is facilitated by a network of proteins that maintain a very low intracellular calcium concentration(Catterall,

2000). Thus, a small influx of calcium ions could result in a transient, many-fold increase in concentration able to initiate a wide range of downstream pathways, such as the contraction of a heart cell or the electrical signaling of a neuron.

Calcium channels were first recognized in crab muscle fibers in the early 1950's (Fatt & Katz, 1953) however, very little progress in the study of these channels could occur without the ability to study these proteins in isolation. It was not until over 30 years later before technological advancements made it possible to purify large amounts of protein, resulting in a flood of research into the function of individual channel subunits (Curtis & Catterall, 1984). Protein-protein interaction assays, sequence alignment and cloning mutagenesis have been critical in identifying key functional regions of all subunits.

Historically, Ca_Vs have been classified based on their electrical properties: low voltage activated (LVA) channels that open near physiological resting membrane potential and high voltage activated (HVA) channels that require greater depolarization to open (Catterall, Perez-Reyes, Snutch, & Striessnig, 2005). Advances in gene sequencing and phylogenetics have further classified HVA Ca_V α subunits as either Ca_V1 (L Type) or Ca_V2 (P/Q, R and N type), while LVA Ca_Vs are classified as Ca_V3 (T type) (Ertel et al., 2000). In HVA Ca_Vs, the pore forming α subunit is found in a complex with the accessory β, α2δ, and in some cases, γ subunits **(Fig. 4A)**. Without the presence of these accessory proteins, the α subunit fails to express at the cell membrane entirely (Birnbaumer et al., 1998; Dolphin, 2016). In addition to differences in electrical properties due to channel subtype, variations in calcium currents can also be attributed to differences in accessory proteins. Thus, understanding the mechanisms by which these accessory subunits regulate the trafficking and opening of this α subunit is critical to understanding the entire channel's innate function.

As with Na_V and Kv α subunits, the S5 and S6 segments of each domain of the Ca_V α subunit act as a selectivity filter **(Fig. 4B)**. In HVA Ca_Vs, the carboxyl oxygen atoms of four glutamate (E) residues form high affinity binding sites for Ca^{2+} ions. The same principle is true with LVA Ca_Vs, with a replacement of two aspartates for two glutamates at the same sites (Heinemann, Terlau, Stühmer, Imoto, & Numa, 1992).

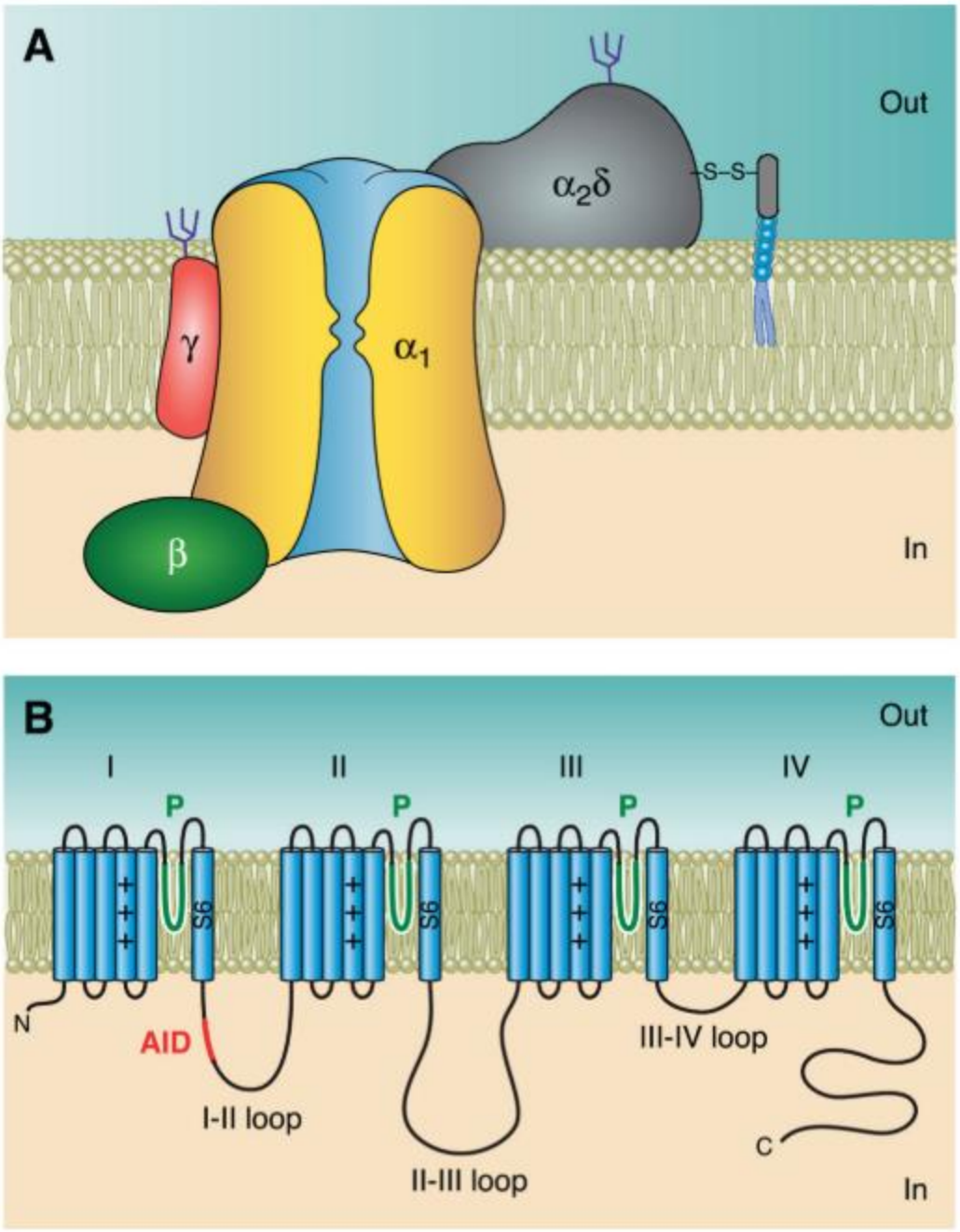

Figure 4: Structure of a voltage-gated calcium channel. (A) Subunit composition of Ca_V1 and Ca_V2 channels. **(B)** Schematic representation of the protein topology of the α subunit with domains I-IV indicated. The α-interaction domain (AID) is highlighted in red. (From Buraei and Yang 2010).

$Ca_V\beta$ subunits are cytosolic proteins that directly bind to Ca_V1 and Ca_V2 α subunits to modulate both voltage dependent opening and expression at the cell membrane. Protein-protein interaction assays, sequence alignment and cloning mutagenesis have identified the interacting domains between the α and β subunits (De Waard, Scott, Pragnell, & Campbell, 1996; Olcese et al., 1994). The β subunit binds to a short intracellular region of the α subunit linking domains I and II, aptly named the α interaction domain (AID) (Pragnell et al., 1994; Wu et al., 2016). Ca_V3 α subunits lack this domain and are thought to not be modulated by β subunits (Buraei & Yang, 2010). The two domains of the β subunit which mediate the interaction between the α subunit are a conserved, but enzymatically inactive, guanylate kinase (GK) domain and a conserved Src-homology 3 (SH3) domain (Buraei & Yang, 2010). The mechanism by which $Ca_V\beta$ subunits increase cell surface expression is still not completely understood. Two general hypotheses are that the β subunit binds to the AID of the pore-forming subunit and masks an endoplasmic reticulum retention signal (Bichet et al., 2000). Alternatively, it has been proposed that the β subunits inhibits proteosomal degradation (Altier et al., 2011).

Once the α subunit is integrated into the cell membrane, binding of the β subunit powerfully regulates the voltage dependent conformational changes of the α subunit (Butcher, Leroy, Richards, Pratt, & Dolphin, 2006; Patil, Brody, & Yue, 1998; Yasuda, Lewis, & Adams, 2004). The exact mechanism by which β subunits modulate both voltage-dependent changes to the channel remains to be resolved. One hypothesis is that Cavβ binding to the AID shifts the energetically favorable conformations of the S6 region of the α subunit, resulting in an increased probability to shift to a different conformational state given a change in voltage (Buraei & Yang, 2010; Yasuda et al., 2004).

In comparison to $Ca_V\beta$ subunits, $Ca_V\alpha2\delta$ subunits have a less significant effect on voltage-dependent properties of the channel (Yasuda et al., 2004). Like $Ca_V\beta$, $Ca_V\alpha2\delta$ subunits increase calcium currents by promoting cell surface expression through increased trafficking and/ or retention (Cantí, Page, Stephens, & Dolphin, 1999; Hoppa, Lana, Margas, Dolphin, & Ryan, 2012; Yasuda et al., 2004).

γ subunits were originally identified as part of the macromolecular calcium channel complex in skeletal muscle and were thought to have a primary role in modulating channel properties (Eberst, Dai, Klugbauer, & Hofmann, 1997). However, this assumption has been increasingly challenged and more recent studies indicate a role in Ca_V trafficking and an additional role in AMPA receptor trafficking and gating (Qiao & Meng, 2003).

Evolution of voltage-gated ion channels

The increased affordability of genomic sequencing and widespread availability of non-mammalian genomic data have led to new insights in the evolution of voltage-gated ion channels. The presence of Ca_V α subunits across multiple phyla support the hypothesis that α subunits appeared early in eukaryote evolution (Jeziorski, Greenberg, & Anderson, 2000; Piontkivska & Hughes, 2003; Senatore, Raiss, & Le, 2016). Based on phylogenetic analyses, Na_V and Ca_V channels are thought to have evolved by two rounds of gene duplication from an ancestral Kv channel. K_V channels, unlike Ca_V and Na_V channels, consist of four subunits, with each subunit encoding a single domain. It is hypothesized that the duplication of a single domain into a two-domain protein, followed by another duplication would lead to an ancestral four-domain channel (Y. Moran, Barzilai, Liebeskind, & Zakon, 2015; Piontkivska & Hughes, 2003).

Additional gene duplication events are thought to mediate the expansion of this single ancestral four-domain channel alpha subunit to three distinct Ca_V pore forming channels, resulting in CaV1, Ca_V2 and Ca_V3 families (Jeziorski et al., 2000; Piontkivska & Hughes, 2003). The duplication of this four-domain protein and subsequent modifications of core structural elements resulted in a diversity of channels with specialized functional properties (Pohorille, Schweighofer, & Wilson, 2005). Gene duplication events in early mammals have resulted in four Ca_V1, three Ca_V2 and three Ca_V3 channels (Perez-Reyes, 2003; Yu & Catterall, 2004). In contrast, cnidarian Ca_V channels expanded independently to result in one Ca_V1, three Ca_V2, two Ca_V3 channels (Yehu Moran & Zakon, 2014).

Diversification in ion channel sequences led to changes in ion selectivity, gating, localization and protein-protein interactions that have resulted in evolutionarily advantageous methods for channel regulation (Senatore et al., 2016). Calcium channels with distinct voltage-dependent properties can alter the responsiveness of channels to various depolarizing stimuli. Additionally, alterations to calcium channel properties can adjust the duration, and thus net influx, of calcium ions, which has important implications for downstream second messenger pathways, as well as preventing calcium-induced cytotoxicity.

Calcium channel accessory subunits have also undergone expansion and diversification through gene duplications. β subunits, which were found in the last common ancestor of bilaterians and choanoflagellates, have also undergone multiple, independent gene duplication events. Bilaterians have four genes encoding $Ca_V\beta$, with many splice variants, whereas single genes have been identified in various cnidarian species and in Trichoplax (C. Bouchard et al., 2006; Grabner et al., 1994; Jeziorski, Greenberg, & Anderson, 1999; Smith et al., 2017). α2δ subunits can be found in

bilaterians as well as cnidarians, however, γ subunits appear to be exclusive to bilaterians (Y. Moran et al., 2015).

Chapter 1

Introduction

Jellyfish, sea anemones, and hydrozoans of the Cnidarian phylum use specialized cells called cnidocytes to facilitate both sensation and secretion required for prey capture and defense (Watson & Hessinger, 1994). Two major types of cnidocytes contribute to prey capture by the tentacles of the starlet sea anemone (*Nematostella vectensis*, **Fig. 5A**): (1) spirocytes, anthozoan-specific cells that extrude a thread-like organelle to ensnare prey, and (2) nematocytes, pan-cnidarian cells which eject a single-use venom-covered barb to mediate stinging (Babonis & Martindale, 2017). Sensory cues from prey act on nematocytes to trigger the explosive discharge of a specialized organelle (nematocyst) at an acceleration of up to $5.41x10^6$ g, among the fastest of any biological process (Holstein & Tardent, 1984; Nüchter et al., 2006) (**Fig. 5B**). The nematocyst can only be discharged once and therefore stinging represents an energetically expensive process that is likely tightly regulated (Babonis & Martindale, 2014; Watson & Hessinger, 1994). Indeed, simultaneously presented chemical and mechanical (chemo-tactile) cues are required to elicit nematocyte discharge (Anderson & Bouchard, 2009; Pantin, 1942a; Watson & Hessinger, 1989, 1992). Electrical stimulation of nematocytes increases the probability of discharge in a calcium (Ca^{2+})-dependent manner (Anderson & Bouchard, 2009; Anderson & McKay, 1987; Gitter et al., 1994; McKay & Anderson, 1988a; Santoro & Salleo, 1991; Watson & Hessinger, 1994), but direct recordings from nematocytes are limited and thus mechanisms by which environmental signals control discharge are not well studied. Here, we demonstrate that nematocytes from *Nematostella vectensis* use a specialized $Ca_v2.1$ voltage-gated calcium channel orthologue (nCa_V) to integrate dynamic voltage signals produced by distinct sensory stimuli. We show nematocytes are intrinsically mechanosensitive but nCa_V exhibits unique voltage-dependent inactivation that basally inhibits cellular activity, thereby preventing responses to extraneous mechanical stimuli,

such as background water turbulence. We further show that sensory neurons make synaptic contact with nematocytes, and the neurotransmitter acetylcholine (ACh) elicits a hyperpolarizing response that relieves nCa_V inactivation to allow for subsequent cellular stimulation and chemo-tactile-elicited discharge. Thus, we propose that the specialized voltage dependence of nCa_V acts as a molecular filter for sensory discrimination.

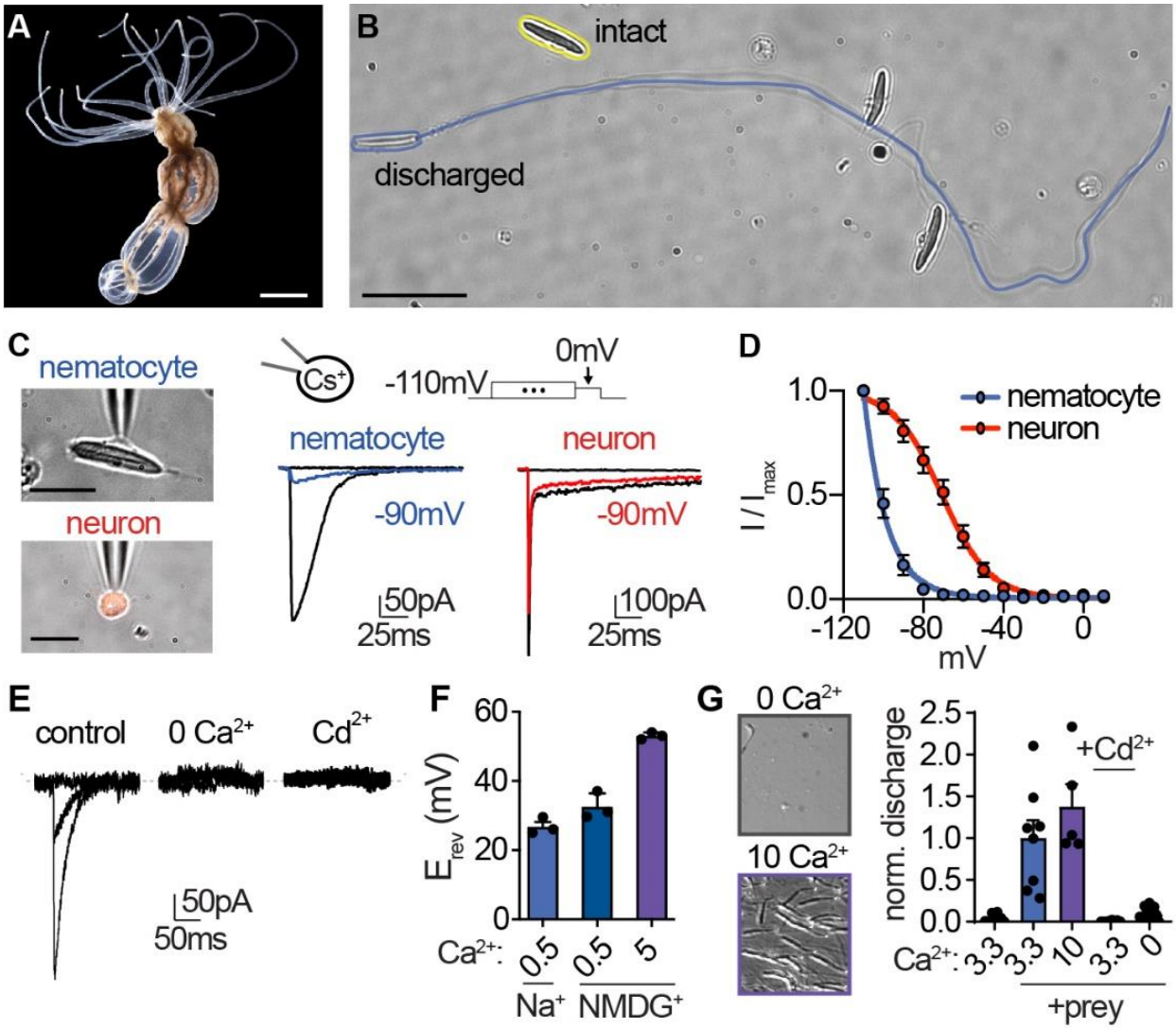

Figure 5: Nematocyte voltage-gated Ca^{2+} currents exhibit sensitive voltage-dependent inactivation. (A) Starlet sea anemone (*Nematostella vectensis).* Scale bar = 3mm. **(B)** Intact (yellow) and discharged nematocyte (blue). Scale bar = 20µm. **(C)** *Left*: Representative patch clamp experiments from a nematocyte and tentacle neuron. Scale bar = 10µm. *Right*: Nematocyte or neuron voltage-gated currents elicited by a maximally activating voltage pulse following 1s pre-pulses to -110mV (max current), -90mV (colored), or 0mV (inactivated, no current). **(D)** Nematocyte voltage-gated currents inactivated at very negative voltages compared with neurons.

Nematocyte inactivation occurred at voltages more negative than could be measured compared with a sigmoidal inactivation relationship in neurons: nematocyte estimated $V_{i1/2}$ = -100.2 ± 0.4mV, n = 13 and neuron $V_{i1/2}$ = -70.8 ± 1.0mV, n = 9. Apparent activation thresholds were similar (Fig. 1 - supplement 1A). **(E)** Nematocyte voltage-gated currents elicited by -40mV and 0mV pulses were abolished in absence of external Ca^{2+} and blocked by cadmium (Cd^{2+}). Representative of n = 4 for 0 Ca^{2+} and 3 for Cd^{2+}, $p < 0.001$ paired two-tailed student's t-test. **(F)** Nematocyte voltage-gated currents were Ca^{2+}-sensitive. Substitution of extracellular Ca^{2+}, but not Na^{+} for $NMDG^{+}$, affected the reversal potential. n = 3 - 4, $p < 0.001$ for 5mM Ca^{2+} versus other conditions, one-way ANOVA with post-hoc Tukey test. **(G)** Nematocyte discharge was minimal or absent in response to mechanical stimulation alone (n = 11, 3.3mM Ca^{2+}). In the presence of prey extract, mechanically-evoked discharge was similar in standard and higher concentration of extracellular Ca^{2+} (n = 8 for 3.3mM Ca^{2+}, n = 5 for 10mM) and blocked by Cd^{2+} (n = 8) or the removal of extracellular Ca^{2+} (n = 15). Discharged nematocysts embedded in presented gelatin-coated coverslips were quantified. $p < 0.001$ for + prey with 3.3 or 10mM Ca^{2+} versus other conditions, one-way ANOVA with post-hoc Bonferroni test. Data represented as mean ± sem.

Results

Nematocyte Ca_V channels

We first obtained whole-cell patch clamp recordings from acutely dissociated nematocytes to investigate nematocyte signal transduction. Using intracellular cesium (Cs^+) to block potassium (K^+) currents revealed a voltage-gated inward current that was activated by positive or depolarized membrane voltages (I_{CaV}, **Fig. 5C**). In response to sustained positive voltage, voltage-activated ion channels enter a non-conducting, inactivated state and cannot be activated until returned to a resting state by negative membrane voltage. This property generally serves to limit responses to repetitive or prolonged stimulation, similar to receptor desensitization. Remarkably, I_{CaV} began to inactivate at voltages more negative than we could technically measure, thus demonstrating an unusual voltage sensitivity of this conductance (**Fig. 5C, D**). To determine whether these properties were specific to nematocytes, we used a transgenic sea anemone with fluorescently-labeled neurons to facilitate direct comparison between these excitable cell types (Nakanishi, Renfer, Technau, & Rentzsch, 2012) (**Fig. 5C**). Neuronal voltage-gated currents had a lower threshold for activation and exhibited much weaker voltage-dependent inactivation (**Fig. 5C, D, Fig. 6A-D**), similar to currents found in neurons of other animals (Hille, 2001), indicating that nematocytes exhibit unusual voltage-dependent properties. Ion substitution and pore blocker experiments confirmed I_{CaV} is a Ca^{2+}-sensitive current (**Fig. 5E, F**), consistent with the contribution of extracellular Ca^{2+} to chemo-tactile-induced discharge (Gitter et al., 1994; Watson & Hessinger, 1994) (**Fig. 5G**). Increased concentrations of extracellular Ca^{2+} did not affect inactivation of I_{CaV} (**Fig. 6E**), suggesting the enhanced voltage-dependent inactivation is intrinsic to the channel complex. This observation is important because it suggests I_{CaV} renders nematocytes

completely inactivated at typical resting membrane voltages and thus cells could not be stimulated from resting state.

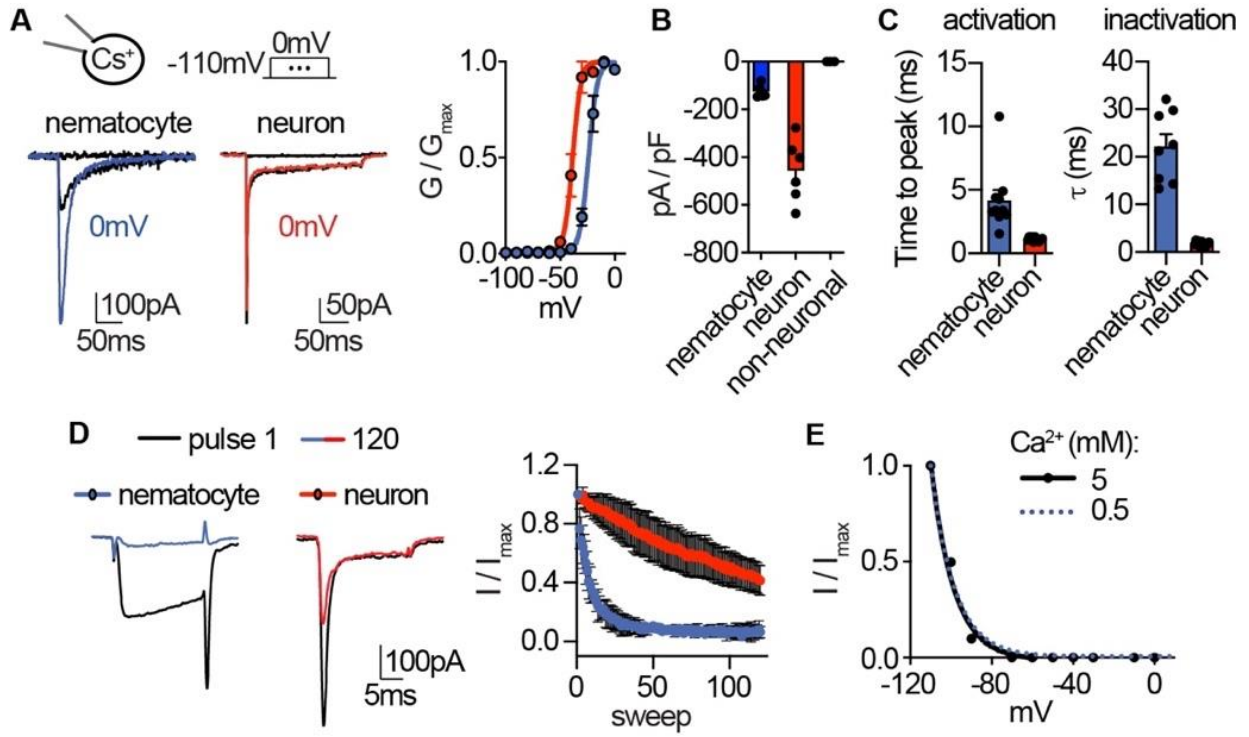

Figure 6: Native nematocyte Ca_V properties. (A) Voltage-gated currents from a nematocyte and tentacle neuron elicited by -40mV or 0mV pulses. Conductance-voltage curves: nematocyte $V_{a1/2}$ = -24.0 ± 0.5mV, n = 10 and neuron $V_{a1/2}$ = -38.6 ± 0.6mV, n = 7. **(B)** Peak current density elicited by 0mV pulse in nematocytes (n = 5), neurons (n = 6), and non-neuronal cells (n = 3). **(C)** Inward currents activated and inactivated more slowly in nematocytes compared with neurons. n = 10 nematocytes, 11 neurons. $p < 0.0001$ two-tailed student's t-test. **(D)** Nematocyte inward currents inactivated more quickly with repetitive stimulation compared with neurons. Protocol: 3.33 Hz stimulation with 20ms pulses to -10mV from -90mV. n = 4 of each cell type, multiple row two-tailed student's t-test with significance of $p < 0.05$ by sweep 5 and $p < 0.0001$ by 120. **(E)** Inactivation of inward currents does not vary with external Ca^{2+}. 0.5 mM Ca^{2+} estimated $V_{i1/2}$ = -100.2 ± 0.4mV, n = 13, from Fig 1. 5 mM Ca^{2+} estimated $V_{i1/2}$ = -99.8 ± 0.9mV, n = 3. Data represented as mean ± sem.

To identify the ion channel mediating I_{CaV}, we generated a tentacle-specific transcriptome and aligned reads from nematocyte-enriched cells (Sunagar et al., 2018). This strategy allowed us to search for differentially expressed transcripts that might encode Ca_V channel subunits (pore-forming α and auxiliary β and α2δ subunits). The orthologue of *cacnb2*, a β subunit of Ca_V channels, was the highest expressed Ca_V transcript in nematocyte-enriched cells, with levels 14-fold higher than other cells in the sea anemone (**Fig. 7A**). β subunits can modulate voltage-dependence and trafficking in diverse ways depending on their splice isoform, interacting subunits, and cellular context (Buraei & Yang, 2010). Importantly, β subunits only interact with α subunits of high voltage-activated (HVA) calcium channels (Perez-Reyes, 2003). In agreement with robust β subunit expression, we found significant enrichment for *cacna1a*, the pore-forming subunit of HVA $Ca_V2.1$, and high expression of *cacna2d1* (**Fig. 8A, B**). These observations are consistent with a previous report demonstrating specific expression of *cacna1a* in nematocytes of sea anemone tentacles and expression of β subunits in nematocytes from jellyfish (C. Bouchard et al., 2006; Christelle Bouchard & Anderson, 2014; Yehu Moran & Zakon, 2014). Expression of *cacna1h*, which does not interact with auxiliary subunits (Buraei & Yang, 2010), was also observed, albeit at lower levels and across all cells (**Fig. 8A**). Thus, it remains possible that voltage-gated currents in nematocytes are not carried exclusively by one Ca_V subtype.

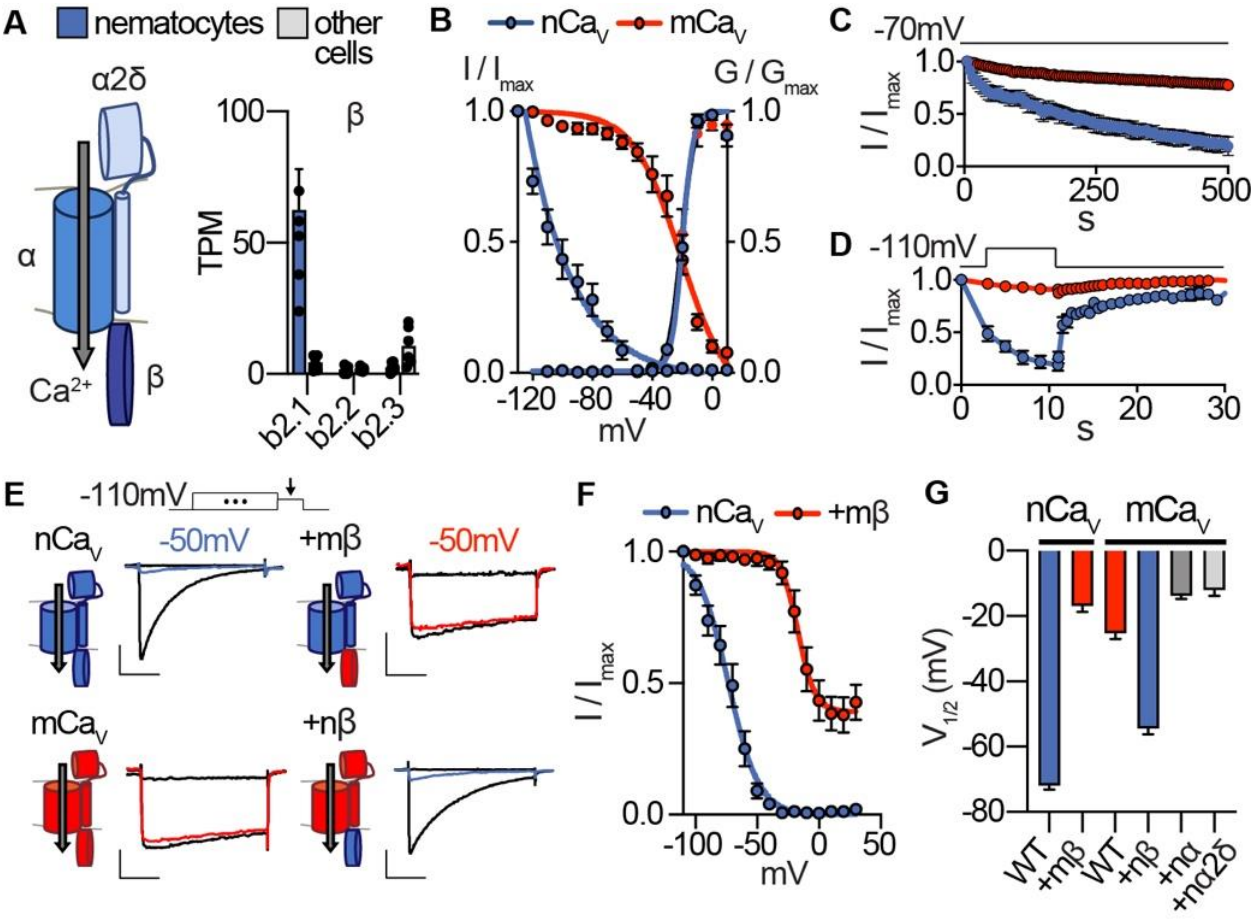

Figure 7: *Nematostella* Ca_V exhibits unique voltage-dependent properties conferred by its β subunit. (A) Ca_V channel complex with α, β, and α2δ subunits. mRNA expression (transcripts per million, TPM) of voltage-gated calcium (Ca_V) channel β subunits in nematocyte-enriched cells (blue) and non-enriched cells (grey). n = 6, $p < 0.0001$ for *cacnb2.1* in nematocytes versus other cells, two-way ANOVA with post-hoc Bonferroni test. **(B)** Heterologously-expressed nCav channels (*Nematostella cacna1a*, *cacnb2*, *cacna2d1*) inactivated at very negative voltages (estimated $V_{i1/2}$ = -101.5 ± 1.6mV, n = 5) versus mammalian orthologues (mCa_V, $V_{i1/2}$ = -20.9 ± 3.4mV, n = 10). Apparent activation thresholds were the same: nCa_V $V_{a1/2}$ = -9.8 ± 0.3mV, n = 5, mCa_V $V_{a1/2}$ = -10.4 ± 0.5mV, n = 9. Inactivation was measured in response to 1s pre-pulses from -110mV to 10mV with an inter-sweep holding potential of -90mV. **(C)** nCa_V exhibited slow

inactivation with -70mV holding potential (0.2 Hz stimulation, 5s inter-pulse interval) that was best fit by two exponential functions with time constants of 10.0 and 369.5s. n = 6, multiple row two-tailed student's t-test with significance of $p < 0.05$ by 15s and $p < 0.0001$ by 500s. **(D)** nCav inactivated at -40mV and quickly recovered at negative holding potentials. n = 7 for nCa_V, n = 6 for mCa_V. **(E)** Voltage-gated currents recorded from nCa_V or mCa_V following a -110mV pre-pulse, -50mV pre-pulse (colored), and 20mV pre-pulse. $Ca_V\beta$ subunits were substituted as indicated (mammalian β in red and *Nematostella* β in blue). Scale bars = 100pA, 25ms. **(F)** Mammalian β shifts nCa_V voltage-dependent inactivation to positive voltages. nCa_V $V_{i1/2}$ = -73.2 ± 1.2mV, n = 6. nCaV + mβ = -16.9 ± 1.9mV, n = 6. **(G)** Half maximal inactivation voltage ($V_{i1/2}$) for Ca_V chimeras. $p < 0.0001$ for nCaV versus nCa_V + mβ, mCa_V versus mCa_V + nβ, one-way ANOVA with post-hoc Tukey test. Inactivation was measured in response to pre-pulses from -100mV to 10mV with an inter-sweep holding potential of -110mV to reduce slow inactivation. Data represented as mean ± sem.

Heterologous expression of *Nematostella* Ca_V (nCa_V: *cacna1a*, *cacnb2*, and *cacna2d1*) produced voltage-gated currents with an apparent activation threshold nearly identical to the Ca_V complex made from respective mammalian orthologues (mCa_V, **Fig. 7B, Fig. 8C, D**). Both channels had similar activation kinetics, but fast inactivation was significantly pronounced in nCa_V, resembling native I_{CaV} (**Fig. 7E, Fig. 8E**). Importantly, nCa_V voltage-dependent inactivation was greatly enhanced compared with mCa_V, regardless of the charge carrier (**Fig. 7B, Fig. 8F, G**). Similar to I_{CaV}, nCa_V exhibited unusually-sensitive voltage-dependence and began to inactivate at voltages more negative than we could measure with an estimated midpoint inactivation voltage ($V_{i1/2}$) ~80mV more negative than mCa_V (**Fig. 7B**). Even with a holding potential of -70mV, nCa_V exhibited slow inactivation resulting in a drastic decrease in responses to depolarizing stimuli over time (**Fig. 7C**). This slow inactivation was largely prevented by adjusting the holding potential to -110mV, suggesting inactivation occurs when channels are in a closed-state at potentials near or more negative than typical resting membrane potential (**Fig. 8H**). Importantly, nCa_V rapidly recovered from inactivation, demonstrating that channels could be reset for subsequent activation following brief exposure to negative voltage (**Fig. 7D**). These distinctive features closely match the unique properties of native I_{CaV}, suggesting nCa_V forms the predominant Ca_V channel in nematocytes.

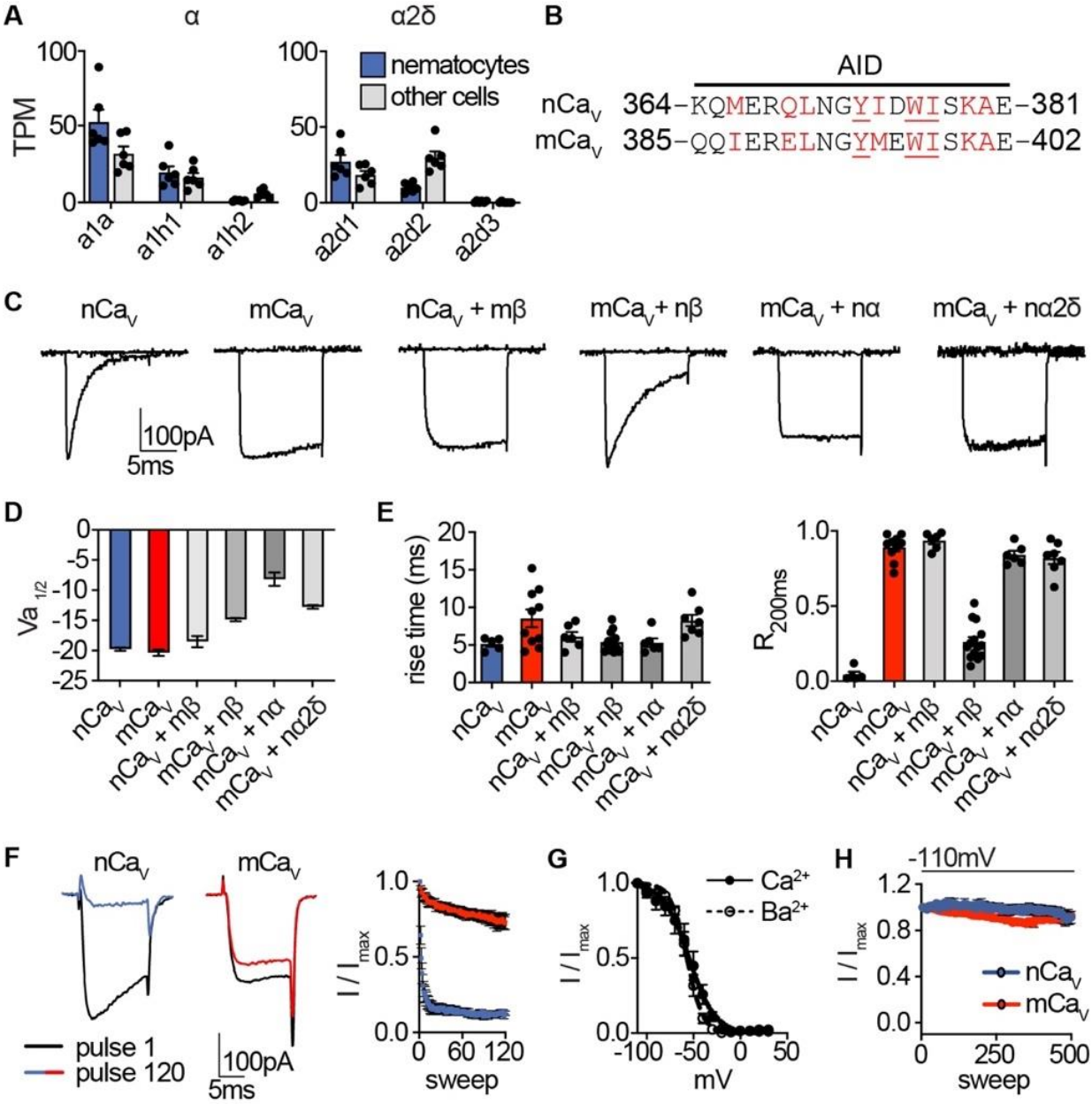

Figure 8: ***Nematostella*** **Cav properties. (A)** mRNA expression (transcripts per million, TPM) of voltage-gated calcium (Cav) channel α and α2δ subunits in nematocyte-enriched cells (blue) versus non-enriched cells (grey). n = 6, $p < 0.01$ for cacna1a in nematocytes versus other cells, two-way ANOVA with post-hoc Bonferroni test. Expression of other subunits was not significantly different. **(B)** Sequence alignment of *Nematostella* and *Mus musculus* α subunits at the α

interaction domain (AID). Red letters indicate important regions for beta subunit interaction, underlined letters are critical for interaction. **(C)** Representative voltage-activated currents from HEK-293 cells expressing wild-type or chimeric Ca_V channels with specific combinations of mammalian and *Nematostella* subunits. Currents were elicited by 0mV pulses from -110mV. **(D)** Half maximal activation voltage ($V_{a1/2}$) was similar for Ca_V chimeras. n = 6 nCa_V, 6 nCa_V + mβ, 10 mCa_V, 10 mCa_V + nβ, 6 mCa_V + nα, 6 mCa_V + nα2δ. **(E)** *Left*: Rise time of voltage-activated inward current. *Right*: Relative fraction of inward current remaining after a 200ms step to 0mV (R200). n = 6 nCa_V, 6 nCa_V + mβ, 10 mCa_V, 14 mCa_V + nβ, 6 mCa_V + nα, 7 mCa_V + nα2δ. **(F)** nCa_V inactivated more quickly than mCa_V. Protocol: 3.33 Hz stimulation with 20ms pulses to -10mV from -90mV. n = 5 nCa_V, 6 mCa_V, multiple row two-tailed student's t-test with significance of $p < 0.05$ by sweep 2 and $p < 0.0001$ by 120. **(G)** Inactivation curves of mCa_V + nβ were similar when external Ca^{2+} ($V_{i1/2}$ = -54.4 ± 1.8mV, n = 10) was replaced with Ba^{2+} ($V_{i1/2}$ = -57.0 ± 0.9mV, n = 6). **(H)** nCa_V exhibited relatively little slow inactivation from -110mV compared with -70mV holding potential (Fig. 2, 0.2 Hz stimulation, 5s inter-pulse interval). Data represented as mean ± sem.

To determine the molecular basis for nCa_V inactivation, we analyzed chimeric Ca_V complexes containing specific α, β, and α2δ1 subunits from nCa_V or mCa_V orthologues. Using a holding potential of -110mV to compare voltage-dependent inactivation, we found that only transfer of the β subunit significantly affected voltage-dependent inactivation, while α or α2δ1 subunits produced minimal effects on voltage-dependent activation, inactivation, or kinetics (**Fig. 7E, Fig. 8C-E**). Indeed, other β subunits can induce significant hyperpolarized shifts in inactivation of HVA Ca_V channels (Yasuda et al., 2004). In this case, the $mCa_V\beta$ subunit drastically shifted nCa_V inactivation by ~56mV in the positive direction, prevented complete inactivation, and produced slower fast inactivation (**Fig. 7E-G, Fig. 8E**). Furthermore, $nCa_V\beta$ was sufficient to confer greatly enhanced voltage-dependent inactivation to mCa_V (**Fig. 7E, G**). From these results, we conclude that $nCa_V\beta$, the most enriched Ca_V subunit in nematocytes, confers nCa_V's uniquely-sensitive voltage-dependent inactivation.

Nematocyte excitability

Because electrical stimulation has been implicated in nematocyte discharge and some nematocytes can produce action potentials (Anderson & Bouchard, 2009; Anderson & McKay, 1987; McKay & Anderson, 1988b), we used current-clamp to record the electrical responses of nematocytes to depolarizing stimuli. Under our conditions, nematocytes had a resting potential of -64.8 ± 8.9mV and did not produce a voltage spike when injected with current from rest (**Fig. 9A**). We further considered that the strong voltage-dependent inactivation of I_{CaV} could prevent excitability. Consistent with this idea, when nematocytes were first hyperpolarized to -90mV and subsequently stimulated by current injection, we observed a singular long voltage spike (**Fig. 9B, C**). In contrast, tentacle neurons produced multiple narrow spikes when injected with equivalent current amplitudes from a similar resting voltage, consistent with other neural systems (**Fig. 9A-C**).

Differences in spike width and frequency appear suited to mediate distinctive cellular functions: dynamic information processing in neurons and a single robust discharge event in nematocytes. Furthermore, these results indicate strong voltage-dependent inactivation prevents nematocyte activation from rest.

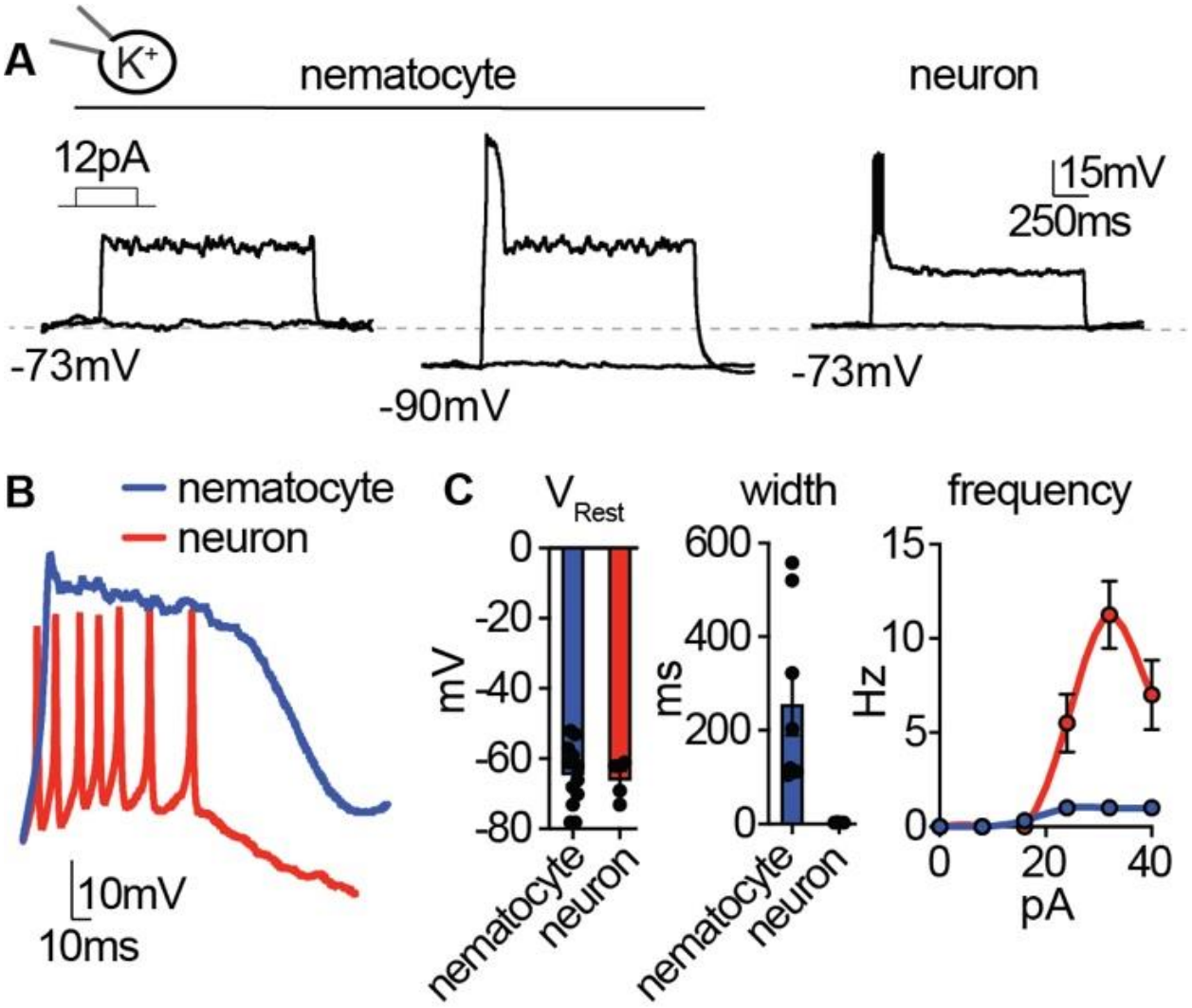

Figure 9: Nematocyte excitability requires hyperpolarized voltages. (A) Depolarizing current injection only elicited spikes from nematocytes first hyperpolarized to relieve inactivation. Nematocyte spike amplitude: 0mV at rest, 41.5 ± 2.2mV from ~-90mV, n = 8, $p < 0.0001$ two-tailed paired student's t-test. In contrast, tentacle neurons spiked from rest (31.5 ± 1.7mV, n = 4). **(B)** Current injection elicited long singular spikes from nematocytes and numerous narrow spikes from neurons. **(C)** Nematocytes and neurons had similar resting membrane potentials but distinct spike width. n = 8 nematocytes, 4 neurons, $p < 0.01$, two-tailed student's t-test. Nematocytes produced only one spike, regardless of injection amplitude (n = 8), whereas neurons produced

varying spike frequency depending on injection amplitude (n = 4). $p < 0.0001$ two-way ANOVA with post-hoc Bonferroni test. Data represented as mean ± sem.

K^+ channels contribute to resting membrane voltage (estimated reversal potential for nematocyte K^+ is ~-100mV) and often modulate repolarization following voltage spikes. Thus, we compared K^+ currents in nematocytes and tentacle neurons to understand how spike width might be differentially regulated. Nematocytes exhibited transient outward K^+ currents that quickly inactivated, while neurons had large sustained K^+ currents, perhaps important for repolarization and repetitive spiking (**Fig. 10A-C**). The transient component of the nematocyte K^+ current was highly sensitive to voltage-dependent inactivation, similar to I_{CaV} (**Fig. 10D**). This K^+ current was abolished by the rapid intracellular Ca^{2+} chelator BAPTA or by removing external Ca^{2+}, similar to the effect of the K^+ channel blocker TEA^+ (**Fig. 101E**). Consistent with this observation, nematocyte-enriched cells expressed numerous Ca^{2+}-activated K^+ channels (**Fig. 10F**). Furthermore, using intracellular Cs^+ to block K^+ currents resulted in prolonged voltage spikes and greatly increased resting membrane voltage, substantiating a role for K^+ channels in modulating membrane voltage (**Fig. 10G**). We propose that these distinct K^+ channel properties could contribute to the singular wide spikes of nematocytes versus the numerous narrow spikes of neurons.

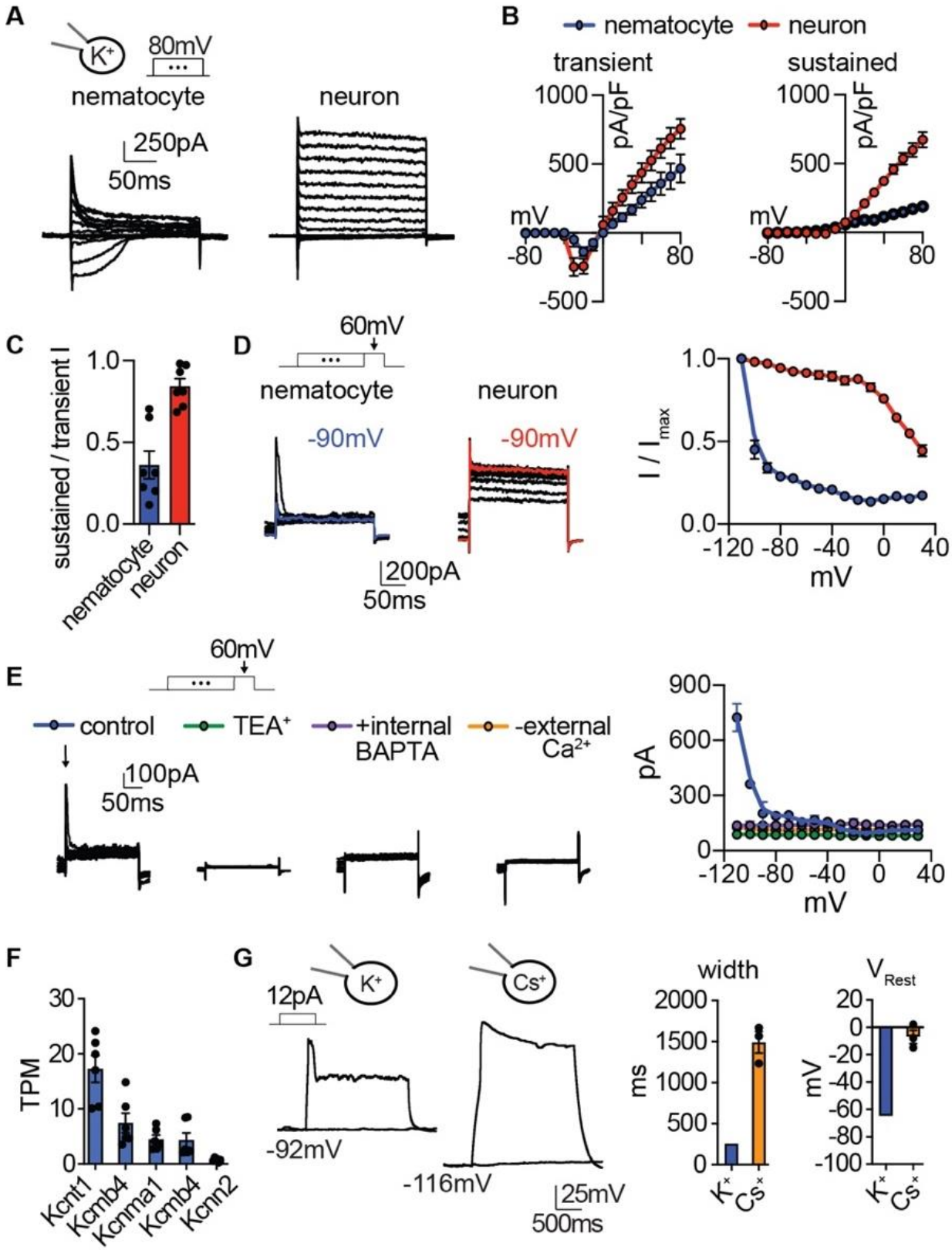
A
K+
80mV
nematocyte
neuron
250pA
50ms
B
nematocyte
neuron
transient
sustained
1000
500
pA/pF
mV
-80
80
-500
C
sustained / transient I
1.0
0.5
0.0
nematocyte
neuron
D
60mV
nematocyte
neuron
-90mV
-90mV
200pA
50ms
I / I max
-120 -80 -40 0 40
mV
E
60mV
control
TEA+
+internal BAPTA
-external Ca2+
100pA
50ms
900
600
300
0
pA
F
TPM
30
20
10
0
Kcnt1
Kcnb4
Kcnma1
Kcnb4
Kcnn2
G
K+
Cs+
12pA
-92mV
-116mV
25mV
500ms
width
2000
1500
1000
500
0
ms
K+
Cs+
V Rest
20
0
-20
-40
-60
-80
-100
mV

Figure 10: Nematocyte K^+ current properties. (A) In the presence of intracellular K^+, voltage-activated outward currents were elicited from nematocytes and tentacle neurons. **(B)** Current-voltage relationships of peak transient and sustained (end of 200ms voltage pulse) currents in nematocytes and neurons. n = 7. **(C)** Nematocytes exhibited a lower ratio of sustained / transient outward current, indicating faster inactivation of outward current. n = 7, $p < 0.01$ two-tailed student's t-test. **(D)** Nematocyte transient outward currents exhibited strong voltage-dependent inactivation compared with weak voltage-dependent inactivation of outward currents in neurons. n = 5, $p < 0.0001$ for voltages at -100mV or above, two-way ANOVA with post-hoc Bonferroni test. **(E)** Transient K^+ currents in nematocytes were assessed using voltage protocols to enhance the outward current sensitive to voltage-dependent inactivation. These currents were abolished by the K^+ channel blocker TEA^+ (n = 4), the intracellular Ca^{2+} chelator BAPTA (n = 4), or in the absence of external Ca^{2+} (replaced with $NMDG^+$ + EGTA, n = 3). $p < 0.0001$ for currents measured following pre-pulses to -110 or -100mV, two-way ANOVA with post-hoc Bonferroni test. Smaller sustained outward currents measured following more positive pre-pulses were significantly affected by TEA^+ but not other treatments. **(F)** mRNA expression (transcripts per million, TPM) of Ca^{2+}-activated K^+ channels in nematocyte-enriched cells. n=6. **(G)** Nematocyte spike width and resting membrane potential were affected by the presence of intracellular Cs^+. Cells were first hyperpolarized to elicit spikes with subsequent current injection. Spike width: n = 8 K^+ (from Fig. 3) and 3 Cs^+, $p < 0.05$ two-tailed student's t-test. Resting membrane voltage: n = 12 K^+ (from Fig. 3) and 3 Cs^+, $p < 0.01$ two-tailed student's t-test. Data represented as mean ± sem.

Nematocyte sensory transduction

If nematocytes are basally inhibited due to the unique voltage-dependent inactivation of I_{CaV}, how do they respond to sensory signals to elicit discharge? Nematocyte discharge requires simultaneous detection of chemo- and mechanosensory cues (Pantin, 1942b; Watson & Hessinger, 1992), even though mechanical stimulation of the nematocyte's cilium (cnidocil) within intact tentacles can by itself induce cellular depolarization(Anderson & Bouchard, 2009; Brinkmann et al., 1996). Indeed, we found the deflection of isolated nematocyte cnidocils elicited a mechanically-gated inward current with rapid activation and inactivation kinetics. This current was abolished by gadolinium (Gd^{3+}), which blocks mechanoreceptor and other cation channels, and was not observed in neurons (**Fig. 11A-C**). Furthermore, nematocyte-enriched cells differentially expressed transcripts encoding NompC (no mechanoreceptor potential C, **Fig. 12A**), a widely conserved mechanoreceptor previously found to localize to the cnidocil of nematocytes from *Hydra* (Schüler et al., 2015). Heterologous expression of *Nematostella* NompC (nNompC) resulted in a mechanically-gated current with similar properties to native nematocytes, including rapid kinetics and Gd^{3+} sensitivity (**Fig. 11A-C**). Comparison with the *Drosophila* orthologue (dNompC) demonstrated nNompC had similar rapid kinetics, Gd^{3+} sensitivity, pressure-response relationships, and nonselective cation conductance, all consistent with the conservation of protein regions important for mechanosensitivity and ion selectivity (Jin et al., 2017) (**Fig. 11A-C, Fig. 12B-D**). Thus, we conclude nematocytes are intrinsically mechanosensitive and suggest nNompC contributes to nematocyte mechanosensitivity. Importantly, this mechanically-evoked current is of sufficient amplitude to evoke a spike from very negative membrane voltages, but not from resting voltage at which I_{CaV} is inactivated.

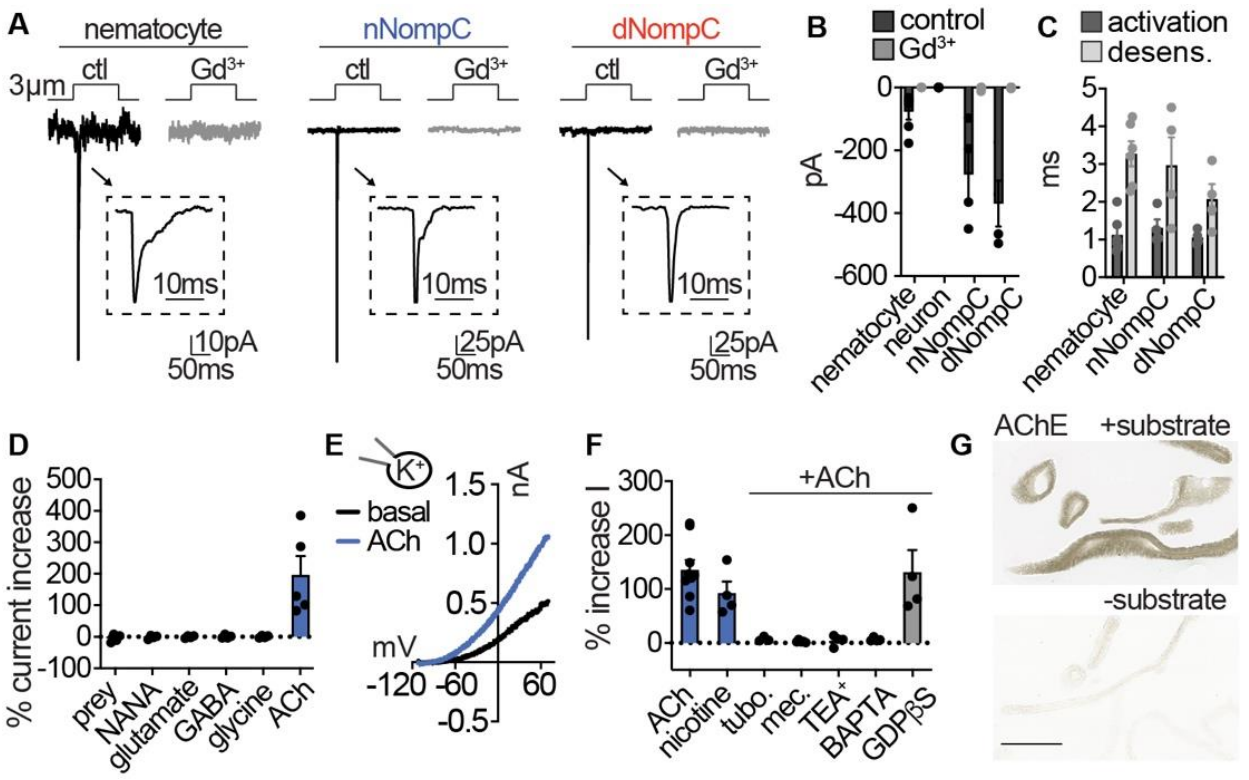

Figure 11: Nematocytes are intrinsically mechanosensitive and indirectly chemosensitive. (A) Mechanical stimulation of nematocytes evoked Gd^{3+}-sensitive, transient inward currents with similar properties to heterologously-expressed *Nematostella* (n) and *Drosophila* (d) NompC channels. Stimulation thresholds (pipette displacement): nematocyte = 1.7 ± 0.3µm (n = 6), nNompC = 4.2 ± 0.6µm (n = 4), dNompC = 4.2 ± 0.5µm (n = 4). Untransfected cells did not respond to similar stimuli (n = 6). **(B)** Mechanically-evoked currents from nematocytes (n = 6), nNompC (n = 4), and dNompC (n = 4) were blocked by Gd^{3+}, while tentacle neurons lacked mechanically-evoked currents (n = 8). $p < 0.01$ two-tailed student's t-test. **(C)** Mechanically-evoked current activation and desensitization kinetics were similar in nematocytes (n = 6), nNompC (n = 4), and dNompC (n = 4). **(D)** Chemosensory stimuli did not directly affect nematocytes but the neurotransmitter acetylcholine (ACh, n = 5) elicited a large outward current. n = 4 for prey extract, NANA, Glutamate, GABA, Glycine, $p < 0.001$ for ACh versus other

conditions, one-way ANOVA with post-hoc Tukey test. **(E)** Representative current-voltage relationship of ACh-elicited response in nematocytes. **(F)** ACh-evoked currents (n = 9) were blocked by nicotinic ACh receptor antagonists (tubocurarine = 4, mecamylamine = 4) and a similar current was elicited by nicotine (n = 4). ACh-evoked outward currents were inhibited by a K^+ channel blocker (TEA^+, n = 4) and an intracellular Ca^{2+} chelator (BAPTA, n = 4), but not the G-protein signaling blocker GDPβS (n = 4). $p < 0.001$ for vehicle versus antagonists, one-way ANOVA with post-hoc Tukey test. **(G)** Acetylcholinesterase staining in tentacles with and without substrate solution (representative of n = 3 animals). Scale bar = 200μm. Data represented as mean ± sem.

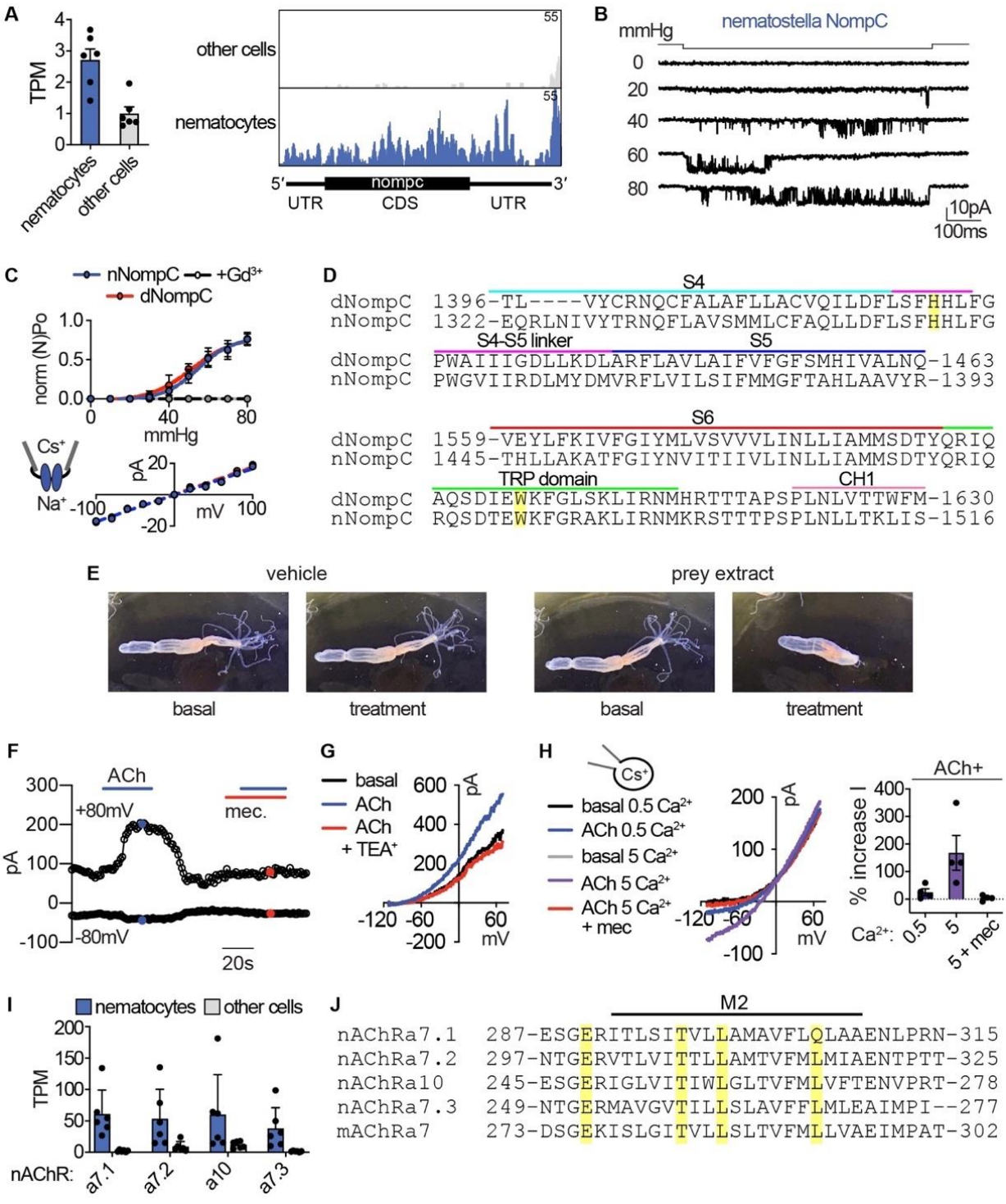
A
TPM
nematocytes
other cells
other cells
nematocytes
nompc
5′
3′
UTR
CDS
UTR
B
nematostella NompC
mmHg
10pA
100ms
C
nNompC
+Gd3+
dNompC
norm (N)Po
mmHg
Cs+
Na+
pA
mV
D
S4
dNompC 1396-TL----VYCRNQCFALAFLLACVQILDFLSFHHLFG
nNompC 1322-EQRLNIVYTRNQFLAVSMMLCFAQLLDFLSFHHLFG
S4-S5 linker
S5
dNompC PWAIIIGDLLKDLARFLAVLAIFVFGFSMHIVALNQ-1463
nNompC PWGVIIRDLMYDMVRFLVILSIFMMGFTAHLAAVYR-1393
S6
dNompC 1559-VEYLFKIVFGIYMLVSVVVLINLLIAMMSDTYQRIQ
nNompC 1445-THLLAKATFGIYNVITIIVLINLLIAMMSDTYQRIQ
TRP domain
CH1
dNompC AQSDIEWKFGLSKLIRNMHRTTTAPSPLNLVTTWFM-1630
nNompC RQSDTEWKFGRAKLIRNMKRSTTTPSPLNLLTKLIS-1516
E
vehicle
prey extract
basal
treatment
basal
treatment
F
ACh
+80mV
mec.
pA
-80mV
20s
G
basal
ACh
ACh
+ TEA+
pA
mV
H
Cs+
basal 0.5 Ca2+
ACh 0.5 Ca2+
basal 5 Ca2+
ACh 5 Ca2+
+ mec
pA
mV
ACh+
% increase I
Ca2+:
0.5
5
5+mec
I
nematocytes
other cells
TPM
nAChR:
α7.1
α7.2
α10
α7.3
J
M2
nAChRa7.1 287-ESGERITLSITVLLAMAVFLQLAAENLPRN-315
nAChRa7.2 297-NTGERVTLVITTLLAMTVFMLMIAENTPTT-325
nAChRa10 245-ESGERIGLVITIWLGLTVFMLVFTENVPRT-278
nAChRa7.3 249-NTGERMAVGVTILLSLAVFFLMLEAIMPI--277
mAChRa7 273-DSGEKISLGITVLLSLTVFMLLVAEIMPAT-302

Figure 12: Sensory transduction properties. (A) *Left*: mRNA expression (transcripts per million, TPM) of NompC (no mechanoreceptor potential) ion channels in nematocyte-enriched cells (blue) vs. non-enriched cells (grey). n = 6, $p < 0.05$, two-tailed student's t-test. *Right*: Numerous reads mapped across the entire NompC sequence. The transcript architecture is shown below the mapping. CDS, coding sequence; UTR, untranslated regions. The maximum read counts was set as the same value between samples. **(B)** A representative single *Nematostella* NompC (nNompC) channel expressed in an excised membrane patch was sensitive to increasing pressure applied via the patch pipette. Vm = -80mV. **(C)** nNompC and *Drosophila* NompC (dNompC) exhibited similar pressure-open probability (NP_O) relationships and slope conductance. nNompC was blocked by Gd^{3+}. 95% confidence interval for pressure required to induce half maximal P_O: nNompC = 51.9 – 59.4 mmHg, dNompC = 47.4 – 59.7 mmHg. n = 5. Slope conductance: nNompC = 168 ± 4 pS, dNompC = 175 ± 4 pS. n = 4. Patches from untransfected cells did not respond to similar stimuli (n = 6). **(D)** Alignment of *Drosophila* (dNompC) and *Nematostella* (nNompC) protein sequences revealed high conservation with overall sequence identity of 44.3% (62.7% similarity). Yellow indicates residues important for mechanosensitivity. **(E)** Application of filtered prey extract, but not vehicle, elicited a feeding response (contraction of tentacles) in a representative *Nematostella*. **(F)** Representative nematocyte response to acetylcholine (ACh) shows an outwardly-rectifying current, which was blocked by mecamylamine (Mec). K^+ was the major intracellular cation. **(G)** Representative current-voltage relationship shows that the ACh-evoked current was inhibited by the K^+ channel blocker TEA^+. **(H)** In the presence of intracellular Cs^+ to block K^+ currents, ACh mediated a mecamylamine-sensitive, inward current that was enhanced by extracellular Ca^{2+}. **(I)** mRNA expression (transcripts per million, TPM) of nicotinic acetylcholine-like receptors (nAChRs) in nematocyte-enriched cells (blue) vs. non-enriched cells

(grey). n = 6, $p < 0.05$ for nACHRa7.1, two-way ANOVA with post-hoc Bonferroni test. **(J)** Alignment of *Nematostella* nAChRs and mouse nAChRa7 protein sequences revealed conserved residues that facilitate Ca^{2+} permeability. Data represented as mean ± sem.

Because nematocyte discharge is mediated by combined chemical and mechanical cues (Pantin, 1942b; Watson & Hessinger, 1992), we wondered if chemosensory signals could modulate nematocyte membrane voltage to allow for I_{CaV} activation and cellular responses. While prey-derived chemicals (<3kDa extract from brine shrimp) evoked robust behavioral responses, similar treatments did not elicit electrical responses from isolated nematocytes (**Fig. 11D, Fig. 12E**). Considering *in vivo* cellular and discharge activity requires the presence of prey-derived chemicals with simultaneous mechanical stimulation, chemoreception may occur indirectly through functionally-coupled cells (Price & Anderson, 2006). Previous studies suggest the presence of synaptic connections between nematocytes and other unknown cell types(Oliver, Brinkmann, Sieger, & Thurm, 2008; Westfall, Landers, & McCallum, 1998). To test this possibility, we screened isolated nematocytes for responses to well-conserved neurotransmitters and found only acetylcholine (ACh) elicited a significant response (**Fig. 11D, E**). ACh-evoked outward currents were abolished by nicotinic acetylcholine receptor (nAChR) antagonists and recapitulated by nicotine (**Fig. 11F, Fig. 12F**). The K^+ channel blocker TEA^+ and the intracellular Ca^{2+} chelator BAPTA inhibited responses, suggesting ACh elicits K^+ channel activity downstream of increased intracellular Ca^{2+}. While the G-protein signaling inhibitor GDPβS did not affect outward currents, blockade of K^+ currents with intracellular Cs^+ revealed an ACh-elicited inward current that was enhanced by increased extracellular Ca^{2+} and blocked by the nAChR antagonist mecamylamine (**Fig. 11F, Fig. 12G, H**). These results suggest ACh evokes a Ca^{2+}-permeable nAChR-like signaling pathway to engage Ca^{2+}-activated K^+ channels, consistent with the absence of muscarinic ACh receptors in *Nematostella* (Faltine-Gonzalez & Layden, 2019). In agreement with this observation, nematocyte-enriched cells expressed numerous nAChR-like transcripts which had well-conserved domains involved in Ca^{2+} permeability (Fucile, 2004) (**Fig. 12I, J**). Finally, we

found robust acetylcholinesterase activity in tentacles, further suggesting a role for ACh signaling in nematocyte function (**Fig. 11G**). These results demonstrate that nematocytes use cholinergic signaling to regulate K^+ currents, similar to how efferent cholinergic innervation of vertebrate hair cells modulates nAChR-K^+ channel signaling to inhibit auditory responses (Elgoyhen & Katz, 2012).

To identify the origin of cellular connections to nematocytes, we used serial electron microscopy reconstruction to visualize nematocytes and neighboring cells. We analyzed similar tentacle tissues from which we carried out physiological experiments and readily observed neurons and nematocytes in close proximity (**Fig. 14A, B**). In resulting micrographs, nematocytes were clearly identified by their distinct nematocyst and cnidocil (**Fig. 14C**). Interestingly, each nematocyte exhibited a long process, of presently unknown function, that extended into the ectoderm (**Fig. 14D**). We also observed numerous spirocytes, indicated by the presence of a large intracellular thread-like structure (**Fig. 13A, Fig. 14C**). Putative sensory neurons were identified based on their synaptic contacts and extracellular projections (**Fig. 13A, Fig. 14E, F**). Importantly, dense core vesicles were localized to electron-dense regions at the junction between each nematocyte and one other cell type, either sensory neurons or spirocytes (**Fig. 13A, Fig. 15A-E**). Thus, nematocytes receive synaptic input from both neurons and spirocytes and likely serve as a site for integrating multiple signals (**Fig. 15F, G**). This observation is consistent with the ability of cnidarians to simultaneously discharge multiple cnidocyte types to most efficiently capture prey (Pantin, 1942a).

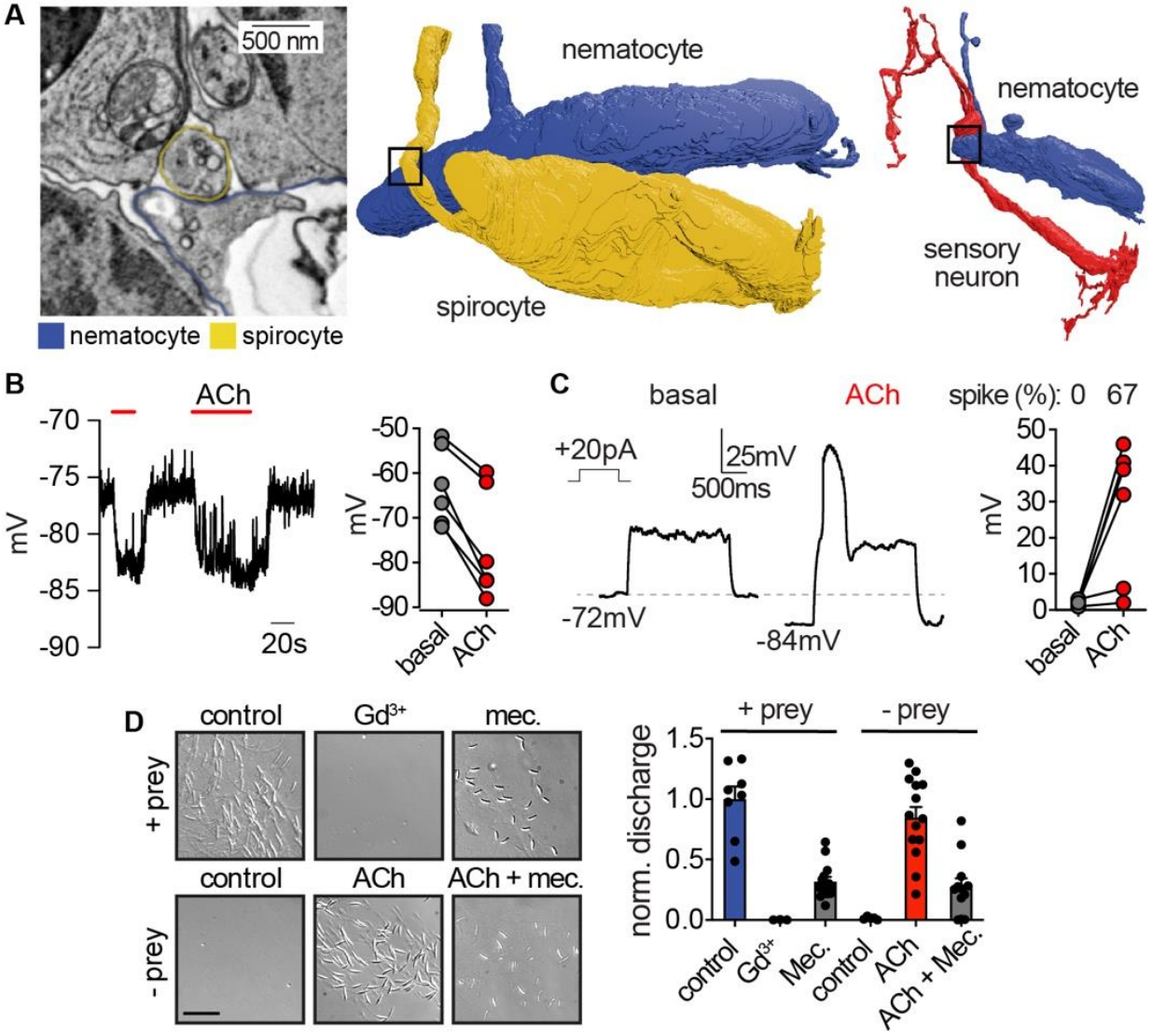

Figure 13: Nematocyte voltage-dependence facilitates signal integration required for stinging. (A) *Left*: Electron micrograph demonstrating dense-core vesicles in the vicinity of an electron-dense zone localized at the junction between a spirocyte and nematocyte. *Middle*: 3D reconstruction of the nematocyte and spirocyte shown in the left panel. The box indicates the position of the synapse. *Right*: 3D reconstruction of a different nematocyte making a synapse with a putative sensory neuron. The box indicates the position of the synapse shown in Fig. 5 - supplement 2C and E. **(B)** ACh induced hyperpolarization of nematocytes. n = 6, $p < 0.01$ paired two-tailed student's t-test. **(C)** Depolarizing current injection did not induce active properties from

rest, but did elicit a voltage spike from most nematocytes hyperpolarized by ACh. $n = 6$, $p < 0.01$ paired two-tailed student's t-test. **(D)** Chemo-tactile-induced nematocyte discharge (touch + prey extract, $n = 8$) was inhibited by the mechanoreceptor current blocker Gd^{3+} ($n = 7$) and nAChR antagonist mecamylamine ($n = 14$). In the absence of chemical stimulation (touch - prey extract, $n = 5$), touch + ACh ($n = 14$) was sufficient to induce discharge, which was inhibited by mecamylamine ($n = 12$). $p < 0.0001$ for controls versus respective treatments, one-way ANOVA with post-hoc Bonferroni test. Data represented as mean ± sem.

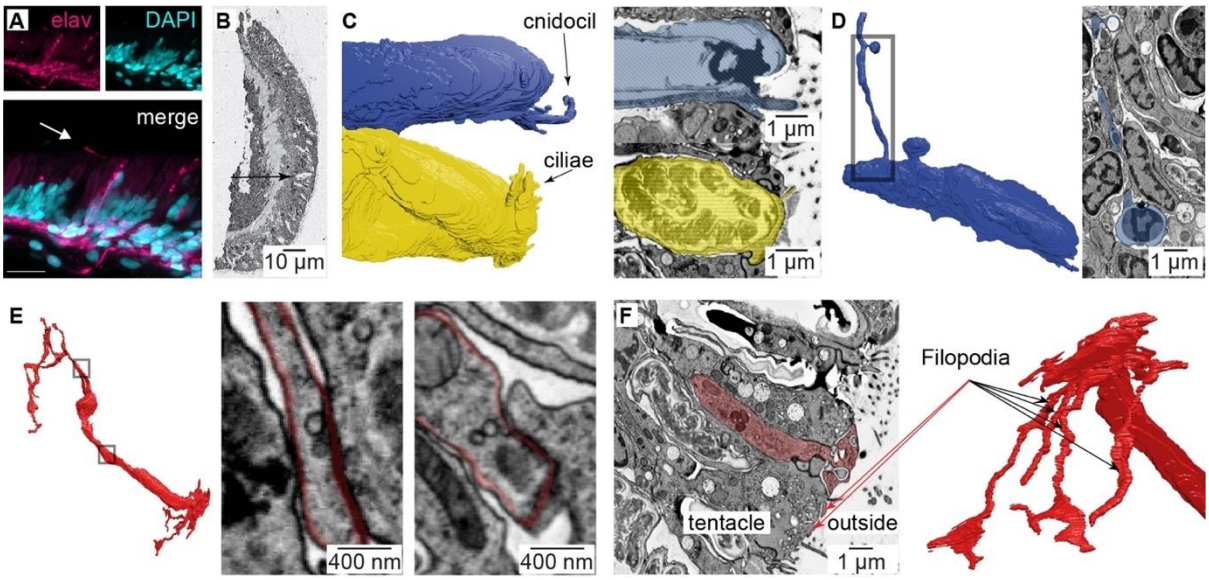

Figure 14: Nematocyte morphology. (A) Tentacle from elav::mOrange *Nematostella* stained with dsRed (red) indicated neural processes beneath ectodermal nematocytes and putative sensory neurons located within the ectoderm. DAPI (blue) stains nuclei and nematocysts. White arrow indicates putative sensory projection. Scale bar = 10µm. **(B)** Electron micrograph of *Nematostella* tentacle section (50nm thickness). Arrow indicates regions containing nematocytes, spirocytes and sensory neurons which were imaged at higher magnification as illustrated in Fig. 5 and Fig. 5 - supplement 2. **(C)** Cnidocil of a nematocyte (blue) and ciliae of a spirocyte (orange). *Left*: 3D reconstruction. *Right*: Electron micrograph of one section of the nematocyte (*top*) and one section of the spirocyte (*bottom*). **(D)** Nematocyte process. *Left*: 3D reconstruction of the nematocyte. *Right*: Electron micrograph of one section across the nematocyte process, indicated by the region boxed on the left panel. **(E)** Synapses made between the neuron and other cells than a nematocyte. Two examples are shown (middle and right panels). **(F)** Sensory terminal of the neuron shown in Fig. 5A with multiple filopodia extending in the outside environment. *Left*: Electron micrograph of one section of the sensory neuron. *Right*: 3D reconstruction of the sensory neuron.

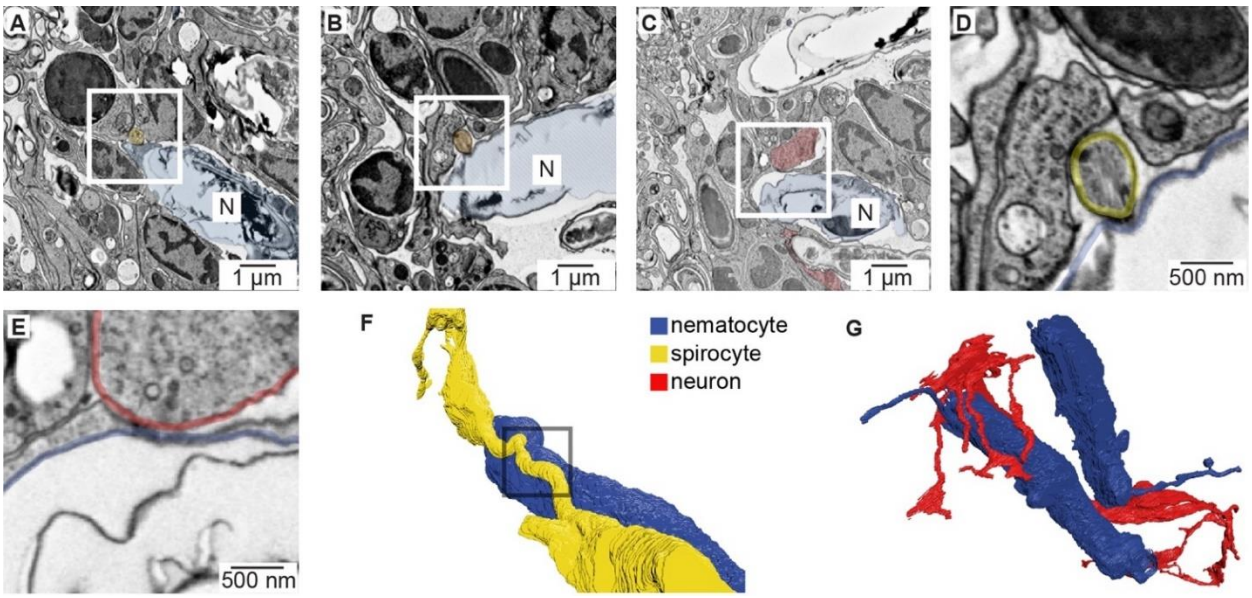

Figure 15: Nematocyte synaptic connections. (A) Putative synapse between a nematocyte (N, blue) and a spirocyte (yellow). Higher magnification is shown in Fig. 5A. **(B)** Putative synapse between a nematocyte (N, blue) and a spirocyte (orange). **(C)** Putative synapse between a nematocyte (N, blue) and a sensory neuron (red). **(D)** Higher magnification of the regions boxed in B. **(E)** Higher magnification of the regions boxed in C. **(F)** Reconstruction of the synapse between a nematocyte (N, blue) and a spirocyte (S, yellow). Box indicates site of synaptic contact shown in panel A and Fig. 5A. **(G)** 3D reconstruction of the sensory neuron and the two nematocytes shown in Fig. 5A (blue).

Voltage-dependence mediates signal integration

How do distinct mechanosensory and chemosensory signals converge to elicit discharge? In agreement with our observation that nAChR activation increases K^+ channel activity, ACh hyperpolarized nematocytes to negative voltages from which they were capable of producing robust voltage spikes (**Fig. 13B, C**). A select number of cells with a more positive resting voltage still failed to produce spikes, and therefore additional regulation could exist through the modulation of resting membrane voltage (**Fig. 16A, B**). These results suggest that the voltage-dependence for I_{CaV} prevents basal activation to depolarizing signals, such as mechanical stimulation, but activation of nAChR hyperpolarizes the cell to relieve I_{CaV} inactivation, thereby amplifying depolarizing signals to mediate cellular responses.

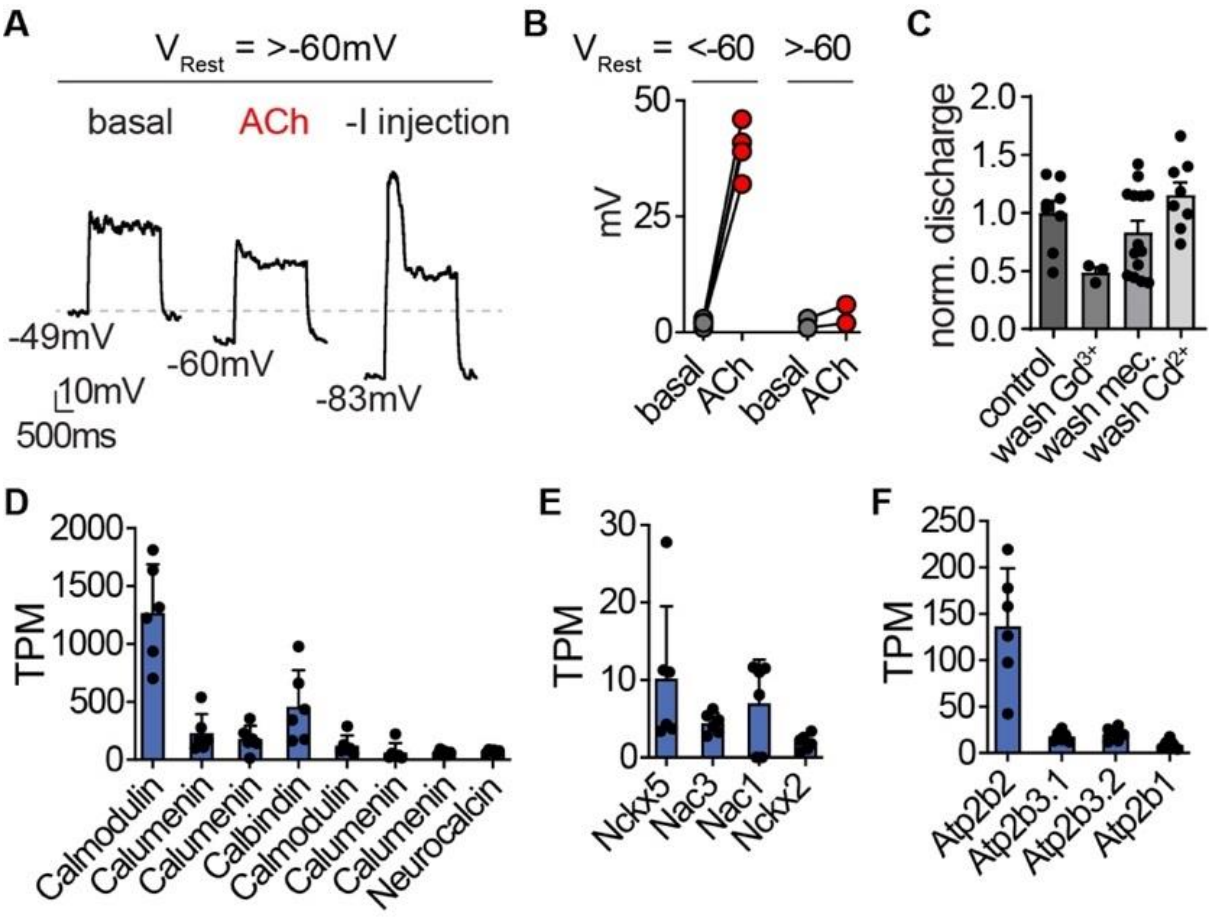

Figure 16: Nematocyte signaling pathways. (A) For nematocytes with a resting membrane voltage (V_{Rest}) more positive than -60mV, ACh was insufficient to hyperpolarize cells enough to mediate a spike following depolarizing current injection. Representative of n = 2. **(B)** For nematocytes with V_{Rest} more negative than -60mV, all ACh-hyperpolarized cells produced voltage spikes following depolarizing current injection. n = 4, $p < 0.001$ two-tailed student's t-test. **(C)** Controls (related to Figs. 1G and 5D) for nematocyte discharge. Control = 8, Gd^{3+} wash = 7, Mec wash = 14, Cd^{2+} wash = 8. **(D-F).** mRNA expression (transcripts per million, TPM) of calcium-binding proteins (**D**), calcium exchangers (**E**), and calcium ATPases (**F**) in nematocyte-enriched cells.

Consistent with a requirement for both mechano- and chemosensory input, we found the mechanoreceptor current blocker Gd^{3+} inhibited chemo-tactile stimulation of discharge. Additionally, the nAChR antagonist mecamylamine greatly reduced chemo-tactile-induced discharge (**Fig. 13D**). Washout of both treatments recovered the ability of nematocytes to discharge (**Fig. 16C**). Moreover, the requirement for prey-derived chemicals was completely recapitulated by ACh (**Fig. 13D**). These results are consistent with a role for ACh signaling downstream of chemosensory stimulation. Thus, we propose that the unique I_{CaV} voltage-dependent inactivation provides a mechanism by which nematocytes filter extraneous depolarizing mechanical signals, but can integrate chemosensory-induced hyperpolarization together with a depolarizing stimulus to elicit robust signal amplification and discharge responses (**Fig. 17**).

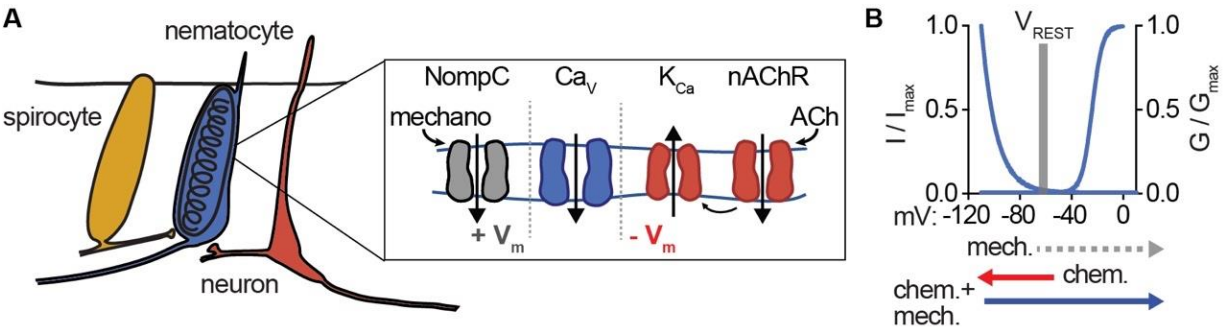

Figure 17: Nematocyte Ca_V properties filter salient chemo-tactile signals. (A) Model for nematocyte signal integration. **(B)** Nematocyte Ca_V is inactivated at rest and thus does not amplify extraneous NompC-mediated mechanical signals. Chemosensory stimuli hyperpolarize nematocytes through ACh signaling to relieve inactivation of Ca_V channels, which can then amplify mechanical stimuli to engage discharge.

Discussion

Here, we demonstrate that nematocytes use the specialized properties of nCa_V to filter salient chemo-tactile signals from environmental noise. The involvement of Ca^{2+} signaling in this process is consistent with a well-established role for Ca^{2+} influx in mediating discharge across multiple cnidarian species (McKay & Anderson, 1988a; Santoro & Salleo, 1991; Watson & Hessinger, 1994). However, the exact mechanism by which Ca^{2+} influx mediates discharge is unclear. It has been proposed that Ca^{2+} influx alters the permeability of the nematocyst capsule and/or initiates the rapid dissociation of ions within the cyst to induce osmotic changes within the organelle (R. Lubbock, Gupta, & Hall, 1981; Roger Lubbock & Amos, 1981; Tardent, 1995; Weber, 1990). Our transcriptomic analyses demonstrate that nematocytes express multiple Ca^{2+} handling proteins (**Fig. 16D-F**), which could control Ca^{2+} signaling domains in response to spatially-restricted sensory transduction cascades. This organization would be consistent with the necessity for I_{CaV}-mediated amplification of receptor-mediated nonselective cation conductances. Indeed, Ca_V currents could mediate an increase of >500μM Ca^{2+} considering a uniform distribution across the small cytoplasmic volume (5%) not occupied by the nematocyst. Future studies will provide insight into the coupling between sensory transduction and organellar physiology.

Our results suggest one mechanism by which nematocytes integrate combined mechanical and chemical cues to filter salient environmental information and appropriately engage nematocyte discharge. However, cnidarians occupy distinct ecological niches and may have evolved different biophysical features to account for increased turbulence, specific behaviors, or particular prey and predatory targets. Numerous sea anemones occupy turbulent tidal pools, whereas others, like *Nematostella vectensis*, live in calmer regions. Similarly, cnidarians can undergo developmental transitions between immobile and free-floating medusa phases while maintaining the use of

nematocytes for prey capture (Martin & Archer, 1997). Although forces generated from swimming prey are likely negligible in comparison with physical contact of the cnidocil, strong tidal waves may be sufficient to elicit mechanoreceptive responses which could interfere with pertinent chemo-tactile sensation and subsequent stinging responses. These ecological differences might require distinct filtering mechanisms for distinguishing salient prey or predator signals. For example, anatomical organization and pharmacological dependence for cellular and discharge activity in anthozoan nematocytes differs from hydrozoans (Anderson & McKay, 1987; Kass-Simon & Scappaticci, Jr., 2002; Oliver et al., 2008). Indeed, nematocysts vary extensively in morphology, differing in the length of the extruded thread, the presence of spines, and the composition of toxins (Kass-Simon & Scappaticci, Jr., 2002), likely reflecting the diversity of organismal needs.

The modularity provided by synaptic connections could increase the diversity of signals which regulate nematocyte discharge. For instance, distinct chemoreceptor cells could form synaptic connections with specific nematocyte populations to mediate discrete behavioral responses. In addition to chemical mixtures, such as prey extract, numerous amino acids, lipids, and N-acetylated sugars can individually modulate nematocyte discharge (Watson & Hessinger, 1992). While these are broadly-distributed molecules, it is possible distinct prey- or predator-derived compounds regulate specific chemosensory cells to engage predatory or defensive nematocytes, respectively (Brace, 1990). Indeed, we observed that both spirocytes and neurons make synaptic contacts with nematocytes, thus either could release ACh in response to specific stimuli. Future identification and characterization of chemosensory cells and the ecologically-relevant compounds which activate them will provide insight regarding chemical coding and mechanisms of synaptic signaling. Discharge can be also regulated by organismal nutritional state (Sandberg, Kanciruk, &

Mariscal, 1971), suggesting nematocytes could receive input from digestive cells or hormones. Additionally, various cnidocyte types are found across the cnidarian phylum and regulated by stimuli relevant to their behavioral purpose. For example, the freshwater cnidarian, *Hydra vulgaris*, uses a specific cnidocyte to grasp surfaces for phototaxis, suggesting that these cells could be regulated downstream of a photoreceptor (Plachetzki, Fong, & Oakley, 2012). Within anthozoans, nematocytes and spirocytes may use similar or distinct mechanisms to control discharge. Functional comparisons will reveal whether specific proteins, domains, or signaling mechanisms are conserved or give rise to the evolutionary novelties across these incredibly specialized cell types (Babonis & Martindale, 2014).

The ability to distinguish behaviorally-relevant stimuli, such as prey, from background noise is especially critical because nematocytes are single-use cells that must be replaced following discharge. Multiple species have taken advantage of these specialized conditions by adapting to evade and exploit nematocyte discharge for their own defensive purposes. For example, clownfish can live among the tentacles of sea anemones without harmful effects, although the exact mechanism by which this occurs is unclear (R. Lubbock, 1980). Certain species of nudibranchs and ctenophores acquire undischarged nematocysts from prey and store them for later defense, indicating that these organisms are able to initially prevent discharge responses (Greenwood, 2009). Understanding such regulation could reveal additional mechanisms by which cells process diverse stimuli and provide insight into the evolution of these interspecies relationships.

Materials and methods:

Animals and Cells

Starlet sea anemones (*Nematostella vectensis*) were provided by the Marine Biological Laboratory (Woods Hole, Massachusetts), Nv-Elav1::mOrange transgenic animals were a gift from F. Rentzsch. We used adult animals of both sexes, which were fed freshly-hatched brine shrimp (*Artemia*) twice a week and kept on a 12hr light/dark cycle in 1/3 natural sea water (NSW). Nematocytes and neurons were isolated from tentacle tissue, which was harvested by anesthetizing animals in high magnesium solution containing (mM): 140 NaCl, 3.3 Glucose, 3.3 KCl, 3.3 HEPES, 40 $MgCl_2$. Cells were isolated from tentacles immediately prior to electrophysiology experiments by treatment with 0.05% Trypsin at 32°C for 30 min and mechanical dissociation in divalent free recording solution (mM): 140 NaCl, 3.3 Glucose, 3.3 KCl, 3.3 HEPES, pH 7.6. Basitrichous isorhiza nematocytes were isolated from tentacles and identified by a thick-walled capsule containing a barbed thread, with a characteristic high refractive index, oblong shape and presence of a cnidocil. Spirocytes were identified by a thin-walled capsule containing a thin, unarmed thread, used for ensnaring prey. Neurons were identified by mOrange expression.

HEK293T cells (ATCC, Cat# CRL-3216, RRID:CVCL_0063, authenticated and validated as negative for mycoplasma by vendor) were grown in DMEM, 10% fetal calf serum, and 1% penicillin/streptomycin at 37°C, 5% CO2. Cells were transfected using lipofectamine 2000 (Invitrogen/Life Technologies) according to the manufacturer's protocol. 1µg of *Nematostella cacna1a, cacnb2.1, cacna2d1. M. musculus* (mouse) *cacna1a, R. norvegicus (*rat*) cacnb2a*, or rat *cacna2d1* was coexpressed with 0.5µg GFP. Mechanosensitive proteins were assayed using HEK293T cells transfected with 1µg of either *Drosophila* NompC or *Nematostella* NompC. To enhance channel expression, cells were transfected for 6-8h, plated on coverslips, and then

incubated at 28°C for 2-6 days before experiments. *Drosophila* NompC-GFP was a gift from YN Jan. Rat *cacna2d1* (RRID:Addgene_26575) and *cacna1a* (RRID:Addgene_26578) were gifts from D. Lipscombe and *cacnb2a* (RRID:Addgene_107424) was a gift from A. Dolphin.

Molecular biology

RNA was prepared from tentacles of adult *Nematostella* using published methods (Stefanik, Friedman, & Finnerty, 2013). Briefly, 50mg of tentacle tissue were homogenized and RNA was extracted using TRIzol. RNA was isolated and DNase treated (Zymo Research), then used for cDNA library synthesis (NEB E6560). Full-length sequence for a *Nematostella* calcium channel beta subunit was obtained with a RACE strategy using specific primers (GATTACGCCAAGCTTTATGCGTCCAATCGTACTTGTCGGC and GATTACGCCAAGCTTGCCGACAAGTACGATTGGACGCATA) on the amplified tentacle-tissue library. The final sequence was confirmed using primers corresponding to the end of the derived sequence (CAGAGCCAGGCCTGAGCGAG and GCCCCGTTAAAAGTCGAGAG) to amplify a full-length cDNA from tentacle mRNA, which was sequenced to confirm identity. *Cacna1a, cacna2d1, cacnb2,* and nNompC-GFP were synthesized by Genscript (Piscataway, NJ). Sequence alignments were carried out using Clustal Omega.

Transcriptomics

Tentacle tissue was ground to a fine powder in the presence of liquid nitrogen in lysis buffer (50mM Tris-HCl pH 7.5, 250mM KCl, 35mM $MgCl_2$, 25mM EGTA-KOH pH 8, 5mM DTT, murine RNase inhibitor (NEB), 1% (w/v) NP-40, 5% (w/v) sucrose, 100µg ml^{-1} cycloheximide (Sigma), 500µg ml^{-1} heparin (Sigma)). Lysate was incubated on ice for 5min, triturated 5 times with an 18 g needle, and insoluble material was removed by centrifugation at 16000g for 5 min at

4 °C. Polyadenylated RNA was used to make sequencing libraries and sequenced on an Illumina HiSeq 4000 (Novogene). Quality filtering and adapter trimming was performed using Cutadapt (martin 2011), and a *de novo* transcriptome was assembled using Trinity (Grabherr et al., 2011). Annotation was performed using InterProScan (Jones et al., 2014) with Panther member database analysis, HMMER(Eddy, 2009) with the Pfam (El-Gebali et al., 2019) database, and DIAMOND (Buchfink, Xie, & Huson, 2014) with the UniProt/TrEMBL database.

Reads from sorted cnidocytes (Bioproject PRJNA391807) (Sunagar et al., 2018), enriched for nematocytes, were quality and adapter trimmed as described above, and transcript abundance (TPM) was quantified using Kallisto (Bray, Pimentel, Melsted, & Pachter, 2016) and the tentacle transcriptome. For read mapping visualization, mapping was performed with Bowtie2 (Langmead & Salzberg, 2012), output files were converted to indexed bam files using Samtools (Li et al., 2009), and visualization was performed with the Integrated Genomics Viewer (Robinson et al., 2011).

Electrophysiology

Recordings were carried out at room temperature using a MultiClamp 700B amplifier (Axon Instruments) and digitized using a Digidata 1550B (Axon Instruments) interface and pClamp software (Axon Instruments). Whole-cell recording data were filtered at 1kHz and sampled at 10kHz. For single-channel recordings, data were filtered at 2kHz and sampled at 20kHz. Data were leak-subtracted online using a p/4 protocol, and membrane potentials were corrected for liquid junction potentials. For whole-cell nematocyte and neuron recordings, borosilicate glass pipettes were polished to 8-10MΩ. The standard *Nematostella* medium was used as the extracellular solution and contained (in mM): 140 NaCl, 3.3 glucose, 3.3 KCl, 3.3 HEPES, 0.5 $CaCl_2$, 0.5 $MgCl_2$, pH 7.6. Two intracellular solutions were used for recording. For isolating inward currents

(mM): 133.3 cesium methanesulfonate, 1.33 $MgCl_2$, 3.33 EGTA, 3.33 HEPES, 10 sucrose, 10 CsEGTA, pH 7.6. For outward currents (mM) 166.67 potassium gluconate, 3.33 HEPES, 10 sucrose, 1.33 $MgCl_2$, 10 KEGTA, pH 7.6. In some experiments, BAPTA was substituted for EGTA. For whole-cell recordings in HEK293 cells, pipettes were 3-4MΩ. The standard extracellular solution contained (in mM): 140 NaCl, 5 KCl, 10 HEPES, 2 $CaCl_2$, 1 $MgCl_2$, pH 7.4. The intracellular solution contained (mM): 140 cesium methanesulfonate, 1 $MgCl_2$, 3.33 EGTA, 3.33 HEPES, 10 sucrose, pH 7.2. In ion substitution experiments, equimolar Ba^{2+} was substituted for Ca^{2+}. Single-channel recording extracellular solution contained (mM): 140 NaCl, 10 HEPES, 1 NaEGTA, pH 7.4. The intracellular solution used (mM): 140 CsCl, 10 HEPES, 1 CsEGTA, pH 7.4.

The following pharmacological agents were used: N-Acetylneuraminic acid (NANA, 100µM, Sigma), glycine (100µM, Sigma), acetylcholine (1mM), mecamylamine (100µM, 500µM for behavioral experiments, Tocris), $GdCl_3$ (100µM, Sigma), glutamate (1mM), GABA (1mM), nicotine (100µM, Tocris), tubocurarine (10µM, Tocris), TEA^+ (10mM, Sigma), BAPTA (10mM, Tocris), GDPβS (1mM, Sigma), and Cd^{2+} (500µM, 250µM for behavioral experiments). All were dissolved in water. Prey extract was isolated from freshly-hatched *Artemia*. *Artemia* were flash-frozen, ground with mortar and pestle, filtered with 0.22µM pores or 3kDa ultracentrifugal filters (Amicon UFC500324). Pharmacological effects were quantified as differences in normalized peak current from the same cell following bath application of the drug ($I_{treatment}/I_{control}$). Whole-cell recordings were used to assess mechanical sensation together with a piezoelectric-driven (Physik Instrumente) fire-polished glass pipette (tip diameter 1µm). Mechanical steps in 0.5µm increment were applied every 5s while cells were voltage-clamped at -90mV. Single mechanosensitive channels were studied using excised outside-out patches exposed to pressure applied via a High-

Speed Pressure Clamp system (HSPC, ALA-scientific). Pressure-response relationships were established using pressure steps in 10mmHg increments. Voltage-dependence of currents was measured from -100mV to 100mV in 20mV increments while applying repetitive 60mmHg pressure pulses.

Unless stated otherwise, voltage-gated currents were measured in response to a 200ms voltage pulse in 10mV increments from a -110mV holding potential. G-V relationships were derived from I-V curves by calculating G: $G=I_{CaV}/(V_m-E_{rev})$ and fit with a Boltzman equation. Voltage-dependent inactivation was measured during -10mV (Ca^{2+} currents in native cells), 0mV (Ca^{2+} currents in heterologously expressed channels), 60mV (K^+ currents in native cells) voltage pulses following a series of 1s pre-pulses ranging from -110mV to 60mV. Voltage-dependent inactivation was quantified as I/I_{max}, with I_{max} occurring at the voltage pulse following a -110mV prepulse. In some instances, inactivation curves could not be fit with a Boltzman equation and were instead fitted with an exponential. The time course of voltage-dependent inactivation was measured by using a holding voltage of -110mV or -70mV and applying a 0mV test pulse every 5s. Recovery from inactivation was quantified by normalizing inactivated and recovered currents to those elicited from the same cell in which a 0mV voltage pulse was applied from -110mV. Test pulses from a holding voltage of -40mV were used to assess inactivation, followed by pulses from -110mV where currents quickly recovered to maximal amplitude. Repetitive stimulation using 20ms pulses to -10mV or 0mV from a holding voltage of -90mV was also used to measure inactivation in response to repetitive stimulation. Current inactivation kinetics were quantified by the portion of current remaining at the end of 200ms pulse (R200) or fit with a single exponential. Activation was quantified as the time from current activation until peak amplitude. 200ms voltage

ramps from -120 to 100mV were used to measure ACh-elicited currents. Stimulus-evoked currents were normalized to basal currents measured at the same voltage of 80mV.

Single channel currents were measured from the middle of the noise band between closed and open states or derived from all-points amplitude histograms fit with Gaussian relationships at closed and open peaks for each excised patch record. Conductance was calculated from the linear slope of I–V relationships. $N(P_O)$ was calculated during pressure steps while voltage was held at -80mV. In current clamp recordings, effects of ACh or intracellular ions on resting membrane potential was measured without current injection (I=0). 1s depolarizing current steps of various amplitudes were injected to measure spikes which were quantified by frequency (spikes/second) or width (duration of spike). To test whether resting membrane potential affects the ability to generate spikes, hyperpolarizing current was injected to bring cells to negative voltages (<-90mV) or ACh was locally perfused before depolarizing current injection.

The change in Ca^{2+} concentration from a nematocyte voltage spike was estimated based on the integral of Ca^{2+}-selective nematocyte currents elicited by a 0mV step, the same amplitude and slightly shorter duration than a voltage spike. Nematocyte volume was estimated from serial electron microscopy reconstruction with a non-nematocyst volume of approximately 5% of the total volume of the cell. We did not consider the volume occupied by other organelles, making for a conservative estimate. Furthermore, calculations were made with extracellular recording solution containing 0.5mM Ca^{2+}, which is approximately 6-fold less than physiological concentrations. Thus, the large increase we calculated likely underestimates the total Ca^{2+} influx.

Immunohistochemistry

Neural staining: Adult Nv-Elav1::mOrange *Nematostella* were paralyzed in anesthetic solution, then placed in a 4% solution of PFA overnight. Animals were cryoprotected using a gradient of increasing sucrose concentrations (10% to 50%) in PBS over two days. Cryostat sections (20µm thick) were permeabilized with 0.2% Triton-X and 4% normal goat serum (NGS) at room temperature for 1 hour, followed by incubation with DsRed Polyclonal Antibody (Takara Bio Cat# 632496, RRID:AB_10013483) overnight in PBST (0.2%) and NGS at 4°C. Tissue was rinsed 3 times with PBST before secondary was applied (Goat anti-rabbit 647, Abcam) for 2 hours at room temperature. Tissue was rinsed with PBS and mounted with Vectashield containing DAPI (Novus Biologicals).

Acetylcholinesterase staining: Tentacles were stained for the presence of acetylcholinesterase as described (Paul, Beltz, & Berger-Sweeney, 2010) using 40µm thick cryosections mounted on glass slides. Slides were incubated in acetylthiocholine and copper-buffered solution at 40ºC until tentacles appeared white. The stain was developed with a silver solution so that stained areas appear brown. Slides were incubated in the presence of the silver staining solution (+substrate) or saline (-substrate), rinsed according to protocol, and mounted in Fluoromount-G (SouthernBiotech) and imaged using a scanning, transmitted light microscope.

Behavior

Discharge of nematocysts was assessed based on well-established assays (Gitter et al., 1994; Watson & Hessinger, 1994). Adult *Nematostella* were placed in petri dishes containing a modified *Nematostella* medium, containing 16.6mM $MgCl_2$. Animals were given appropriate time to acclimate before presented with stimuli. For assaying discharge, 5 mm round coverslips were coated with a solution of 25% gelatin (w/v) dissolved in medium, and allowed to cure overnight prior to use. Coverslips were presented to the animal's tentacles for 5 seconds and then

immediately imaged at 20X magnification using a transmitted light source. To assay behavioral response to prey-derived chemicals, freshly hatched brine shrimp were flash frozen and pulverized, then filtered through a 0.22µm filter. Coverslips were dipped in the prey extract and immediately presented to the animal. All pharmacological agents were bath applied, except for acetylcholine (1mM), which was delivered as a bolus immediately prior to coverslip presentation. Acetylcholine exposure did not produce movement or contraction of tentacles. Experiments carried out in the absence of extracellular Ca^{2+} were nominally Ca^{2+} free and did not use extracellular chelators. The highest density of discharged nematocytes on the coverslip was imaged at 20X. Nematocyte discharge involves everting the barbed thread, causing them to embed in the gelatin-coated coverslips. Therefore, if nematocytes do not discharge, they are not captured by the gelatin-coated coverslip or visualized for quantification. Images were blindly analyzed using a custom Matlab routine (available in supplemental material) in which images were thresholded and the fraction of pixels corresponding to nematocytes was compared across experiments.

Electron microscopy

Tentacles from an individual *Nematostella vectensis* were placed between two sapphire coverslips separated by a 100um spacer ring (Leica) and frozen in a high-pressure freezer (EM ICE, Leica). This was followed by freeze-substitution (EM AFS2, Leica) in dry acetone containing 1 % ddH2O, 1 % OsO4 and 1 % glutaraldehyde at −90°C for 48 hrs. The temperature was then increased at 5°C/h up to 20°C and samples were washed at room temperature in pure acetone 3x10min RT and propylene oxide 1x10min. Samples were infiltrated with 1:1 Epon:propylene oxide overnight at 4C. The samples were subsequently embedded in TAAB Epon (Marivac Canada Inc.) and polymerized at 60 degrees C for 48 hrs. Ultrathin sections (about 50nm) were cut on an ultramicrotome (Leica EM UC6) and collected with an automated tape collector (ATUM(Kasthuri

et al., 2015)). The sections were then post-stained with uranyl acetate and lead citrate prior to imaging with a scanning electron microscope (Zeiss SIGMA) using a back-scattered electron detector and a pixel size of 4nm.

Once all the sections were scanned, images were aligned into a stack using the algorithm "Linear Stack Alignment with SIFT" available in Fiji (Schindelin et al., 2012). After alignment, images were imported into VAST (Berger, Seung, & Lichtman, 2018) so that every cell could be manually traced. By examining sections and following cellular processes contacts between cells of interest (e.g. neurons and nematocytes) were identified and assessed for the presence of dense-core vesicles in the vicinity (~500nm). Such instances were labeled as putative synapses. Cells were then rendered in 3 dimensions using 3D Studio Max 2019 (Autodesk, San Rafael, CA).

Nematocytes were readily identified because resin does not infiltrate the nematocyst capsule, making for an 'empty' appearance (large white area). Spirocytes were also readily identified based on their capsule containing a long, coiled filament. Sensory neurons were identified according to the higher number of dense core vesicles, higher number of synapses and the presence of sensory processes extending into the external environment.

Statistical analysis

Data were analyzed with Clampfit (Axon Instruments) or Prism (Graphpad) and are represented as mean ± s.e.m. *n* represents independent experiments for the number of cells/patches or behavioral trials. Data were considered significant if $p < 0.05$ using paired or unpaired two-tailed Student's t-tests or one- or two-way ANOVAs. All significance tests were justified considering the experimental design and we assumed normal distribution and variance, as is common for

similar experiments. Sample sizes were chosen based on the number of independent experiments required for statistical significance and technical feasibility.

Data availability

Deep sequencing data are available via the Sequence Read Archive (SRA) repository under the accession code PRJNA627705 and GenBank accession numbers are: cacna2d1 - MT334780, cacna1a - MT334781, cacnb2 - MT334782, nompC - MT334783.

Chapter 2

Introduction:

Ca_V accessory subunits have many well documented roles in modulating channel properties (Buraei & Yang, 2010; Dolphin, 2016). In the case of the $Ca_V\beta$ accessory subunit, binding to Ca_V1 and Ca_V2 channels both increases trafficking of the channel to the cell membrane and changes the voltage-dependence of gating (Josephson & Varadi, 1996; Lacerda et al., 1991; Shistik, Ivanina, Puri, Hosey, & Dascal, 1995; Varadi, Lory, Schultz, Varadi, & Schwartz, 1991). As discussed in Chapter 1, the *Nematostella* Ca_V channel displays unusually strong voltage-dependent inactivation due to binding of the β subunit. While the hyperpolarizing shift in the voltage-dependence of inactivation has been noted in previous studies (Birnbaumer et al., 1998; He, Zhang, Chen, Yamada, & Yang, 2007; Olcese et al., 1994), a shift of this magnitude by a β subunit has not been previously described. These results demonstrate a potentially new mechanism by which the β subunit interacts and modulates the opening of the α subunit.

The mammalian genome contains four β subunit genes, all of which can bind to Ca_V1 and Ca_V2 α subunits (Dawson et al., 2014). The binding between the α and β subunit is mediated by a region on the α subunit called the alpha interaction domain (AID), a well-conserved 18 amino acid sequence found intracellularly linking domains I and II (Pragnell et al., 1994). Point-mutations in the AID of the α subunit greatly attenuate $Ca_V\beta$-enhanced current (De Waard et al., 1996), suggesting an important role for the AID to β subunit binding. Unlike the α subunit, the β subunit does not have a clearly delineated interacting region. Instead, multiple regions of the protein are thought to influence the opening and closing of the α subunit.

Binding of the β subunit at the AID affects both the voltage-dependence of channel opening from a closed state, as well as the rate at which the channel enters the non-conducting, inactivated state. β subunit binding increases the amplitude of voltage-gated calcium currents from Ca_V1 and Ca_V2

channels by both decreasing the size of the depolarizing stimulus needed to open the channel, often referred to as "shifting" the voltage dependence of activation, and by hastening the channel opening by increasing the probability of single channel openings (Buraei & Yang, 2010; Josephson & Varadi, 1996; Neely, Wei, Olcese, Birnbaumer, & Stefani, 1993).

The $Ca_V\beta$ protein can be divided into five regions based on structure, sequence homology, and function. The "core" of the protein contains well-conserved, although catalytically inactive, homologous Src homology 3 (SH3) and guanylate kinase (GK) domains. These domains are separated by a flexible, variable length HOOK region. This core region is bordered by poorly conserved N- and C-terminal regions that, like the HOOK region, are sites for alternative splicing (Buraei & Yang, 2010; Olcese et al., 1994; Opatowsky, Chomsky-Hecht, Kang, Campbell, & Hirsch, 2003; Richards, Leroy, Pratt, & Dolphin, 2007).

The mechanism by which β subunits change the voltage-dependence of inactivation is still unknown and is hindered in part by an incomplete understanding of the structural basis for inactivation in Ca_Vs. In contrast to K_V and Na_V, where inactivation can be directly linked to the movement of a region of the protein known as "the inactivation gate", the equivalent region has not been identified in Ca_Vs (Hille, 2001). Crystal structures of the β subunit bound to the α subunit revealed the GK domain of the β subunit in close proximity to the AID and suggest that the interaction of the β subunit induces a helical formation in the AID-containing region (Chen et al., 2004; Opatowsky, Chen, Campbell, & Hirsch, 2004; Van Petegem, Clark, Chatelain, & Minor, 2004; Wu et al., 2016). This rigidity is then predicted to create more energetically favorable positions of S6 and the voltage-sensing domain (VSD) II, both of which are implicated in channel gating (Chen et al., 2004; Opatowsky et al., 2004; Van Petegem et al., 2004; Wu et al., 2016).

Experiments using cloning and site-directed mutagenesis have been critical for establishing the function of each domain of the mammalian β subunit and have generated new hypotheses regarding the structural basis of β-enhanced inactivation. With the exception of the C-terminal domain, the remaining four domains of the β subunit have all been implicated in mediating the voltage-dependent effects on the α subunit (He et al., 2007).

Due to the limitations of available calcium channel sequences and a bias to study mammalian proteins, very little research has been conducted on the regulatory effects of non-mammalian Ca_V accessory subunits. Furthermore, the study of non-mammalian subunits may shed new light into the mechanism by which this regulation occurs. Using a combination of site directed mutagenesis and cloning, I have shown that the N-terminal region of the *Nematostella* β (NVE β) subunit is uniquely capable of producing strong voltage-dependent inactivation. These results have revealed a new function for this protein region and highlight the importance of comparative physiology to molecular physiology.

Results

To identify the region of the NVE β subunit mediating the unusual voltage-dependence of inactivation described in Chapter 1, I generated chimera proteins using mammalian β (Rat β) and NVE β subunit sequences. By interchanging homologous domains between these differentially acting proteins, any changes in voltage-dependent properties could be directly attributed to the mutated regions. The function of β subunit chimeras was assessed using a heterologous expression system in which mammalian *cacna1a* and *cacna2d1* were expressed with a mutant β subunit in HEK-293 cells (**Fig. 18**).

Except for mammalian β2 splice variants, interaction of the β with the α subunit shifts the voltage dependence of inactivation, both by decreasing the amplitude of the depolarizing stimulus needed to move the channel into an inactivated state and by increasing the rate at which this state change occurs (He et al., 2007; Patil et al., 1998). Interestingly, this transition to the inactivated state is thought to be promoted when the channel is in a closed configuration, a process referred to as "ultra-slow" or "closed-state inactivation" (Bähring & Covarrubias, 2011; Yasuda et al., 2004). NVE β on promotes a shift to an inactivated state at typical resting membrane potentials, consistent with closed-state inactivation. Heterologous expression of NVE β confers unusually negative voltage-dependent inactivation compared to the mammalian homologue (**Fig. 19**). Calcium currents begin to inactivate at -90mV, which likely contributes to the non-sigmoidal shape of the current-voltage plot (**Fig. 19A**). NVE β shifts the midpoint inactivation voltage ($V_{i1/2}$) by approximately ~100mV. This voltage-dependence closely resembles that of the *Nematostella* Ca_V. NVE β also increased the rate of fast inactivation (**Fig. 19B**). Altogether, these results suggest that channels readily move into an inactive state without entering an open, conductive state. Thus, the number of channels available to amplify a depolarizing stimulus at typical resting membrane potentials is decreased.

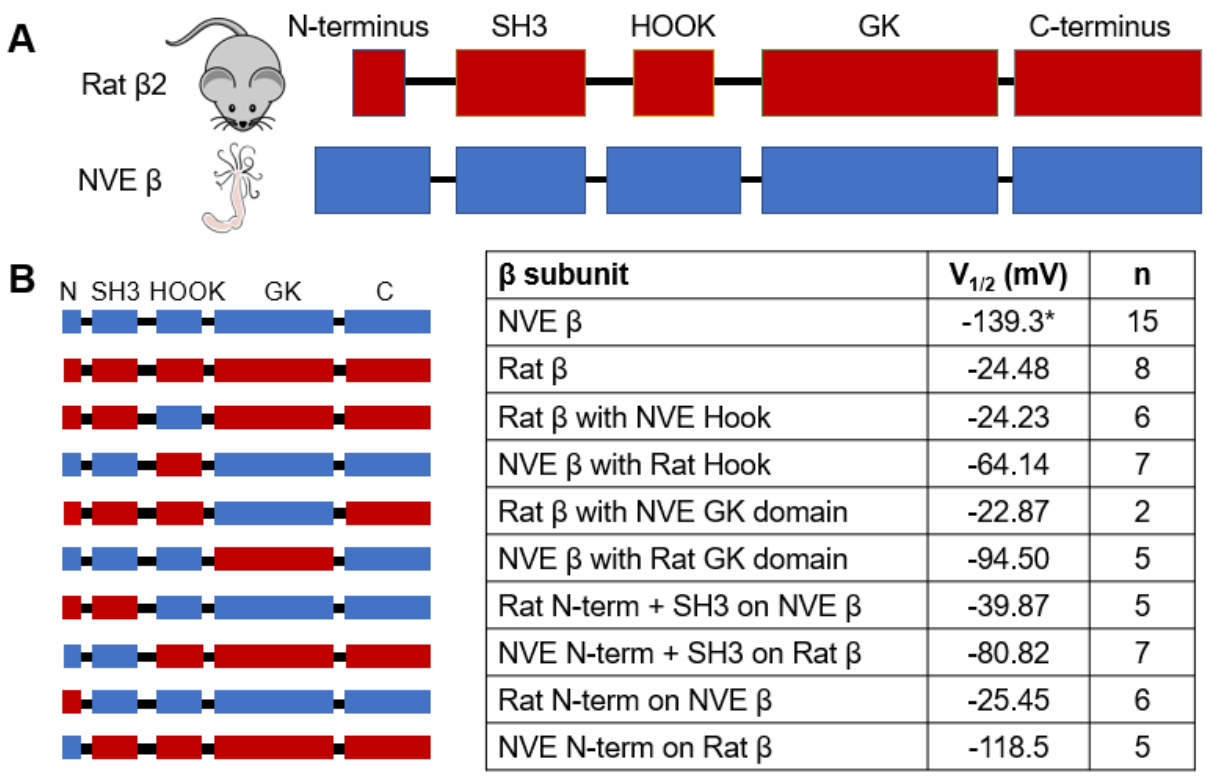

β subunit	$V_{1/2}$ (mV)	n
NVE β	-139.3*	15
Rat β	-24.48	8
Rat β with NVE Hook	-24.23	6
NVE β with Rat Hook	-64.14	7
Rat β with NVE GK domain	-22.87	2
NVE β with Rat GK domain	-94.50	5
Rat N-term + SH3 on NVE β	-39.87	5
NVE N-term + SH3 on Rat β	-80.82	7
Rat N-term on NVE β	-25.45	6
NVE N-term on Rat β	-118.5	5

Figure 18: $Ca_V\beta$ subunit chimera proteins generated. (A) Schematic representation of β subunit domains for rat (top, red) and *Nematostella* (bottom, blue). **(B)** Chimeric proteins generated (left); colors indicate animal origin of each domain. Summary table with the measured voltage at which half of the maximally evoked current was inactivated, as estimated with a sigmoidal fit (right). Asterisk indicates a non-sigmoidal inactivation relationship, n indicates number of cells.

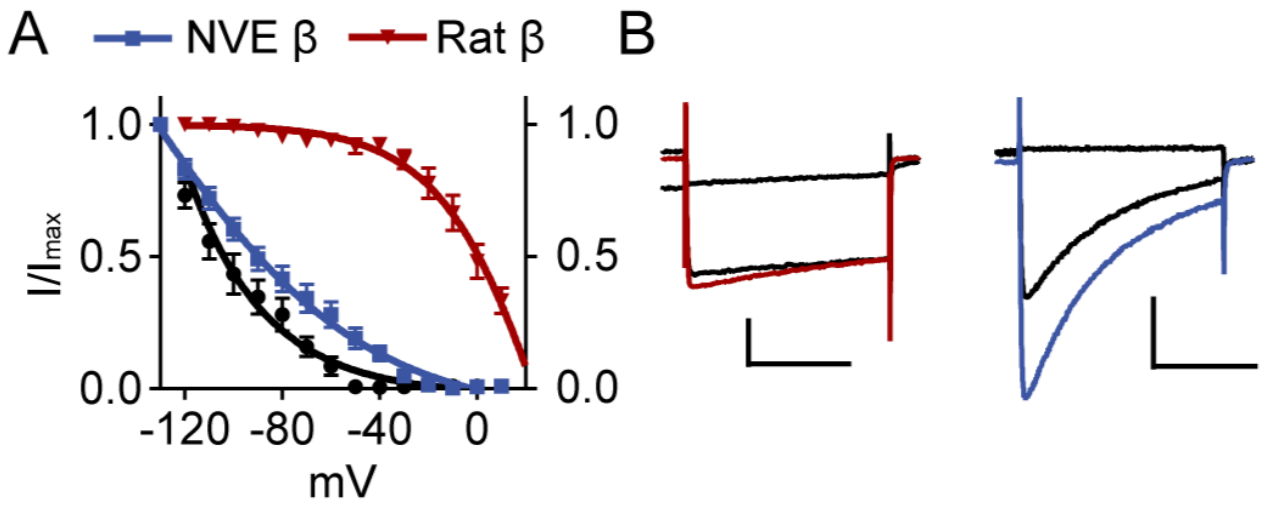

Figure 19: *Nematostella* Cavβ confers unusually negative voltage-dependent inactivation. Voltage-gated currents recorded from heterologously-expressed Ca_V channels (mammalian *cacna1a* and *cacna2d1*) with $Ca_V\beta$ subunits substituted as indicated (mammalian β in red and NVE β in blue). **(A)** NVE β shifts the voltage-dependence of inactivation to negative voltages (estimated $V_{i1/2}$ = -139.3 ± 47.44 mV, n = 15) versus mammalian β ($V_{i1/2}$ = -24.48 ± 0.09mV, n = 8). Inactivation was measured in response to 1s pre-pulses from -110mV to 20mV with an inter-sweep holding potential of -90mV. *Nematostella* Ca_V is plotted for comparison (black). **(B)** Representative voltage-activated currents following a -130mV (colored) pre-pulse, -70mV pre-pulse, and -10mV pre-pulse. Scale bars = 200pA, 100ms.

It is unclear if the HOOK region directly interacts with the α subunit because it is adjacent to the GK domain, which has a more established role in interacting with the AID domain. Despite a lack of structural data to indicate direct binding with the α subunit, convincing evidence using chimeric proteins has shown that switching the HOOK domains between the differentially acting β1 and β2 subunits switches the effects of each on voltage-dependent inactivation (He et al., 2007). Given the disparity in length between the HOOK domains of both β subunits, I generated chimeras that exchanged these domains. Heterologous expression of these chimeras produced currents very similar to the original proteins (**Fig. 20**), indicating that the HOOK domain does not confer a shift in the voltage-dependence of inactivation by NVE β.

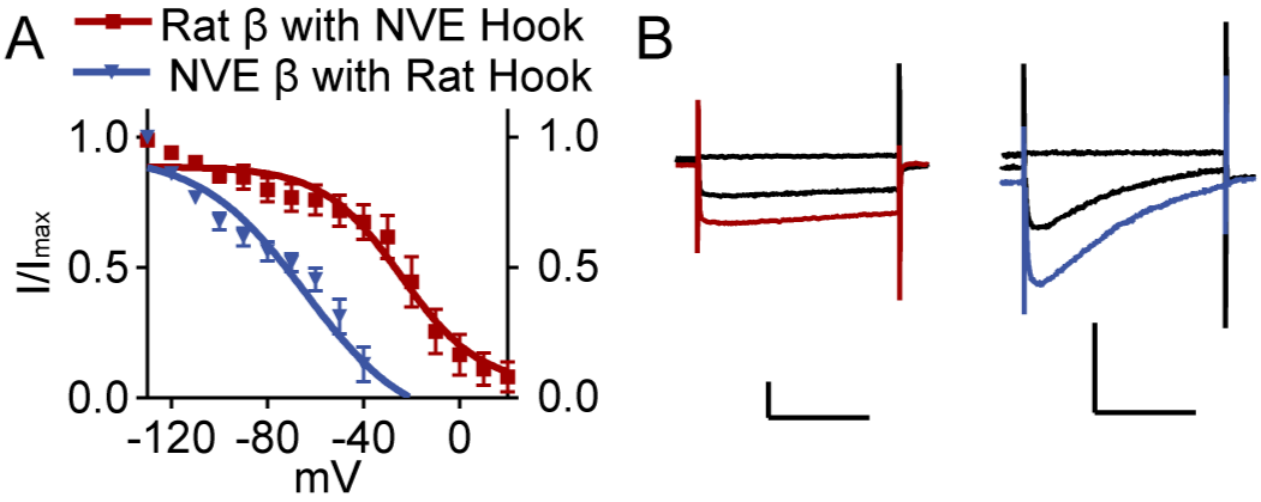

Figure 20: The HOOK domain does not confer a large shift in the voltage-dependence of inactivation. (A) Chimera β subunits with interchanged HOOK domains does not dramatically alter the voltage-dependence from the native protein. Mammalian β chimera $V_{i1/2}$ = -24.32 ± 3.12mV, n = 2)(red) versus NVEβ chimera ($V_{i1/2}$ = -64.14 ± 2.61mV, n = 5)(blue). Inactivation was measured in response to 1s pre-pulses from -110mV to 20mV with an inter-sweep holding potential of -90mV. *Nematostella* Ca_V is plotted for comparison (black). **(B)** Representative voltage-activated currents following a -130mV (colored) pre-pulse, -70mV pre-pulse, and -10mV pre-pulse. Scale bars = 200pA, 100ms.

Taking into account the high conservation of the GK domain among all four β subtypes, it is not surprising that all GK domains been shown to similarly shift the voltage-dependence of inactivation to more negative potentials (He et al., 2007). Structural data indicate that the GK domain has closely interacts with the α subunit by forming a hydrophobic pocket that binds tightly with the AID, which may be critical to the activity of the β subunit (Van Petegem et al., 2004). However, chimera β subunits with interchanged GK domains did not have dramatically different voltage-dependence properties compared to the native proteins (**Fig. 21**).

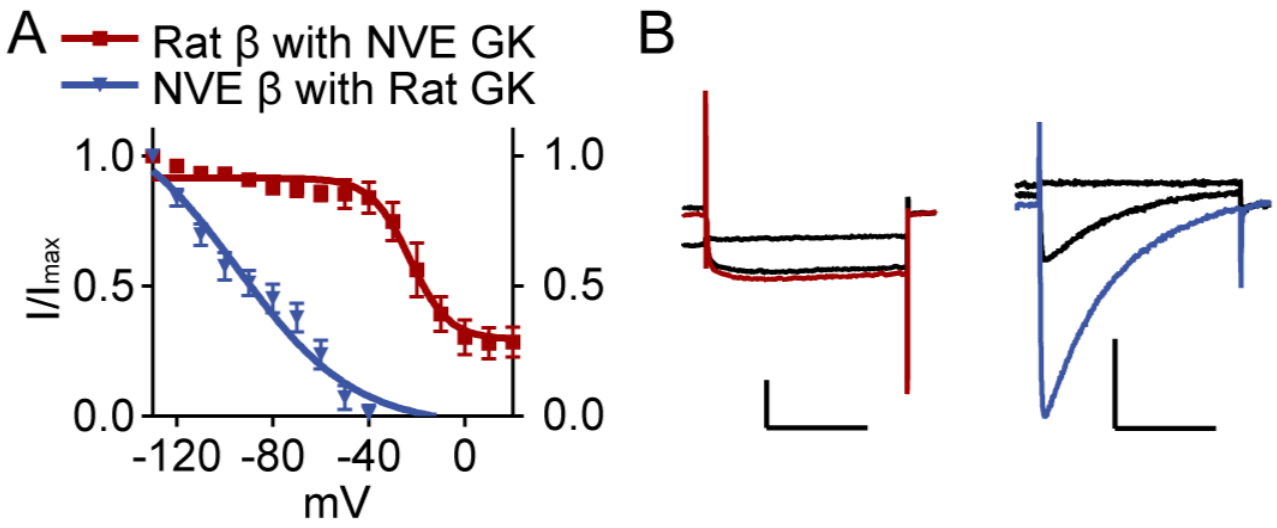

Figure 21: The GK domain does not confer a shift in the voltage-dependence of inactivation. **(A)** Chimera β subunits with interchanged GK domains does not dramatically alter the voltage-dependence from the native protein. Mammalian β chimera ($V_{i1/2}$ = -22.87 ± 1.92mV, n = 6)(red) versus NVEβ chimera ($V_{i1/2}$ = -94.50 ± 6.26mV, n = 5)(blue). Inactivation was measured in response to 1s pre-pulses from -110mV to 20mV with an inter-sweep holding potential of -90mV. *Nematostella* Ca_V is plotted for comparison (black). **(B)** Representative voltage-activated currents following a -130mV (colored) pre-pulse, -70mV pre-pulse, and -10mV pre-pulse. Scale bars = 200pA, 100ms.

While there is little structural data to support a functional role for the N-terminal of the β subunits in modulating the pore-forming α subunit, truncations of this region have been shown to change voltage-properties (Jangsangthong et al., 2010; Olcese et al., 1994; Stephens et al., 2000). In general, truncating or deleting N-terminal domain diminished the hyperpolarizing shift on inactivation (Jangsangthong et al., 2010; Olcese et al., 1994; Stephens, Page, Bogdanov, & Dolphin, 2000). Initially, both the N-terminus and the neighboring SH3 domain was interchanged (**Fig. 22**). Substituting the mammalian N-terminal region and SH3 domain with the *Nematostella* homologous regions left shifted $V_{i1/2}$ by ~50mV **(Fig. 22A)** and conferred the fast-inactivation seen with NVE β (**Fig. 22B**). The reverse was also true where the mammalian N-terminal domain and SH3 domains conferred mammalian-like properties to the largely *Nematostella* β chimera.

To further isolate the region responsible for these properties, chimeras containing only interchanged N-terminal regions were generated (**Fig. 23**). Exchanging only the N-terminal regions of the β subunits almost completely recapitulated the voltage-properties seen in the native proteins. The N-terminal region from the *Nematostella* β conferred an approximately 90mV hyperpolarizing shift in $V_{i1/2}$ (**Fig. 23A**) and also increased the rate of fast-inactivation (**Fig. 23B**).

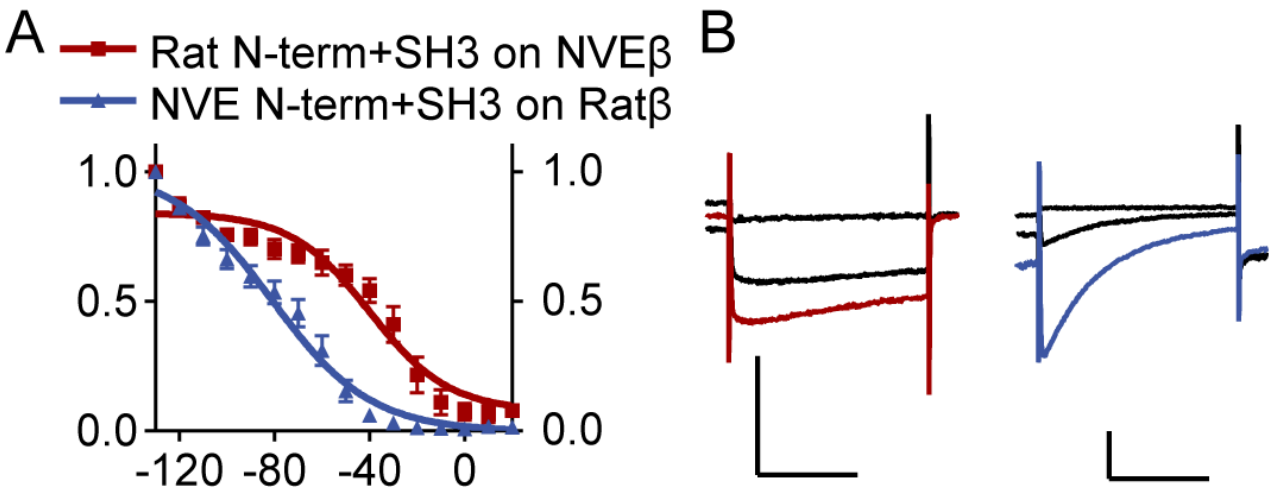

Figure 22: The N-terminal and SH3 domains confer a shift in the voltage-dependence of inactivation. (A) Interchanging the N-terminal and SH3 domains from the NVEβ to the mammalian β confers the unusual voltage-dependent properties. Mammalian β chimera $V_{i1/2}$ = -80.82 ± 2.91mV, n = 7)(blue) versus NVEβ chimera ($V_{i1/2}$ = -39.87 ± 2.62mV, n = 5) (red). Inactivation was measured in response to 1s pre-pulses from -110mV to 10mV with an inter-sweep holding potential of -90mV. *Nematostella* Ca_V is plotted for comparison (black). **(B)** Representative voltage-activated currents following a -130mV (colored) pre-pulse, -70mV pre-pulse, and -10mV pre-pulse. Scale bars = 200pA, 100ms.

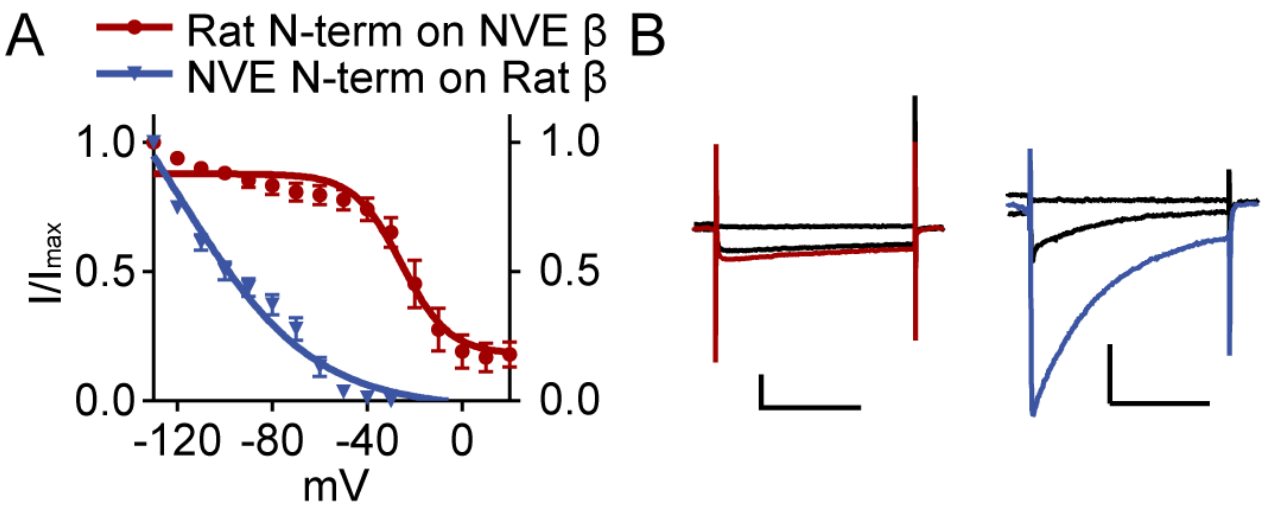

Figure 23: **The N-terminal region confers a shift in the voltage-dependence of inactivation.** **(A)** Interchanging only the N-terminal region of the NVE β and mammalian β subunits switches the voltage-dependent properties. Mammalian β chimera $V_{i1/2}$ = -25.45 ± 2.01mV, n = 5)(blue) versus NVEβ chimera ($V_{i1/2}$ = -118.5 ± 10.64mV, n = 6) (red). Inactivation was measured in response to 1s pre-pulses from -110mV to 20mV with an inter-sweep holding potential of -90mV. *Nematostella* Ca_V is plotted for comparison (black). **(B)** Representative voltage-activated currents following a -130mV (colored) pre-pulse, -70mV pre-pulse, and -10mV pre-pulse. Scale bars = 200pA, 100ms.

Discussion

From these results, we can conclude that the N-terminal region of the *Nematostella* β subunit confers uniquely-sensitive voltage-dependent inactivation to the calcium channel. The N-terminal region does not appear to have strong sequence homology with other known bilaterian and cnidarian β subunits, although this region of the protein is often missing from transcriptomic data sets. It is possible that *Nematostella* β subunits independently acquired mutations in this region resulting in this acquired function. Increased diversity of cnidarian genomic data may help resolve the evolutionary history of this protein.

Protein binding assays and structural data only support direct binding between the AID and a hydrophobic pocket formed by GK domain. The S6 region and the linker regions between domains I and II of the α subunit are both thought to play key roles in inactivation (Berjukow et al., 2001). However, given that the AID is directly adjacent to S6 of domain 1, it is easy to infer that indirect interactions between various domains of the β subunit, such as the N-terminal region, could also cause conformational changes in S6.

Additional structural data could provide critical new insight into the contribution of the N-terminus to the conformational state of the α subunit. The currently available structural data is inherently limited. Methods used to produce these structures limit the conformational state of the channel in an open or inactivated state, and even then, the state of the channel cannot be determined with certainty. Furthermore, the flexibility of the N- and C- termini of the β subunit greatly reduces the ability to resolve the interaction of these protein regions with the α subunit. Advances in cryo-EM, including the use of lipid nano-disks, will likely resolve additional conformational states in the near future. However, with the currently available structural data, it is difficult to gain a complete picture of the conformational changes that occur at the pore.

β subunits also play a critical, albeit indirect, role in inactivation of the α subunit through other regulatory proteins, including Gβγ subunits, calmodulin (CaM), and the RGK subfamily of proteins. G-protein coupled receptors are common molecular targets of signaling molecules, including neurotransmitters and peptides. Once the receptor is activated, Gβγ subunits can dissociate from the complex and bind to downstream targets such as Ca_V α subunits. Gβγ binding acts to inhibit Ca_V activity by binding at the linker between domains I and II with concomitant binding of the β subunit (Cantí et al., 1999). Similarly, CaM, an intracellular calcium-binding protein, can also inactivate Ca_V in a β subunit-dependent manner. CaM is activated upon high intracellular calcium levels and binds to the α subunit at a modified isoleucine-glutamine (IQ) domain on the C-terminal region (Findeisen & Minor, 2009; Ivanina, Blumenstein, Shistik, Barzilai, & Dascal, 2000). CaM binding results in a shift of the α subunit to an inactivated state, thus acting as a form of negative feedback to Ca_V mediated calcium influx (Simms & Zamponi, 2014). Although the binding domain is less clear, the RGK subfamily of proteins also inhibits Ca_V opening in a β-subunit dependent manner (Béguin et al., 2007). It is possible that the *Nematostella* β subunit regulation may be dependent on additional binding proteins, however, considering the similar phenotype present in both native cells from *Nematostella* and in the heterologous cell expression system, the likelihood is small. Nevertheless, the diversity of proteins that can regulate Ca_V activity and allow for cell-specific, and even compartment specific, tuning of Ca_V mediated calcium influx is remarkable and cannot be ruled out.

β subunits have also been described as inducing significant hyperpolarizing shifts in inactivation of HVA Ca_V channels in a dose-dependent manner (Yasuda et al., 2004). In this study, while plasmids encoding chimera proteins were generated using the same codon optimization and plasmid backbone, it is possible that some chimeras generated greater protein levels in the cytosol.

To determine the contribution of dose-dependent effects, future work could utilize xenopus oocytes, where the amount of injected RNA more closely corresponds with the amount of protein expressed, to determine if expression level variation could account for these physiological findings.

Ultimately, these results demonstrate a novel function for a protein domain and underscore the importance of electrophysiological study of non-bilaterian channels.

Methods:

Cells:

HEK293T cells (ATCC, Cat# CRL-3216, RRID:CVCL_0063, authenticated and validated as negative for mycoplasma by vendor) were grown in DMEM, 10% fetal calf serum, and 1% penicillin/streptomycin at 37°C, 5% CO2. Cells were transfected using lipofectamine 2000 (Invitrogen/Life Technologies) according to the manufacturer's protocol. 1µg of one of the mutant β subunit proteins in the table below, along with 1µg of *M. musculus* (mouse) *cacna1a*, *cacna2d1* (rat) was coexpressed with 0.5µg GFP. To enhance channel expression, cells were transfected for 6-8h, plated on coverslips, and then incubated at 28°C for 2-6 days before experiments. Rat *cacna2d1* (RRID:Addgene_26575) and *cacna1a* (RRID:Addgene_26578) were gifts from D. Lipscombe and *cacnb2a* (RRID:Addgene_107424) was a gift from A. Dolphin.

Proteins generated:

Protein name	Amino Acid Sequence
Nematostella cacnb2.1 (NVE β)	MEPEPGLSEQDIELDSLEQVSTASSFHSDIQRHYNDGREASRFIGADDF NRDSDPAYRASDTSSIEEDRETSRRELERRAWDALQAARSKPVAFAVR TNLRYDGSEDDDSPVHGAAVSFEAKDFLHVKEKFNDDWWIGRVVKE GCDIGFIPTPSKLKSLQQIGGTASGRGMRNSKRDVFQFDMVNQAQSPT NTSPSRHSSTSVDAENGVEYDDDQQSPTSPTNKTLPRSASGTTVSSQPG TATGTQGKPKKGLFKKQEQLPPYDVVPSMRPIVLVGPSLKGYEVTDM MQKALLDFMKHRFSGRVLIARVTSDISLAKRTNMSNPGKQTIMERTKN

	KNTGLAEVQQEIERIFELARGLNLVVLDCETVNHPTQLAKTSLAPMIV YIKIAAPKVLQRLIKTRGKSQSRNLSIQLVAAEKLAQCSEDMYDLVLEE TQLDDACEHLGEFLESYWRATHPPNQPGSRPPNVQPSNSTPQYNVIEG GERPSVYL
Rat cacnb2a (Rat β)	MQCCGLVHRRRVRVSYGSADSYTSRPSDSDVSLEEDREAVRREAERQ AQAQLEKAKTKPVAFAVRTNVRYSAAQEDDVPVPGMAISFEAKDFLH VKEKFNNDWWIGRLVKEGCEIGFIPSPVKLENMRLQHEQRAKQGKFY SSKSGGNSSSSLGDIVPSSRKSTPPSSAIDIDATGLDAEENDIPANHRSPK PSANSVTSPHSKEKRMPFFKKTEHTPPYDVVPSMRPVVLVGPSLKGYE VTDMMQKALFDFLKHRFEGRISITRVTADISLAKRSVLNNPSKHAIIERS NTRSSLAEVQSEIERIFELARTLQLVVLDADTINHPAQLSKTSLAPIIVYV KISSPKVLQRLIKSRGKSQAKHLNVQMVAADKLAQCPPQESFDVILDE NQLEDACEHLADYLEAYWKATHPPSSNLPNPLLSRTLATSTLPLSPTLA SNSQGSQGDQRTDRSAPRSASQAEEEPCLEPVKKSQHRSSSATHQNHR SGTGRGLSRQETFDSETQESRDSAYVEPKEDYSHEHVDRYVPHREHNH REESHSSNGHRHREPRHRTRDMGRDQDHNECSKQRSRHKSKDRYCD KEGEVISKRRSEAGEWNRDVYIRQ
Rat β with NVE Hook	MQCCGLVHRRRVRVSYGSADSYTSRPSDSDVSLEEDREAVRREAERQ AQAQLEKAKTKPVAFAVRTNVRYSAAQEDDVPVPGMAISFEAKDFLH VKEKFNNDWWIGRLVKEGCEIGFIPSPSKLKSLQQIGGTASGRGMRNS KRDVFQFDMVNQAQSPTNTSPSRHSSTSVDAENGVEYDDDQQSPTSPT NKTLPRSASGTTVSSQPGTATGTQGKPKKGLFKKQEQLPPYDVVPSMR PVVLVGPSLKGYEVTDMMQKALFDFLKHRFEGRISITRVTADISLAKRS VLNNPSKHAIIERSNTRSSLAEVQSEIERIFELARTLQLVVLDADTINHP AQLSKTSLAPIIVYVKISSPKVLQRLIKSRGKSQAKHLNVQMVAADKL AQCPPQESFDVILDENQLEDACEHLADYLEAYWKATHPPSSNLPNPLL SRTLATSTLPLSPTLASNSQGSQGDQRTDRSAPRSASQAEEEPCLEPVK KSQHRSSSATHQNHRSGTGRGLSRQETFDSETQESRDSAYVEPKEDYS HEHVDRYVPHREHNHREESHSSNGHRHREPRHRTRDMGRDQDHNEC SKQRSRHKSKDRYCDKEGEVISKRRSEAGEWNRDVYIRQ
NVE β with Rat Hook	MEPEPGLSEQDIELDSLEQVSTASSFHSDIQRHYNDGREASRFIGADDF NRDSDPAYRASDTSSIEEDRETSRRELERRAWDALQAARSKPVAFAVR TNLRYDGSEDDDSPVHGAAVSFEAKDFLHVKEKFNDDWWIGRVVKE GCDIGFIPTPVKLENMRLQHEQRAKQGKFYSSKSGGNSSSSLGDIVPSS RKSTPPSSAIDIDATGLDAEENDIPANHRSPKPSANSVTSPHSKEKRMPF FKKTEHTPPYDVVPSMRPIVLVGPSLKGYEVTDMMQKALLDFMKHRF SGRVLIARVTSDISLAKRTNMSNPGKQTIMERTKNKNTGLAEVQQEIER IFELARGLNLVVLDCETVNHPTQLAKTSLAPMIVYIKIAAPKVLQRLIK TRGKSQSRNLSIQLVAAEKLAQCSEDMYDLVLEETQLDDACEHLGEFL ESYWRATHPPNQPGSRPPNVQPSNSTPQYNVIEGGERPSVYL
Rat β with NVE GK domain	MQCCGLVHRRRVRVSYGSADSYTSRPSDSDVSLEEDREAVRREAERQ AQAQLEKAKTKPVAFAVRTNVRYSAAQEDDVPVPGMAISFEAKDFLH VKEKFNNDWWIGRLVKEGCEIGFIPSPVKLENMRLQHEQRAKQGKFY SSKSGGNSSSSLGDIVPSSRKSTPPSSAIDIDATGLDAEENDIPANHRSPK PSANSVTSPHSKEKRMPFFKKTEHTPPYDVVPSMRPIVLVGPSLKGYEV TDMMQKALLDFMKHRFSGRVLIARVTSDISLAKRTNMSNPGKQTIME

	RTKNKNTGLAEVQQEIERIFELARGLNLVVLDCETVNHPTQLAKTSLA PMIVYIKIAAPKVLQRLIKTRGKSQSRNLSIQLVAAEKLAQCSEDMYDL VLEETQLDDACEHLGEFLESYWRATHPPNQPGSRPPNVQPSNSTPQYN VIEGGERPSVYL
NVE β with Rat GK domain	MEPEPGLSEQDIELDSLEQVSTASSFHSDIQRHYNDGREASRFIGADDF NRDSDPAYRASDTSSIEEDRETSRRELERRAWDALQAARSKPVAFAVR TNLRYDGSEDDDSPVHGAAVSFEAKDFLHVKEKFNDDWWIGRVVKE GCDIGFIPTPSKLKSLQQIGGTASGRGMRNSKRDVFQFDMVNQAQSPT NTSPSRHSSTSVDAENGVEYDDDQQSPTSPTNKTLPRSASGTTVSSQPG TATGTQGKPKKGLFKKQEQLPPYDVVPSMRPVVLVGPSLKGYEVTDM MQKALFDFLKHRFEGRISITRVTADISLAKRSVLNNPSKHAIIERSNTRS SLAEVQSEIERIFELARTLQLVVLDADTINHPAQLSKTSLAPIIVYVKISS PKVLQRLIKSRGKSQAKHLNVQMVAADKLAQCPPQESFDVILDENQLE DACEHLADYLEAYWKATHPPSSNLPNPLLSRTLATSTLPLSPTLASNSQ GSQGDQRTDRSAPRSASQAEEEPCLEPVKKSQHRSSSATHQNHRSGTG RGLSRQETFDSETQESRDSAYVEPKEDYSHEHVDRYVPHREHNHREES HSSNGHRHREPRHRTRDMGRDQDHNECSKQRSRHKSKDRYCDKEGE VISKRRSEAGEWNRDVYIRQ
Rat N-term on NVE β	MQCCGLVHRRRVRVSYGSADSYTSRPSDSDVSLEEDREAVRREAERQ AQAQLEKAKTKPVAFAVRTNLRYDGSEDDDSPVHGAAVSFEAKDFLH VKEKFNDDWWIGRVVKEGCDIGFIPTPSKLKSLQQIGGTASGRGMRNS KRDVFQFDMVNQAQSPTNTSPSRHSSTSVDAENGVEYDDDQQSPTSPT NKTLPRSASGTTVSSQPGTATGTQGKPKKGLFKKQEQLPPYDVVPSMR PIVLVGPSLKGYEVTDMMQKALLDFMKHRFSGRVLIARVTSDISLAKR TNMSNPGKQTIMERTKNKNTGLAEVQQEIERIFELARGLNLVVLDCET VNHPTQLAKTSLAPMIVYIKIAAPKVLQRLIKTRGKSQSRNLSIQLVAA EKLAQCSEDMYDLVLEETQLDDACEHLGEFLESYWRATHPPNQPGSR PPNVQPSNSTPQYNVIEGGERPSVYL
Rat N-term + SH3 on NVE β	MQCCGLVHRRRVRVSYGSADSYTSRPSDSDVSLEEDREAVRREAERQ AQAQLEKAKTKPVAFAVRTNVRYSAAQEDDVPVPGMAISFEAKDFLH VKEKFNNDWWIGRLVKEGCEIGFIPSPSKLKSLQQIGGTASGRGMRNS KRDVFQFDMVNQAQSPTNTSPSRHSSTSVDAENGVEYDDDQQSPTSPT NKTLPRSASGTTVSSQPGTATGTQGKPKKGLFKKQEQLPPYDVVPSMR PIVLVGPSLKGYEVTDMMQKALLDFMKHRFSGRVLIARVTSDISLAKR TNMSNPGKQTIMERTKNKNTGLAEVQQEIERIFELARGLNLVVLDCET VNHPTQLAKTSLAPMIVYIKIAAPKVLQRLIKTRGKSQSRNLSIQLVAA EKLAQCSEDMYDLVLEETQLDDACEHLGEFLESYWRATHPPNQPGSR PPNVQPSNSTPQYNVIEGGERPSVYL
NVE N-term + SH3 on Rat β	MEPEPGLSEQDIELDSLEQVSTASSFHSDIQRHYNDGREASRFIGADDF NRDSDPAYRASDTSSIEEDRETSRRELERRAWDALQAARSKPVAFAVR TNVRYSAAQEDDVPVPGMAISFEAKDFLHVKEKFNNDWWIGRLVKEG CEIGFIPSPVKLENMRLQHEQRAKQGKFYSSKSGGNSSSSLGDIVPSSR KSTPPSSAIDIDATGLDAEENDIPANHRSPKPSANSVTSPHSKEKRMPFF KKTEHTPPYDVVPSMRPVVLVGPSLKGYEVTDMMQKALFDFLKHRFE GRISITRVTADISLAKRSVLNNPSKHAIIERSNTRSSLAEVQSEIERIFELA RTLQLVVLDADTINHPAQLSKTSLAPIIVYVKISSPKVLQRLIKSRGKSQ

	AKHLNVQMVAADKLAQCPPQESFDVILDENQLEDACEHLADYLEAY WKATHPPSSNLPNPLLSRTLATSTLPLSPTLASNSQGSQGDQRTDRSAP RSASQAEEEPCLEPVKKSQHRSSSATHQNHRSGTGRGLSRQETFDSET QESRDSAYVEPKEDYSHEHVDRYVPHREHNHREESHSSNGHRHREPR HRTRDMGRDQDHNECSKQRSRHKSKDRYCDKEGEVISKRRSEAGEW NRDVYIRQ
NVE N-term on Rat β	MEPEPGLSEQDIELDSLEQVSTASSFHSDIQRHYNDGREASRFIGADDF NRDSDPAYRASDTSSIEEDRETSRRELERRAWDALQAARSKPVAFAVR TNLRYDGSEDDDSPVHGAAVSFEAKDFLHVKEKFNDDWWIGRVVKE GCDIGFIPTPVKLENMRLQHEQRAKQGKFYSSKSGGNSSSSLGDIVPSS RKSTPPSSAIDIDATGLDAEENDIPANHRSPKPSANSVTSPHSKEKRMPF FKKTEHTPPYDVVPSMRPVVLVGPSLKGYEVTDMMQKALFDFLKHRF EGRISITRVTADISLAKRSVLNNPSKHAIIERSNTRSSLAEVQSEIERIFEL ARTLQLVVLDADTINHPAQLSKTSLAPIIVYVKISSPKVLQRLIKSRGKS QAKHLNVQMVAADKLAQCPPQESFDVILDENQLEDACEHLADYLEAY WKATHPPSSNLPNPLLSRTLATSTLPLSPTLASNSQGSQGDQRTDRSAP RSASQAEEEPCLEPVKKSQHRSSSATHQNHRSGTGRGLSRQETFDSET QESRDSAYVEPKEDYSHEHVDRYVPHREHNHREESHSSNGHRHREPR HRTRDMGRDQDHNECSKQRSRHKSKDRYCDKEGEVISKRRSEAGEW NRDVYIRQ

Electrophysiology

Recordings were carried out at room temperature using a MultiClamp 700B amplifier (Axon Instruments) and digitized using a Digidata 1550B (Axon Instruments) interface and pClamp software (Axon Instruments). Whole-cell recording data were filtered at 1kHz and sampled at 10kHz. For single-channel recordings, data were filtered at 2kHz and sampled at 20kHz. Data were leak-subtracted online using a p/4 protocol, and membrane potentials were corrected for liquid junction potentials. For whole-cell recordings in HEK293 cells, pipettes were 3-4MΩ. The standard extracellular solution contained (in mM): 140 NaCl, 5 KCl, 10 HEPES, 2 $CaCl_2$, 1 $MgCl_2$, pH 7.4. The intracellular solution contained (mM): 140 cesium methanesulfonate, 1 $MgCl_2$, 3.33 EGTA, 3.33 HEPES, 10 sucrose, pH 7.2.

Unless stated otherwise, voltage-gated currents were measured in response to a 200ms voltage pulse in 10mV increments from a -110mV holding potential. G-V relationships were derived from

I-V curves by calculating G: $G=I_{CaV}/(V_m-E_{rev})$ and fit with a Boltzman equation. Voltage-dependent inactivation was measured during -10mV (Ca^{2+} currents in native cells), 0mV (Ca^{2+} currents in heterologously expressed channels), 60mV (K^+ currents in native cells) voltage pulses following a series of 1s pre-pulses ranging from -130mV to 60mV. Voltage-dependent inactivation was quantified as I/I_{max}, with I_{max} occurring at the voltage pulse following a -130mV prepulse. In some instances, inactivation curves could not be fit with a Boltzman equation and were instead fitted with an exponential.

Statistical analysis

Data were analyzed with Clampfit (Axon Instruments) or Prism (Graphpad) and are represented as mean ± s.e.m. *n* represents independent experiments for the number of cells. Data were considered significant if $p < 0.05$ using paired or unpaired two-tailed Student's t-tests or one- or two-way ANOVAs. All significance tests were justified considering the experimental design and we assumed normal distribution and variance, as is common for similar experiments. Sample sizes were chosen based on the number of independent experiments required for statistical significance and technical feasibility.

Conclusion

Cnidarians occupy a diverse range of aquatic environments that vary with salinity, temperature, and the presence of different prey and predators. For example, the freshwater hydrozoan, *Hydra*, is found in shallow ponds and streams in both temperature and tropic climates and feeds on small, aquatic invertebrates (Lenhoff & Loomis, 1961). In contrast, *Crossota millsae*, another small hydrozoan, live at depths greater than 1000m (Thuesen, 2003). *Physalia physalis*, or more commonly known as the Portuguese man of war, is a siphonophore known to float for hundreds of miles in tropical oceans, dragging tentacles up to 100 feet long that can deliver deadly stings to both fish and humans (Munro, Vue, Behringer, & Dunn, 2019).

Additionally, cnidocytes, the cell type by which the phylum is named after, are exceptionally diverse themselves. Cnidocytes can be categorized into at least 28 distinct cell types based on the appearance of the discharged thread (Kass-Simon & Scappaticci, Jr., 2002; Östman, 2000). In organisms that contain multiple types of cnidocytes, it has been shown that different cnidocytes can be deployed for different tasks. For example, *Hydra* uses atrichous isorhiza nematocytes for locomotion by placing its tentacles on the floor and discharging these adhesive nematocytes to provide the traction needed for the organism to pull or lift itself from one location to another (Ewer. & Fox, 1947). Similarly, spirocytes, which are an anthozoan-specific cnidocyte, are distinguished by a sticky thread that is used for ensnaring prey, rather than piercing and envenomating (Krayesky et al., 2010). Cnidocytes are also localized to different regions of the organism to complement their function. For instance, while most nematocytes are localized to the tentacles where they can passively entangle and sting prey, some species of sea anemones also have nematocytes contained in specialized sacs along the body column called acrorhagi. These sacs act as nematocyst-filled "grenades" to inflict damage to neighboring sea anemones competing for territory (Brace, 1990).

As discussed in Chapter 1, nematocytes from the sea anemone *Nematostella vectensis* use a specialized CaV to distinguish salient sensory cues and control the explosive discharge of its penetrant nematocytes. Given that all cnidarians possess these specialized stinging cells, it is possible that other cnidarians utilize a similar molecular strategy to control the discharge of these cells. One strategy to investigate this would be to compare the physiological properties of nematocytes in *Nematostella* to a closely related sea anemone such as *Aiptasia* (Kayal et al., 2018). *Aiptasia* is a hardy sea anemone found in warm, shallow saltwater environments around the world (Baumgarten et al., 2015). Like *Nematostella*, *Aiptasia* have a crown of tentacles densely populated with nematocytes for capturing prey. Despite a close phylogenetic relationship (Kayal et al., 2018) and a similar body pattern, key differences between these organisms may play a critical role in regulating the use of their nematocytes. Unlike *Nematostella*, *Aiptasia* exhibit phototaxis and can move a few centimeters a day (Foo, Liddell, Grossman, & Caldeira, 2020). *Aiptasia* are hosts to endosymbiotic algae in specialized cells, which provide the *Aiptasia* with additional nutrients in the form of photosynthate in exchange for nitrogen, amino acids, and other critical nutrients to the algae (Davy, Allemand, & Weis, 2012). *Aiptasia* also possess threads of tissue, called acontia, which are released from pores on the side of its body column or from its mouth upon stimulation. These nematocyte-packed threads are thought to serve a defense function against predation (Lam et al., 2017).

Taking into consideration the added nutritional source provided by the photosynthetic algae, one can hypothesize that *Aiptasia* have less selective pressure for precise and controlled discharge of their nematocytes compared to *Nematostella*. Indeed, as much as 90% of the photosynthate produced by the algae is given to the host (Burriesci, Raab, & Pringle, 2012). To test the effect of immediate nutrient availability on nematocyst discharge, two manipulations can be carried out:

changing the availability of food to the *Aiptasia* and removing the algae from the host. Algae can be effectively expelled from *Aiptasia* by incubating animals for 8 h in 0.2 mM menthol (Matthews et al., 2016). Over the course of a week with such treatment, *Aiptasia* will become lighter in color, gradually turning white (**Fig. A1**). Preliminary behavioral experiments to assay the nematocyte discharge response in *Aiptasia*, similar to those described in Chapter 1, indicate aposymbiotic *Aiptasia* discharge nematocytes in similar numbers as those hosting algae. Similarly, *Aiptasia* that were deprived of their typical prey, artemia, showed no difference in the probability of discharging their nematocytes compared to their well-fed controls (**Fig. A2**). These preliminary findings suggest that short term changes in nutritional state do not influence the stinging response of nematocytes in *Aiptasia*. However, further analysis is needed to determine if nutritional state may impact the type of nematocysts utilized. *Aiptasia* contain at least three different types of cnidae: spirocysts, microbasic p-mastigophores and basitrichous isorhizas, whose expression may be dependent upon both nutritional state and the presence of symbionts (Gundlach & Watson, 2019). Furthermore, the responses to nutritional state may be dependent upon the localization of the nematocytes such that nematocytes from tentacles may respond to nutritional changes differently than those found in acontia. It is possible that there are no physiological changes to nematocytes in response to nutrition availability. This would suggest that *Aiptasia* may have evolved to use a different, less stringent filter to initiate discharge due to continued presence of algae in their evolution. Thus, a close examination of the physiological properties of these cells in both tissues of the organism may shed important insight to cell regulation by nutrition.

Preliminary examination of the physiological properties suggests that *Aiptasia* have a different system for filtering environmental cues than *Nematostella*. Like *Nematostella*, nematocyte discharge is calcium dependent, and likely is mediated by mechanical cues (**Fig. A2**). Importantly,

nematocyte discharge does not appear to be modulated by the presence of prey-derived chemicals, which are thought to play a critical role in priming the discharge of cell in *Nematostella*. An initial whole-cell recording from a tentacle-derived basitrichous isorhiza nematocyte in *Aiptasia* showed very different voltage-dependent inward currents. Although the charge carrier is not known in this recording, the current inactivates at much more positive potentials, which would indicate that the channels mediating this current would be in closed state at rest and able to open with a depolarizing stimulus (**Fig. A3**). Future work to identify the molecular underpinnings of this current will provide important clues as to the evolution of the filtering and signal amplification used in nematocytes of *Nematostella* and other cnidarians.

Although much of my work has focused on mechanisms mediating nematocyte discharge, another equally fascinating topic is the inhibition nematocyte discharge. Multiple cnidarian predators, including nudibranchs and ctenophores, have evolved to protect themselves from the venomous stings of their prey. While the mechanisms by which they inhibit discharge are not clear, and likely vary by species, one hypothesis is that chemicals within the mucus of these predators inhibit nematocyte discharge (Greenwood, Garry, Hunter, & Jennings, 2004). Perhaps even more astoundingly, some predators can acquire and utilize undischarged nematocysts for their own defenses. These externally acquired nematocysts, termed "kleptocnidae", are ingested by the predator, then sequestered to peripheral tissues, where in some cases they are believed to be functional (Greenwood, 2009). Many questions remain in this area of research, starting with understanding the basic mechanism by which predators are able to inhibit nematocyte discharge. Future research aimed at understanding the method by which these predators can ingest and acquire these single-cell weapons will undoubtably shed light on cell signaling and endocytosis.

Why study native cells?

The last few decades of physiology research have been dominated by work in mammalian model organisms and heterologous cell expression systems, likely due to the availability of genetic tools and the potential translational benefits of this research to human health. However, such defined experimental systems may miss critical opportunities to learn about cell physiology that may only come from studying a range of cell and animal models in their native conditions.

Before the widespread availability of genetic tools, much of the work in the first half of the 20th century in electrical properties of cell membranes was done in what are now considered "unconventional" model organisms. At the time, the selection of model organisms and cells was driven by availability and cell size. In order to study ion currents at the single cell level, early electrophysiologists turned to large, single cells where electrodes could be inserted intracellularly. These included plant cells, such as *Nitella,* which could reach lengths of many centimeters (Findlay, 1959) and muscle cells, such as those from the giant barnacle *Balanus nubilus* (Hagiwara & Naka, 1964). The most famous example of such large cells is the discovery of the squid giant axon by J.Z. Young and the groundbreaking work by A.L Hodgkin and A.F. Huxley (Hodgkin & Huxley, 1952; Young, 1939). The squid giant axon is an incredibly wide 500 µm, which is large enough to allow a wire to be threaded up the length of this part of the neuron. Experiments in the early 50's by Hodgkin and Huxley and later the development of the patch-clamp technique by E. Neher and B. Sakmann would lay the foundation for the study of ion channel structure and properties, including voltage-dependence, permeation, and selectivity.

Much of the early principles of cell electrophysiology came from studying native cells, which greatly benefited the understanding of the native cell physiology by maintaining physiological solutes and native protein interactions. These native cell recordings led to the discovery of the slowing of heart rate by acetylcholine in cardiac pacemaker cells (Logothetis, Kurachi, Galper,

Neer, & Clapham, 1987), and calcium release activated calcium currents, also known as store-operated currents (Parekh & Putney, 2005). It would take many years before the proteins involved in both examples would be identified, in large part because of difficulties in replicating the native cell conditions in reduced experimental preparations (Bourne, 1987; Peinelt et al., 2006). Genetic tools have aided in the ability to label and record native cells, such as the use of the transgenic *Nematostella* to identify neurons in Chapter 1. However, genetic tools alone cannot reveal a cell or protein's native function. Without the continued study of native characteristics of cells, our understanding of cell physiology will be greatly limited.

Appendix

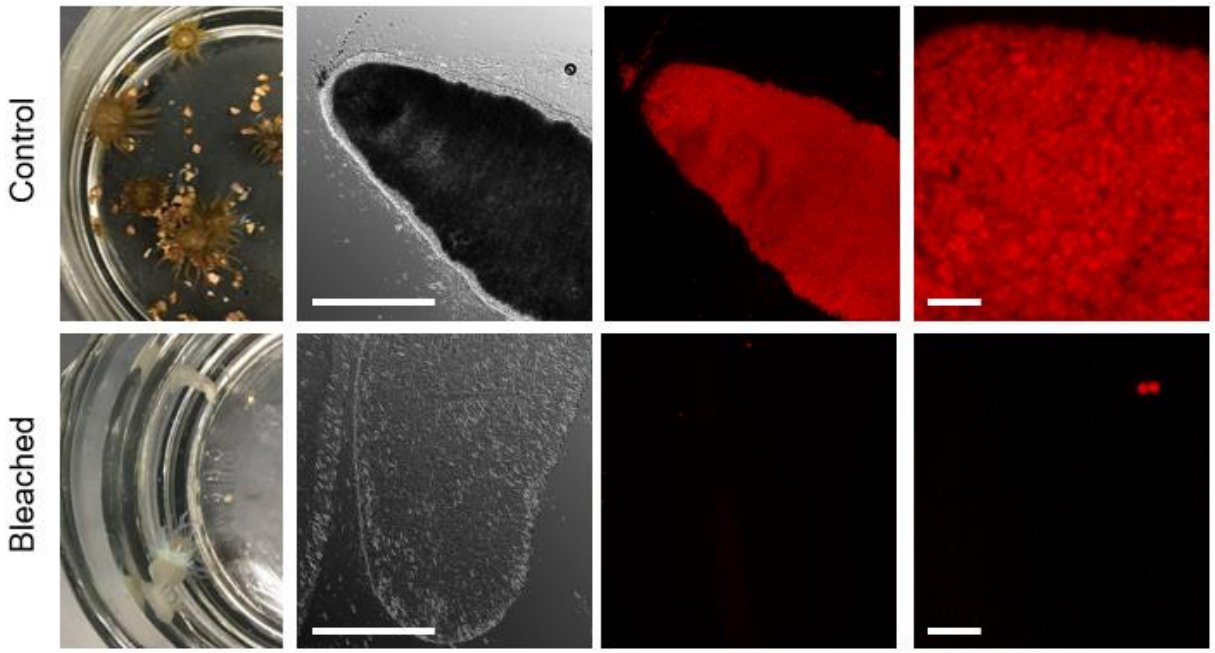

Figure A1: Menthol-treated *Aiptasia* expel autofluorescent algae. Top row, left to right: control *Aiptasia* are brown due to the presence of symbiotic algae in the tentacles. Transmitted light image of a squashed tentacle, scale bar is 500µm. Algae are autofluorescent under red light. Higher resolution image of tentacle, each red dot is a single symbiont, scale bar is 50µm. Bottom row: *Aiptasia* treated with menthol appear white due to the lack of algae.

Chemical tested	Behavioral response: **Nematostella**	Behavioral response: **Aiptasia**
Cd^{2+} (250µM)	No discharge	No discharge
Gd^{3+} (100µM)	No discharge	No discharge
No food chemicals	No discharge	Discharge
Food chemicals	Discharge	Discharge

Figure A2: Behavioral response of *Aiptasia* to gelatin-coated coverslips. *Aiptasia* nematocyte discharge was assessed using the behavioral assay described in Chapter 1. As with *Nematostella,* nematocytes from *Aiptasia* were inhibited by the presence of calcium channel and mechanosensitive channel blockers. However, unlike *Nematostella,* discharge was not dependent upon the presence of prey-derived chemicals.

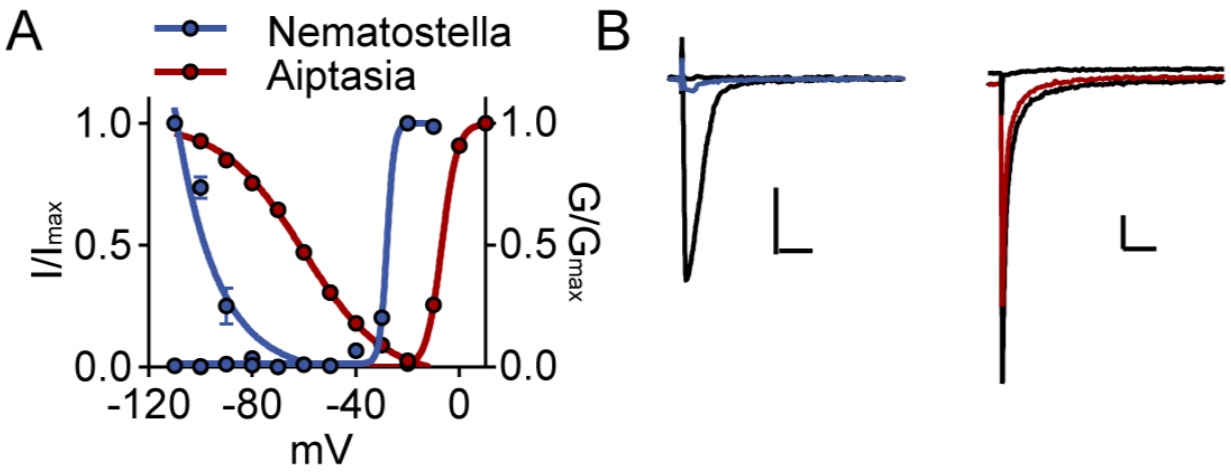

Figure A3: *Aiptasia* nematocytes have different voltage-dependent currents. (A) Voltage-gated currents recorded from nematocytes of *Aiptasia* (red) and *Nematostella* (blue) have different voltage-dependent properties. **(B)** Representative voltage-activated currents following a -120mV pre-pulse, -80mV(colored) pre-pulse, and -20mV pre-pulse. Scale bars = 100pA, 25ms.

References

Altier, C., Garcia-Caballero, A., Simms, B., You, H., Chen, L., Walcher, J., … Zamponi, G. W. (2011). The Cavβ subunit prevents RFP2-mediated ubiquitination and proteasomal degradation of L-type channels. In *Nature Neuroscience* (Vol. 14, pp. 173–182). Nature Publishing Group. https://doi.org/10.1038/nn.2712

Anderson, P. A. V. (1985). Physiology of a Bidirectional , Chemical Synapse, *53*(3).

Anderson, P. A. V., & Bouchard, C. (2009). The regulation of cnidocyte discharge. *Toxicon*, *54*(8), 1046–1053. https://doi.org/10.1016/j.toxicon.2009.02.023

Anderson, P. A. V., & McKay, M. C. (1987). *The Electrophysiology of Cnidocytes*. *Journal of Experimental Biology* (Vol. 133). Retrieved from http://jeb.biologists.org/content/jexbio/133/1/215.full.pdf

Babonis, L. S., & Martindale, M. Q. (2014). Old cell, new trick? Cnidocytes as a model for the evolution of novelty. In *Integrative and Comparative Biology*. https://doi.org/10.1093/icb/icu027

Babonis, L. S., & Martindale, M. Q. (2017). PaxA, but not PaxC, is required for cnidocyte development in the sea anemone Nematostella vectensis. *EvoDevo*, *8*(1), 14. https://doi.org/10.1186/s13227-017-0077-7

Bähring, R., & Covarrubias, M. (2011). Mechanisms of closed-state inactivation in voltage-gated ion channels. *The Journal of Physiology*, *589*(3), 461–479. https://doi.org/10.1113/jphysiol.2010.191965

Baumgarten, S., Simakov, O., Esherick, L. Y., Liew, Y. J., Lehnert, E. M., Michell, C. T., … Knowlton, N. (2015). The genome of Aiptasia, a sea anemone model for coral symbiosis. *Proceedings of the National Academy of Sciences of the United States of America*, *112*(38), 11893–11898. https://doi.org/10.1073/pnas.1513318112

Béguin, P., Ng, Y. J. A., Krause, C., Mahalakshmi, R. N., Mei, Y. N., & Hunziker, W. (2007). RGK small GTP-binding proteins interact with the nucleotide kinase domain of Ca2+-channel β-subunits via an uncommon effector binding domain. *Journal of Biological Chemistry*, *282*(15), 11509–11520. https://doi.org/10.1074/jbc.M606423200

Berger, D. R., Seung, H. S., & Lichtman, J. W. (2018). VAST (Volume Annotation and Segmentation Tool): Efficient Manual and Semi-Automatic Labeling of Large 3D Image Stacks. *Frontiers in Neural Circuits, 12*, 88. https://doi.org/10.3389/fncir.2018.00088

Berjukow, S., Marksteiner, R., Sokolov, S., Weiss, R. G., Margreiter, E., & Hering, S. (2001). Amino Acids in Segment IVS6 and β-Subunit Interaction Support Distinct Conformational Changes during Cav2.1 Inactivation. *Journal of Biological Chemistry*, *276*(20), 17076–17082. https://doi.org/10.1074/jbc.M010491200

Bichet, D., Cornet, V., Geib, S., Carlier, E., Volsen, S., Hoshi, T., … De Waard, M. (2000). The I-II loop of the Ca2+ channel α1 subunit contains an endoplasmic reticulum retention signal antagonized by the β subunit. *Neuron*, *25*(1), 177–190. https://doi.org/10.1016/S0896-6273(00)80881-8

Birnbaumer, L., Qin, N., Olcese, R., Tareilus, E., Platano, D., Costantin, J., & Stefani, E. (1998). Structures and functions of calcium channel β subunits. *Journal of Bioenergetics and Biomembranes*, *30*(4), 357–375. https://doi.org/10.1023/A:1021989622656

Bouchard, C., Price, R. B., Moneypenny, C. G., Thompson, L. F., Zillhardt, M., Stalheim, L., & Anderson, P. A. V. (2006). Cloning and functional expression of voltage-gated ion channel subunits from cnidocytes of the Portuguese Man O'War Physalia physalis. *Journal of Experimental Biology*, *209*(15), 2979–2989. https://doi.org/10.1242/jeb.02314

Bouchard, Christelle, & Anderson, P. A. V. (2014). *Immunolocalization of a Voltage-Gated Calcium Channel Subunit in the Tentacles and Cnidocytes of the Portuguese Man-of-War, Physalia physalis*. Retrieved from http://www.journals.uchicago.edu/t-and-c

Bourne, H. R. (1987). "Wrong" subunit regulates cardiac potassium channels. *Nature*, *325*(6102), 296–297. https://doi.org/10.1038/325296a0

Brace, R. C. (1990). Aggression in a sea anemone: a model of early non-self recognition. *Endeavour*. https://doi.org/10.1016/0160-9327(90)90038-S

Bray, N. L., Pimentel, H., Melsted, P., & Pachter, L. (2016). Near-optimal probabilistic RNA-seq quantification. *Nature Biotechnology*, *34*(5), 525–527. https://doi.org/10.1038/nbt.3519

Brinkmann, M., Oliver, D., & Thurm, U. (1996). Mechanoelectric transduction in nematocytes of a hydropolyp (Corynidae). *Journal of Comparative Physiology A: Sensory, Neural, and Behavioral Physiology*, *178*(1), 125–138. https://doi.org/10.1007/BF00189597

Buchfink, B., Xie, C., & Huson, D. H. (2014, January 1). Fast and sensitive protein alignment using DIAMOND. *Nature Methods*. Nature Publishing Group. https://doi.org/10.1038/nmeth.3176

Buraei, Z., & Yang, J. (2010). The β subunit of voltage-gated Ca2+ channels. *Physiological Reviews*, *90*(4), 1461–1506. https://doi.org/10.1152/physrev.00057.2009

Burriesci, M. S., Raab, T. K., & Pringle, J. R. (2012). Evidence that glucose is the major transferred metabolite in dinoflagellate-cnidarian symbiosis. *Journal of Experimental Biology*, *215*(19), 3467–3477. https://doi.org/10.1242/jeb.070946

Butcher, A. J., Leroy, J., Richards, M. W., Pratt, W. S., & Dolphin, A. C. (2006). The importance of occupancy rather than affinity of Cavβ subunits for the calcium channel I-II linker in relation to calcium channel function. *Journal of Physiology*, *574*(2), 387–398. https://doi.org/10.1113/jphysiol.2006.109744

Cantí, C., Page, K. M., Stephens, G. J., & Dolphin, A. C. (1999). Identification of residues in the N terminus of α1B critical for inhibition of the voltage-dependent calcium channel by Gβγ. *Journal of Neuroscience*, *19*(16), 6855–6864. https://doi.org/10.1523/jneurosci.19-16-06855.1999

Catterall, W. A. (1986). Molecular Properties of Voltage-Sensitive Sodium Channels. In *New Insights into Cell and Membrane Transport Processes* (pp. 3–20). Boston, MA: Springer US. https://doi.org/10.1007/978-1-4684-5062-0_1

Catterall, W. A. (2000). Structure and Regulation of Voltage-Gated Ca 2+ Channels. *Annual Review of Cell and Developmental Biology*, *16*(1), 521–555. https://doi.org/10.1146/annurev.cellbio.16.1.521

Catterall, W. A. (2011). Voltage-gated calcium channels. *Cold Spring Harbor Perspectives in Biology*, *3*(8), 1–23. https://doi.org/10.1101/cshperspect.a003947

Catterall, W. A., Perez-Reyes, E., Snutch, T. P., & Striessnig, J. (2005, December 1). International Union of Pharmacology. XLVIII. Nomenclature and structure-function relationships of voltage-gated calcium channels. *Pharmacological Reviews*. American Society for Pharmacology and Experimental Therapeutics. https://doi.org/10.1124/pr.57.4.5

Chen, Y.-H., Li, M.-H., Zhang, Y., He, L.-L., Yamada, Y., Fitzmaurice, A., … Yang, J. (2004). Structural basis of the α1–β subunit interaction of voltage-gated Ca2+ channels. *Nature*, *429*(6992), 675–680. https://doi.org/10.1038/nature02641

Curtis, B. M., & Catterall, W. A. (1984). Purification of the Calcium Antagonist Receptor of the Voltage-Sensitive Calcium Channel from Skeletal Muscle Transverse Tubules. *Biochemistry, 23*(10), 2113–2118. https://doi.org/10.1021/bi00305a001

Davy, S. K., Allemand, D., & Weis, V. M. (2012). Cell Biology of Cnidarian-Dinoflagellate Symbiosis. *Microbiology and Molecular Biology Reviews, 76*(2), 229–261. https://doi.org/10.1128/mmbr.05014-11

Dawson, T. F., Boone, A. N., Senatore, A., Piticaru, J., Thiyagalingam, S., Jackson, D., … Spafford, J. D. (2014). Gene splicing of an invertebrate beta subunit (LCavβ) in the N-terminal and HOOK domains and its regulation of LCav1 and LCav2 calcium channels. *PLoS ONE, 9*(4). https://doi.org/10.1371/journal.pone.0092941

De Waard, M., Scott, V. E. S., Pragnell, M., & Campbell, K. P. (1996). Identification of critical amino acids involved in α1-β interaction in voltage-dependent Ca2+ channels. *FEBS Letters, 380*(3), 272–276. https://doi.org/10.1016/0014-5793(96)00007-5

Dolphin, A. C. (2016). Voltage-gated calcium channels and their auxiliary subunits: physiology and pathophysiology and pharmacology. *Journal of Physiology, 594*(19), 5369–5390. https://doi.org/10.1113/JP272262

DuBuc, T. Q., Traylor-Knowles, N., & Martindale, M. Q. (2014). Initiating a regenerative response; cellular and molecular features of wound healing in the cnidarian Nematostella vectensis. *BMC Biology, 12*(1). https://doi.org/10.1186/1741-7007-12-24

Eberst, R., Dai, S., Klugbauer, N., & Hofmann, F. (1997). Identification and functional characterization of a calcium channel γ subunit. *Pflugers Archiv European Journal of Physiology, 433*(5), 633–637. https://doi.org/10.1007/s004240050324

Eddy, S. R. (2009). A new generation of homology search tools based on probabilistic inference. *Genome Informatics. International Conference on Genome Informatics, 23*(1), 205–211. https://doi.org/10.1142/9781848165632_0019

El-Gebali, S., Mistry, J., Bateman, A., Eddy, S. R., Luciani, A., Potter, S. C., … Finn, R. D. (2019). The Pfam protein families database in 2019. *Nucleic Acids Research, 47*(D1), D427–D432. https://doi.org/10.1093/nar/gky995

Elgoyhen, A. B., & Katz, E. (2012). The efferent medial olivocochlear-hair cell synapse. *Journal of Physiology Paris, 106*(1–2), 47–56. https://doi.org/10.1016/j.jphysparis.2011.06.001

Ertel, E. A., Campbell, K. P., Harpold, M. M., Hofmann, F., Mori, Y., Perez-Reyes, E., … Catterall, W. A. (2000). Nomenclature of Voltage-Gated Calcium Channels. *Neuron*, *25*(3), 533–535. https://doi.org/10.1016/S0896-6273(00)81057-0

Ewer., R. F., & Fox, H. M. (1947). On the Functions and Mode of Action of the Nematocysts of Hydra. *Proceedings of the Zoological Society of London*, *117*(2–3), 365–376. https://doi.org/10.1111/j.1096-3642.1947.tb00524.x

Faltine-Gonzalez, D. Z., & Layden, M. J. (2019). Characterization of nAChRs in Nematostella vectensis supports neuronal and non-neuronal roles in the cnidarian-bilaterian common ancestor. *EvoDevo*, *10*(1), 27. https://doi.org/10.1186/s13227-019-0136-3

Fatt, P., & Katz, B. (1953). The electrical properties of crustacean muscle fibres. *The Journal of Physiology*, *120*(1–2), 171–204. https://doi.org/10.1113/jphysiol.1953.sp004884

Findeisen, F., & Minor, D. L. (2009). Disruption of the IS6-AID linker affects voltage-gated calcium channel inactivation and facilitation. *Journal of General Physiology*, *133*(3), 327–343. https://doi.org/10.1085/jgp.200810143

Findlay, G. (1959). Studies of Action Potentials in the Vacuole and Cytoplasm of Nitella. *Australian Journal of Biological Sciences*, *12*(4), 412. https://doi.org/10.1071/bi9590412

Foo, S. A., Liddell, L., Grossman, A., & Caldeira, K. (2020). Photo-movement in the sea anemone Aiptasia influenced by light quality and symbiotic association. *Coral Reefs*, *39*(1), 47–54. https://doi.org/10.1007/s00338-019-01866-w

Fucile, S. (2004). Ca2+ permeability of nicotinic acetylcholine receptors. *Cell Calcium*, *35*(1), 1–8. https://doi.org/10.1016/j.ceca.2003.08.006

Gitter, A. H., Oliver, D., & Thurm, U. (1994). Calcium- and voltage-dependence of nematocyst discharge in Hydra vulgaris. *Journal of Comparative Physiology A*, *175*(1), 115–122. https://doi.org/10.1007/BF00217442

Grabherr, M. G., Haas, B. J., Yassour, M., Levin, J. Z., Thompson, D. A., Amit, I., … Regev, A. (2011). Full-length transcriptome assembly from RNA-Seq data without a reference genome. *Nature Biotechnology*, *29*(7), 644–652. https://doi.org/10.1038/nbt.1883

Grabner, M., Wang, Z., Mitterdorfer, J., Rosenthal, F., Charnet, P., Savchenko, A., … Glossmann, H. (1994). Cloning and functional expression of a neuronal calcium channel β

subunit from house fly (Musca domestica). *Journal of Biological Chemistry*, *269*(38), 23668–23674. https://doi.org/10.1016/S0021-9258(17)31567-3

Greene, J. R. (1861). *A manual of the sub-kingdom Cœlentera*. London. Retrieved from https://hollis.harvard.edu/primo-explore/fulldisplay?docid=01HVD_ALMA21193760178000394l&context=L&vid=HVD2&lang=en_US&search_scope=everything&adaptor=Local Search Engine&tab=everything&query=any,contains,Greene Coelenterata&sortby=rank&offset=0

Greenwood, P. G. (2009). Acquisition and use of nematocysts by cnidarian predators. *Toxicon*, *54*(8), 1065–1070. https://doi.org/10.1016/j.toxicon.2009.02.029

Greenwood, P. G., Garry, K., Hunter, A., & Jennings, M. (2004). Adaptable Defense: A Nudibranch Mucus Inhibits Nematocyst Discharge and Changes With Prey Type. *The Biological Bulletin*, *206*(2), 113–120. https://doi.org/10.2307/1543542

Gundlach, K. A., & Watson, G. M. (2019). The effects of symbiotic state and nutrient availability on the cnidom in the model sea anemone, Exaiptasia diaphana. *Marine Biology*, *166*(3), 1–10. https://doi.org/10.1007/s00227-019-3477-5

Gur Barzilai, M., Reitzel, A. M., Kraus, J. E. M., Gordon, D., Technau, U., Gurevitz, M., & Moran, Y. (2012). Convergent Evolution of Sodium Ion Selectivity in Metazoan Neuronal Signaling. *Cell Reports*, *2*(2), 242–248. https://doi.org/10.1016/j.celrep.2012.06.016

Hagiwara, S., & Naka, K. (1964). The Initiation of Spike Potential in Barnacle Muscle Fibers under Low Intracellular Ca++. *Journal of General Physiology*, *48*(1), 141–162. https://doi.org/10.1085/jgp.48.1.141

He, L. L., Zhang, Y., Chen, Y. H., Yamada, Y., & Yang, J. (2007). Functional modularity of the β-subunit of voltage-gated Ca 2+ channels. *Biophysical Journal*, *93*(3), 834–845. https://doi.org/10.1529/biophysj.106.101691

Heinemann, S. H., Terlau, H., Stühmer, W., Imoto, K., & Numa, S. (1992). Calcium channel characteristics conferred on the sodium channel by single mutations. *Nature*, *356*(6368), 441–443. https://doi.org/10.1038/356441a0

Hille, B. (2001). *Ion Channels of Excitable Membranes. 3rd edition. Sinauer Associates, Sunderland*. https://doi.org/10.1007/3-540-29623-9_5640

Hodgkin, A. L., & Huxley, A. F. (1952). A quantitative description of membrane current and its application to conduction and excitation in nerve. *The Journal of Physiology*, *117*(4), 500–544. https://doi.org/10.1113/jphysiol.1952.sp004764

Holstein, T., & Tardent, P. (1984). An ultrahigh-speed analysis of exocytosis: Nematocyst discharge. *Science*, *223*(4638), 830–833. https://doi.org/10.1126/science.6695186

Hoppa, M. B., Lana, B., Margas, W., Dolphin, A. C., & Ryan, T. A. (2012). α2δ expression sets presynaptic calcium channel abundance and release probability. *Nature*, *486*(7401), 122–125. https://doi.org/10.1038/nature11033

Ikmi, A., Steenbergen, P. J., Anzo, M., McMullen, M. R., Stokkermans, A., Ellington, L. R., & Gibson, M. C. (2020). Feeding-dependent tentacle development in the sea anemone Nematostella vectensis. *Nature Communications*, *11*(1), 1–13. https://doi.org/10.1038/s41467-020-18133-0

Ivanina, T., Blumenstein, Y., Shistik, E., Barzilai, R., & Dascal, N. (2000). Modulation of L-type Ca2+ Channels by Gβγ and Calmodulin via Interactions with N and C Termini of α1C. *Journal of Biological Chemistry*, *275*(51), 39846–39854. https://doi.org/10.1074/jbc.M005881200

Jangsangthong, W., Kuzmenkina, E., Khan, I. F. Y., Matthes, J., Hullin, R., & Herzig, S. (2010). Inactivation of L-type calcium channels is determined by the length of the N terminus of mutant β1 subunits. *Pflugers Archiv European Journal of Physiology*, *459*(3), 399–411. https://doi.org/10.1007/s00424-009-0738-z

Jeziorski, M. C., Greenberg, R. M., & Anderson, P. A. V. (1999). Cloning and expression of a jellyfish calcium channel β subunit reveal functional conservation of the α1-β interaction. *Receptors and Channels*, *6*(5), 375–386. Retrieved from https://europepmc.org/article/med/10551269

Jeziorski, M. C., Greenberg, R. M., & Anderson, P. A. V. (2000). The molecular biology of invertebrate voltage-gated Ca2+ channels. *Journal of Experimental Biology*, *203*(5), 841–856.

Jiang, Y., Lee, A., Chen, J., Ruta, V., Cadene, M., Chait, B. T., & MacKinnon, R. (2003). X-ray structure of a voltage-dependent K+ channel. *Nature*, *423*(6935), 33–41. https://doi.org/10.1038/nature01580

Jin, P., Bulkley, D., Guo, Y., Zhang, W., Guo, Z., Huynh, W., … Cheng, Y. (2017). Electron

cryo-microscopy structure of the mechanotransduction channel NOMPC. *Nature*, *547*(7661), 118–122. https://doi.org/10.1038/nature22981

Jones, P., Binns, D., Chang, H.-Y., Fraser, M., Li, W., McAnulla, C., … Hunter, S. (2014). InterProScan 5: genome-scale protein function classification. *Bioinformatics*, *30*(9), 1236–1240. https://doi.org/10.1093/bioinformatics/btu031

Josephson, I. R., & Varadi, G. (1996). The β subunit increases Ca2+ currents and gating charge movements of human cardiac L-type Ca2+ channels. *Biophysical Journal*, *70*(3), 1285–1293. https://doi.org/10.1016/S0006-3495(96)79685-6

Karabulut, A., He, S., Chen, C. Y., McKinney, S. A., & Gibson, M. C. (2019). Electroporation of short hairpin RNAs for rapid and efficient gene knockdown in the starlet sea anemone, Nematostella vectensis. *Developmental Biology*, *448*(1), 7–15. https://doi.org/10.1016/j.ydbio.2019.01.005

Kass-Simon, G., & Scappaticci, Jr., A. A. (2002). The behavioral and developmental physiology of nematocysts. *Canadian Journal of Zoology*, *80*(10), 1772–1794. https://doi.org/10.1139/z02-135

Kasthuri, N., Hayworth, K. J., Berger, D. R., Schalek, R. L., Conchello, J. A., Knowles-Barley, S., … Lichtman, J. W. (2015). Saturated Reconstruction of a Volume of Neocortex. *Cell*, *162*(3), 648–661. https://doi.org/10.1016/j.cell.2015.06.054

Katsuki, T., & Greenspan, R. J. (2013). Jellyfish nervous systems. *Current Biology*, *23*(14), R592–R594. https://doi.org/10.1016/j.cub.2013.03.057

Kayal, E., Bentlage, B., Sabrina Pankey, M., Ohdera, A. H., Medina, M., Plachetzki, D. C., … Ryan, J. F. (2018). Phylogenomics provides a robust topology of the major cnidarian lineages and insights on the origins of key organismal traits. *BMC Evolutionary Biology*, *18*(1), 1–18. https://doi.org/10.1186/s12862-018-1142-0

Krayesky, S. L., Mahoney, J. L., Kinler, K. M., Peltier, S., Calais, W., Allaire, K., & Watson, G. M. (2010). Regulation of spirocyst discharge in the model sea anemone, Nematostella vectensis. *Marine Biology*. https://doi.org/10.1007/s00227-009-1384-x

Lacerda, A. E., Kim, H. S., Ruth, P., Perez-Reyes, E., Flockerzi, V., Hofmann, F., … Brown, A. M. (1991). Normalization of current kinetics by interaction between the α1 and β subunits of the skeletal muscle dihydropyridine-sensitive Ca2+ channel. *Nature*, *352*(6335), 527–530. https://doi.org/10.1038/352527a0

Lam, J., Cheng, Y. W., Chen, W. N. U., Li, H. H., Chen, C. S., & Peng, S. E. (2017). A detailed observation of the ejection and retraction of defense tissue acontia in sea anemone (Exaiptasia pallida). *PeerJ*, *2017*(2), 1–11. https://doi.org/10.7717/peerj.2996

Langmead, B., & Salzberg, S. L. (2012). Fast gapped-read alignment with Bowtie 2. *Nature Methods*, *9*(4), 357–359. https://doi.org/10.1038/nmeth.1923

Layden, M. J., Rentzsch, F., & Röttinger, E. (2016). The rise of the starlet sea anemone Nematostella vectensis as a model system to investigate development and regeneration. *Wiley Interdisciplinary Reviews: Developmental Biology*. https://doi.org/10.1002/wdev.222

Lenhoff, H. M., & Loomis, F. W. (1961). *The biology of hydra and of some other coelenterates, 1961*. University of Miami Press. Retrieved from http://hdl.handle.net/2027/uc1.31822012662540

Li, H., Handsaker, B., Wysoker, A., Fennell, T., Ruan, J., Homer, N., … Durbin, R. (2009). The Sequence Alignment/Map format and SAMtools. *Bioinformatics*, *25*(16), 2078–2079. https://doi.org/10.1093/bioinformatics/btp352

Logothetis, D. E., Kurachi, Y., Galper, J., Neer, E. J., & Clapham, D. E. (1987). The βγ subunits of GTP-Binding proteins activate the muscarinic K+ channel in heart. *Nature*, *325*(6102), 321–326. https://doi.org/10.1038/325321a0

Lubbock, R. (1980). Why are clownfishes not stung by sea anemones? *Proceedings of the Royal Society of London. Series B. Biological Sciences*, *207*(1166), 35–61. https://doi.org/10.1098/rspb.1980.0013

Lubbock, R., Gupta, B. L., & Hall, T. A. (1981). Novel role of calcium in exocytosis: Mechanism of nematocyst discharge as shown by x-ray microanalysis. *Proceedings of the National Academy of Sciences of the United States of America*, *78*(6 I), 3624–3628. https://doi.org/10.1073/pnas.78.6.3624

Lubbock, Roger, & Amos, W. B. (1981). Removal of bound calcium from nematocyst contents causes discharge. *Nature*, *290*(5806), 500–501. https://doi.org/10.1038/290500a0

Marlow, H. Q., Srivastava, M., Matus, D. Q., Rokhsar, D., & Martindale, M. Q. (2009). Anatomy and development of the nervous system of Nematostella vectensis, an anthozoan cnidarian. *Developmental Neurobiology*, *69*(4), 235–254. https://doi.org/10.1002/dneu.20698

Martin, V. J., & Archer, W. E. (1997). Stages of larval development and stem cell population changes during metamorphosis of a hydrozoan planula. *Biological Bulletin*, *192*(1), 41–52. https://doi.org/10.2307/1542574

Matthews, J. L., Sproles, A. E., Oakley, C. A., Grossman, A. R., Weis, V. M., & Davy, S. K. (2016). Menthol-induced bleaching rapidly and effectively provides experimental aposymbiotic sea anemones (Aiptasia sp.) for symbiosis investigations. *Journal of Experimental Biology*, *219*(3), 306–310. https://doi.org/10.1242/jeb.128934

McGee, A. W., Nunziato, D. A., Maltez, J. M., Prehoda, K. E., Pitt, G. S., & Bredt, D. S. (2004). Calcium channel function regulated by the SH3-GK module in β subunits. *Neuron*, *42*(1), 89–99. https://doi.org/10.1016/S0896-6273(04)00149-7

McKay, M. C., & Anderson, P. A. V. (1988a). Materials and methods. *Biological Bulletin*, (147), 47–53. https://doi.org/10.1007/978-3-319-09701-5_6

McKay, M. C., & Anderson, P. a. V. (1988b). Preparation and Properties of Cnidocytes from the Sea Anemone Anthopleura elegantissima. *Biological Bulletin*, *174*(1), 47. https://doi.org/10.2307/1541758

Moran, Y., Barzilai, M. G., Liebeskind, B. J., & Zakon, H. H. (2015). Evolution of voltage-gated ion channels at the emergence of Metazoa. *Journal of Experimental Biology*, *218*(4), 515–525. https://doi.org/10.1242/jeb.110270

Moran, Yehu, & Zakon, H. H. (2014). The evolution of the four subunits of voltage-gated calcium channels: Ancient roots, increasing complexity, and multiple losses. *Genome Biology and Evolution*, *6*(9), 2210–2217. https://doi.org/10.1093/gbe/evu177

Munro, C., Vue, Z., Behringer, R. R., & Dunn, C. W. (2019). Morphology and development of the Portuguese man of war, Physalia physalis. *Scientific Reports*, *9*(1), 1–12. https://doi.org/10.1038/s41598-019-51842-1

Nakanishi, N., Renfer, E., Technau, U., & Rentzsch, F. (2012). Nervous systems of the sea anemone Nematostella vectensis are generated by ectoderm and endoderm and shaped by distinct mechanisms. *Development*, *139*(2), 347–357. https://doi.org/10.1242/dev.071902

Neely, A., Wei, X., Olcese, R., Birnbaumer, L., & Stefani, E. (1993). Potentiation by the β subunit of the ratio of the ionic current to the charge movement in the cardiac calcium channel. *Science*, *262*(5133), 575–578. https://doi.org/10.1126/science.8211185

Noda, M., Ikeda, T., Suzuki, H., Takeshima, H., Takahashi, T., Kuno, M., & Numa, S. (1986). Expression of functional sodium channels from cloned cDNA. *Nature*, *322*(6082), 826–828. https://doi.org/10.1038/322826a0

Nüchter, T., Benoit, M., Engel, U., Özbek, S., & Holstein, T. W. (2006). Nanosecond-scale kinetics of nematocyst discharge. *Current Biology*, *16*(9), R316–R318. https://doi.org/10.1016/j.cub.2006.03.089

Olcese, R., Qin, N., Schneider, T., Neely, A., Wei, X., Stefani, E., & Birnbaumer, L. (1994). The amino terminus of a calcium channel β subunit sets rates of channel inactivation independently of the subunit's effect on activation. *Neuron*, *13*(6), 1433–1438. https://doi.org/10.1016/0896-6273(94)90428-6

Oliver, D., Brinkmann, M., Sieger, T., & Thurm, U. (2008). Hydrozoan nematocytes send and receive synaptic signals induced by mechano-chemical stimuli. *Journal of Experimental Biology*, *211*(17), 2876–2888. https://doi.org/10.1242/jeb.018515

Opatowsky, Y., Chen, C. C., Campbell, K. P., & Hirsch, J. A. (2004). Structural analysis of the voltage-dependent calcium channel β subunit functional core and its complex with the α1 interaction domain. *Neuron*, *42*(3), 387–399. https://doi.org/10.1016/S0896-6273(04)00250-8

Opatowsky, Y., Chomsky-Hecht, O., Kang, M. G., Campbell, K. P., & Hirsch, J. A. (2003). The Voltage-dependent Calcium Channel β Subunit Contains Two Stable Interacting Domains. *Journal of Biological Chemistry*, *278*(52), 52323–52332. https://doi.org/10.1074/jbc.M303564200

Östman, C. (2000). A guideline to nematocyst nomenclature and classification, and some notes on the systematic value of nematocysts. *Scientia Marina*, *64*(SUPPLEMENT 1), 31–46. https://doi.org/10.3989/scimar.2000.64s131

Pantin, C. F. A. (1942a). Excitation of nematocysts [1]. *Nature*. Nature Publishing Group. https://doi.org/10.1038/149109a0

Pantin, C. F. A. (1942b). The Excitation of Nematocysts. *Journal of Experimental Biology*, *19*(3).

Parekh, A. B., & Putney, J. W. (2005, April). Store-operated calcium channels. *Physiological Reviews*. American Physiological Society. https://doi.org/10.1152/physrev.00057.2003

Patil, P. G., Brody, D. L., & Yue, D. T. (1998). Preferential closed-state inactivation of neuronal calcium channels. *Neuron*, *20*(5), 1027–1038. https://doi.org/10.1016/S0896-6273(00)80483-3

Paul, C. A., Beltz, B., & Berger-Sweeney, J. (2010). Staining for acetylcholinesterase in brain sections. *Cold Spring Harbor Protocols*, *5*(8), pdb.prot4806. https://doi.org/10.1101/pdb.prot4806

Peinelt, C., Vig, M., Koomoa, D. L., Beck, A., Nadler, M. J. S., Koblan-Huberson, M., … Kinet, J. P. (2006). Amplification of CRAC current by STIM1 and CRACM1 (Orai1). *Nature Cell Biology*, *8*(7), 771–773. https://doi.org/10.1038/ncb1435

Perez-Reyes, E. (2003). Molecular physiology of low-voltage-activated T-type calcium channels. *Physiological Reviews*, *83*(1), 117–161. https://doi.org/10.1152/physrev.00018.2002

Piontkivska, H., & Hughes, A. L. (2003). Evolution of vertebrate voltage-gated ion channel α chains by sequential gene duplication. *Journal of Molecular Evolution*, *56*(3), 277–285. https://doi.org/10.1007/s00239-002-2399-9

Plachetzki, D. C., Fong, C. R., & Oakley, T. H. (2012). Cnidocyte discharge is regulated by light and opsin-mediated phototransduction. *BMC Biology*, *10*(17). https://doi.org/10.1186/1741-7007-10-17

Pohorille, A., Schweighofer, K., & Wilson, M. A. (2005). The Origin and Early Evolution of Membrane Channels. *Astrobiology*, *5*(1), 1–17. https://doi.org/10.1089/ast.2005.5.1

Pragnell, M., De Waard, M., Mori, Y., Tanabe, T., Snutch, T. P., & Campbell, K. P. (1994). Calcium channel β-subunit binds to a conserved motif in the I-II cytoplasmic linker of the α1-subunit. *Nature*, *368*(6466), 67–70. https://doi.org/10.1038/368067a0

Price, R. B., & Anderson, P. A. V. (2006). Chemosensory pathways in the capitate tentacles of the hydroid Cladonema. *Invertebrate Neuroscience*, *6*(1), 23–32. https://doi.org/10.1007/s10158-005-0015-6

Qiao, X., & Meng, H. (2003, December). Nonchannel Functions of the Calcium Channel γ Subunit: Insight from Research on the Stargazer Mutant. *Journal of Bioenergetics and Biomembranes*. Springer. https://doi.org/10.1023/B:JOBB.0000008030.79380.fb

Richards, M. W., Leroy, J., Pratt, W. S., & Dolphin, A. C. (2007). The hook-domain between the

SH3 and the gk domains of cav-subunits contains key determinants controlling calcium channel inactivation. *Channels*, *1*(2), 92–101. https://doi.org/10.4161/chan.4145

Robinson, J. T., Thorvaldsdóttir, H., Winckler, W., Guttman, M., Lander, E. S., Getz, G., & Mesirov, J. P. (2011, January). Integrative genomics viewer. *Nature Biotechnology*. NIH Public Access. https://doi.org/10.1038/nbt.1754

Sandberg, D. M., Kanciruk, P., & Mariscal, R. N. (1971). Inhibition of nematocyst discharge correlated with feeding in a sea anemone, Calliactis tricolor (Leseur) [15]. *Nature*, *232*(5308), 263–264. https://doi.org/10.1038/232263a0

Santoro, G., & Salleo, A. (1991). The discharge of in situ nematocysts of the acontia of Aiptasia mutabilis is a Ca2+-induced response. *Journal of Experimental Biology*, *156*(1), 173–185. Retrieved from http://jeb.biologists.org/content/156/1/173.abstract

Schindelin, J., Arganda-Carreras, I., Frise, E., Kaynig, V., Longair, M., Pietzsch, T., … Cardona, A. (2012, July). Fiji: An open-source platform for biological-image analysis. *Nature Methods*. Nat Methods. https://doi.org/10.1038/nmeth.2019

Schüler, A., Schmitz, G., Reft, A., Özbek, S., Thurm, U., & Bornberg-Bauer, E. (2015). The rise and fall of TRP-N, an ancient family of mechanogated ion channels, in metazoa. *Genome Biology and Evolution*, *7*(6), 1713–1727. https://doi.org/10.1093/gbe/evv091

Senatore, A., Raiss, H., & Le, P. (2016). Physiology and evolution of voltage-gated calcium channels in early diverging animal phyla: Cnidaria, placozoa, porifera and ctenophora. *Frontiers in Physiology*, *7*(NOV), 1–26. https://doi.org/10.3389/fphys.2016.00481

Shistik, E., Ivanina, T., Puri, T., Hosey, M., & Dascal, N. (1995). Ca2+ current enhancement by alpha 2/delta and beta subunits in Xenopus oocytes: contribution of changes in channel gating and alpha 1 protein level. *The Journal of Physiology*, *489*(1), 55–62. https://doi.org/10.1113/jphysiol.1995.sp021029

Simion, P., Philippe, H., Baurain, D., Jager, M., Richter, D. J., Di Franco, A., … Manuel, M. (2017). A Large and Consistent Phylogenomic Dataset Supports Sponges as the Sister Group to All Other Animals. *Current Biology*, *27*(7), 958–967. https://doi.org/10.1016/j.cub.2017.02.031

Simms, B. A., & Zamponi, G. W. (2014). Neuronal voltage-gated calcium channels: Structure, function, and dysfunction. *Neuron*, *82*(1), 24–45. https://doi.org/10.1016/j.neuron.2014.03.016

Skaer, R. J. (1973). The secretion and development of nematocysts in a siphonophore. *Journal of Cell Science*, *13*(2), 371–393. Retrieved from http://www.ncbi.nlm.nih.gov/pubmed/4148557

Smith, C. L., Abdallah, S., Wong, Y. Y., Le, P., Harracksingh, A. N., Artinian, L., … Senatore, A. (2017). Evolutionary insights into T-type Ca2+ channel structure, function, and ion selectivity from the Trichoplax adhaerens homologue. *Journal of General Physiology*, *149*(4), 483–510. https://doi.org/10.1085/jgp.201611683

Stefanik, D. J., Friedman, L. E., & Finnerty, J. R. (2013). Collecting, rearing, spawning and inducing regeneration of the starlet sea anemone, Nematostella vectensis. *Nature Protocols*, *8*(5), 916–923. https://doi.org/10.1038/nprot.2013.044

Stefanik, D. J., Wolenski, F. S., Friedman, L. E., Gilmore, T. D., & Finnerty, J. R. (2013). Isolation of DNA, RNA and protein from the starlet sea anemone Nematostella vectensis. *Nature Protocols*, *8*(5), 892–899. https://doi.org/10.1038/nprot.2012.151

Stephens, G. J., Page, K. M., Bogdanov, Y., & Dolphin, A. C. (2000). The α1B Ca2+ channel amino terminus contributes determinants for β subunit-mediated voltage-dependent inactivation properties. *Journal of Physiology*, *525*(2), 377–390. https://doi.org/10.1111/j.1469-7793.2000.t01-1-00377.x

Sunagar, K., Columbus-Shenkar, Y. Y., Fridrich, A., Gutkovich, N., Aharoni, R., & Moran, Y. (2018). Cell type-specific expression profiling unravels the development and evolution of stinging cells in sea anemone. *BMC Biology*, *16*(1). https://doi.org/10.1186/s12915-018-0578-4

Tanabe, T., Takeshima, H., Mikami, A., Flockerzi, V., Takahashi, H., Kangawa, K., … Numa, S. (1988). Primary structure of the receptor for calcium channel blockers from skeletal muscle. *Nature*, *328*(6128), 313–318. https://doi.org/10.1038/328313a0

Tardent, P. (1995). The cnidarian cnidocyte, a hightech cellular weaponry. *BioEssays*, *17*(4), 351–362. https://doi.org/10.1002/bies.950170411

Thorington, G. U., & Hessinger, D. A. (1988). Control of Cnida Discharge: I. Evidence for Two Classes of Chemoreceptor. *The Biological Bulletin*, *174*(2), 163–171. https://doi.org/10.2307/1541783

Thuesen, E. V. (2003). Zootaxa 309, *12*(September), 1–12.

Thurm, U., Brinkmann, M., Golz, R., Holtmann, M., Oliver, D., & Sieger, T. (2004). Mechanoreception and synaptic transmission of hydrozoan nematocytes. In *Hydrobiologia* (Vol. 530–531, pp. 97–105). https://doi.org/10.1007/s10750-004-2679-z

Van Petegem, F., Clark, K. A., Chatelain, F. C., & Minor, D. L. (2004). Structure of a complex between a voltage-gated calcium channel β-subunit and an α-subunit domain. *Nature*, *429*(6992), 671–675. https://doi.org/10.1038/nature02588

Varadi, G., Lory, P., Schultz, D., Varadi, M., & Schwartz, A. (1991). Acceleration of activation and inactivation by the β subunit of the skeletal muscle calcium channel. *Nature*, *352*(6331), 159–162. https://doi.org/10.1038/352159a0

Watanabe, H., Fujisawa, T., & Holstein, T. W. (2009). Cnidarians and the evolutionary origin of the nervous system. *Development Growth and Differentiation*, *51*(3), 167–183. https://doi.org/10.1111/j.1440-169X.2009.01103.x

Watson, G. M., & Hessinger, D. A. (1989). Cnidocytes and adjacent supporting cells form receptor-effector complexes in anemone tentacles. *Tissue and Cell*, *21*(1), 17–24. https://doi.org/10.1016/0040-8166(89)90017-7

Watson, G. M., & Hessinger, D. A. (1992). Receptors for N-acetylated sugars may stimulate adenylate cyclase to sensitize and tune mechanoreceptors involved in triggering nematocyst discharge. *Experimental Cell Research*, *198*(1), 8–16. https://doi.org/10.1016/0014-4827(92)90142-U

Watson, G. M., & Hessinger, D. A. (1994). Evidence for calcium channels involved in regulating nematocyst discharge. *Comparative Biochemistry and Physiology -- Part A: Physiology*, *107*(3), 473–481. https://doi.org/10.1016/0300-9629(94)90028-0

Watson, G. M., & Mire, P. (2004). Dynamic tuning of hair bundle mechanoreceptors in a sea anemone during predation. In *Hydrobiologia* (Vol. 530–531, pp. 123–128). https://doi.org/10.1007/s10750-004-2633-0

Weber, J. (1990). Poly(γ-glutamic acid)s are the major constituents of nematocysts in Hydra (Hydrozoa, Cnidaria). *Journal of Biological Chemistry*, *265*(17), 9664–9669. https://doi.org/10.1016/s0021-9258(19)38721-6

Westfall, J. A., Landers, D. D., & McCallum, J. D. (1998). Different nematocytes have different synapses in the sea anemone Aiptasia pallida (Cnidaria, Anthozoa). *Journal of Morphology*, *238*(1), 53–62. https://doi.org/10.1002/(SICI)1097-4687(199810)238:1<53::AID-

JMOR4>3.0.CO;2-O

Wu, J., Yan, Z., Li, Z., Qian, X., Lu, S., Dong, M., … Yan, N. (2016). Structure of the voltage-gated calcium channel Cav1.1 at 3.6 Å resolution. *Nature*, *537*(7619), 191–196. https://doi.org/10.1038/nature19321

Yasuda, T., Lewis, R. J., & Adams, D. J. (2004). Overexpressed Cavβ3 Inhibits N-type (Cav2.2) Calcium Channel Currents through a Hyperpolarizing Shift of "Ultra-slow" and "Closed-state" Inactivation. *Journal of General Physiology*, *123*(4), 401–416. https://doi.org/10.1085/jgp.200308967

Young, J. Z. (1939). Fused neurons and synaptic contacts in the giant nerve fibres of cephalopods. *Philosophical Transactions of the Royal Society of London. Series B, Biological Sciences*, *229*(564), 465–503. https://doi.org/10.1098/rstb.1939.0003

Yu, F. H., & Catterall, W. A. (2004, October 5). The VGL-chanome: a protein superfamily specialized for electrical signaling and ionic homeostasis. *Science's STKE : Signal Transduction Knowledge Environment*. Science Signaling. https://doi.org/10.1126/stke.2532004re15